2020

Proof of Concept for the Development of a Ground Vibration Sensor System for Future Research in Blasting

John Meuth
University of Kentucky, meuthjohn@gmail.com
Digital Object Identifier: https://doi.org/10.13023/etd.2020.118

STUDENT AGREEMENT:

I represent that my thesis or dissertation and abstract are my original work. Proper attribution has been given to all outside sources. I understand that I am solely responsible for obtaining any needed copyright permissions. I have obtained needed written permission statement(s) from the owner(s) of each third-party copyrighted matter to be included in my work, allowing electronic distribution (if such use is not permitted by the fair use doctrine) which will be submitted to UKnowledge as Additional File.

I hereby grant to The University of Kentucky and its agents the irrevocable, non-exclusive, and royalty-free license to archive and make accessible my work in whole or in part in all forms of media, now or hereafter known. I agree that the document mentioned above may be made available immediately for worldwide access unless an embargo applies.

I retain all other ownership rights to the copyright of my work. I also retain the right to use in future works (such as articles or books) all or part of my work. I understand that I am free to register the copyright to my work.

REVIEW, APPROVAL AND ACCEPTANCE

The document mentioned above has been reviewed and accepted by the student's advisor, on behalf of the advisory committee, and by the Director of Graduate Studies (DGS), on behalf of the program; we verify that this is the final, approved version of the student's thesis including all changes required by the advisory committee. The undersigned agree to abide by the statements above.

John Meuth, Student

Dr. Jhon Silva, Major Professor

Dr. Zacharias Agioutantis, Director of Graduate Studies

PROOF OF CONCEPT FOR THE DEVELOPMENT OF A GROUND VIBRATION SENSOR SYSTEM FOR FUTURE RESEARCH IN BLASTING

THESIS

A thesis submitted in partial fulfillment of the
requirements for the degree of Master of Science in the
Mining Engineering in the College of Engineering
at the University of Kentucky

By

John Meuth

Lexington, Kentucky

Director: Dr. Jhon Silva, Professor of Mining Engineering

Lexington, Kentucky

2020

ABSTRACT OF THESIS

PROOF OF CONCEPT FOR THE DEVELOPMENT OF A GROUND VIBRATION SENSOR SYSTEM FOR FUTURE RESEARCH IN BLASTING

Ground vibrations from blasting are one of the leading limitations to mining (underground and surface). There is a need for a low-cost scalable vibration monitoring system to conduct large scale ground vibration projects in the mining industry. Studies conducted on ground vibrations use any number of different sensors to obtain their data, the different sensor capabilities and methods for data processing lead to uncertainties in the research and regulations set for ground vibrations. Commercial Systems do not allow researchers to obtain raw output data, and the data processing procedures are not provided or disclosed for these systems. In order to study ground vibrations and their impact on structures, the University of Kentucky Explosives Research Team is developing a system to obtain raw ground vibration data for their research projects going forward. This study investigates the feasibility of the initial vibration system assembled in conjunction with a significant ground vibrations study happening at a surface coal mine. The assembled system, along with two other systems, were used to study three blast events at structures near the surface coal mine. The two acquired systems were used for data comparison and validation against the assembled system in this document. Additionally, a comparative analysis was performed on the vibration frequency content obtained from the three sensors and a recommendation was made for the continued use of the assembled sensor system in ground vibrations research.

KEYWORDS: Ground Vibrations, Blast Vibrations, Seismograph, Vibration Regulation

John Meuth

04/15/2020

PROOF OF CONCEPT FOR THE DEVELOPMENT OF A GROUND VIBRATION SENSOR SYSTEM FOR FUTURE RESEARCH IN BLASTING

By
John Meuth

Dr. Jhon Silva
Director of Thesis

Dr. Zacharias Agioutantis
Director of Graduate Studies

04/15/2020
Date

DEDICATION

Paul Holmgren (12.15.1995-01.25.2020)

ACKNOWLEDGMENTS

The research compiled for this thesis was made possible thanks to multiple individuals and organizations. First, I would like to thank all the members of the University of Kentucky Explosives Research Team, including Nate Schafer, Dr. Josh Calnan, and Dr. Jhon Silva. Additionally, I would like to thank Andrew Alano with Peabody Energy and Vince Sloan with Dyno Nobel for helping to coordinate the testing done for the project. I would also like to individually thank my academic advisor Dr. Jhon Silva for providing me the opportunity to conduct meaningful research in a creative environment and Dr. Seth Carpenter for his guidance on vibration signal analysis. Lastly, I would like to acknowledge the other two members of my advisory committee, Dr. Joe Sottile and Dr. Steve Schafrik.

TABLE OF CONTENTS

LIST OF TABLES

LIST OF FIGURES

CHAPTER 1. INTRODUCTION

1.1 Background

The purpose of the research project and the framework for the testing are outlined in this chapter. The research questions to be considered are listed, and the key terms and procedures are included.

Vibrations are controlled at mining operations in order to protect nearby structures. Many research studies have been conducted to understand the structural response from vibrations and their impacts on the structures. Vibration monitoring in the mining industry does not have specific guidelines for the requirements or the characteristics of the equipment to be used or the analysis required for the collected raw data (post-processing). While this situation can be enough for the mining industry, it is not enough to conduct accurate and efficient research in ground vibrations. From an academic perspective, it is essential to obtain raw data with a complete understanding of the signal processing that is occurring before producing a "final waveform."

The commercial devices currently used for vibration monitoring are, in many instances expensive and bulky. These devices are adequate for long term vibration monitoring at set locations around the structures but are not conducive to fluid large scale research projects needed to understand the vibration transmission through the ground and the structural responses fully. There is a need in the area of academic and industry research for an inexpensive, scalable device to monitor blast vibrations.

The devices used for mining compliance, and to study structural response and vibrations transmitted through the ground from blast vibrations were developed a considerable number of years ago. The original devices and technologies haven't been updated. The development in the field of electronics and piezoelectric materials in the years since the original research by the bureau of mines regarding blast vibrations has seen exponential growth, and these new technologies provide the opportunity to update the systems and the sensors used in the mining industry. In the long term, this can be used to reevaluate many of the vibration regulations used in the mining industry.

1.2 Statement of Problem

There is a clear lag in the technology used to monitor and study blast vibrations. A new cost-effective system is needed to efficiently and accurately obtain raw vibration data in order to complete large scale research projects on the structural response and ground vibrations transmission from blast vibrations. Such large-scale research projects will require the use of a considerable number of devices to collect vibration data that it will be at some point cost prohibited.

1.3 Conceptual Framework for the Study

Following detonation, an explosive is converted to several types of energy. The confinement of the explosive within the medium converts energy from the explosive into ground vibration waveforms. In order to simplify the problem of ground vibrations, these vibration waveforms are divided into three waveform directions, radial, transverse, and vertical components. Vibration monitoring systems are used to measure the three vibration waveforms in order to understand the impact on structural response and limit its exposure to vibrations from these blast events. These sensors use the mechanical effects of vibrations to produce an electric signal in order to store and analyze the waveforms.

Piezoelectric materials are materials that change their electric response with an input of mechanical energy. These materials have provided the opportunity to miniaturize and improve the sensors used to study blast vibrations.

1.4 Purpose of Study and Research Questions

This thesis aims to provide an outline of a developed vibration system for the use of vibration monitoring. The study provides the outline of the components used to assemble the system and the procedure used to study its feasibility compared to accepted industry devices. This system was assembled in response to a structural response research project being performed at the University of Kentucky and aims to provide an alternative to vibration monitoring systems available on the market today.

Ultimately, two questions are investigated in this research

1. Is the assembled system capable of measuring and recording blast vibrations from a surface mining operation?
2. Is the acquired data accurate and precise enough to be used in research projects moving forward in the field of mining?

A recommendation will be made at the conclusion of the project for the continued use of the system for the ongoing and future University of Kentucky research projects.

1.5 Procedures

A prototype system was developed to best study the range of vibrations typical seen from a surface mining operation. The system was configured to reproduce similar sampling rates used in the mining industry. The system includes a device developed for triggering the sensors and logging the events.

Ground vibrations from three surface blasts in a surface coal mine operation were studied using the prototype system, a commercial seismograph, and an accelerometer used for geophysical research. The systems and the sensors were installed near a structure being studied by the University of Kentucky. The recorded waveform components were logged

for comparison. Cross-correlation and visual comparison were used to analyze the waveforms of the three blast components, and spectral coherence was performed on the frequency content of the waveforms.

1.6 Limitations of the Study

This study utilized components produced by electronic manufacturers and were confined to the configurations of those devices. The components were programmed to best match the needs of vibration monitoring. Still, it is necessary to keep in mind that this was not the original purpose of the electronic components of the system.

The events studied for this research project were part of ongoing mining operations, and therefore the research had no control over the types or locations of the blasts and would frequently obtain this information with minimal lead time.

This developed system is the first iteration of the device and this research is meant to provide a recommendation for future work and feasibility for a more complex and comprehensive blast vibration monitoring system.

1.7 Organization of the Study

This thesis provides a literature review and background information on ground vibration response and types of sensors and their role in studying ground vibrations. The developed prototype system is outlined and explained. The vibrations project from the University of Kentucky is outlined and the procedure for testing the prototype system is provided. Following the data analysis and comparison, results, concluding remarks, and recommendations for future work are given. A full outline of the chapters for this can be viewed in the table of content.

The three main characteristics of time histories that are important to evaluate wave motions are amplitude, frequency, and duration. A brief review of these components follows.

2.1.1 *Amplitude, or the intensity of particle velocity:*

A blast time history is made up of peaks and troughs of motion, the height of any wave is the amplitude (OSMRE). The largest value of the ground vibration amplitude is called the peak particle velocity (PPV) as marked in the radial direction in Figure 2.1.

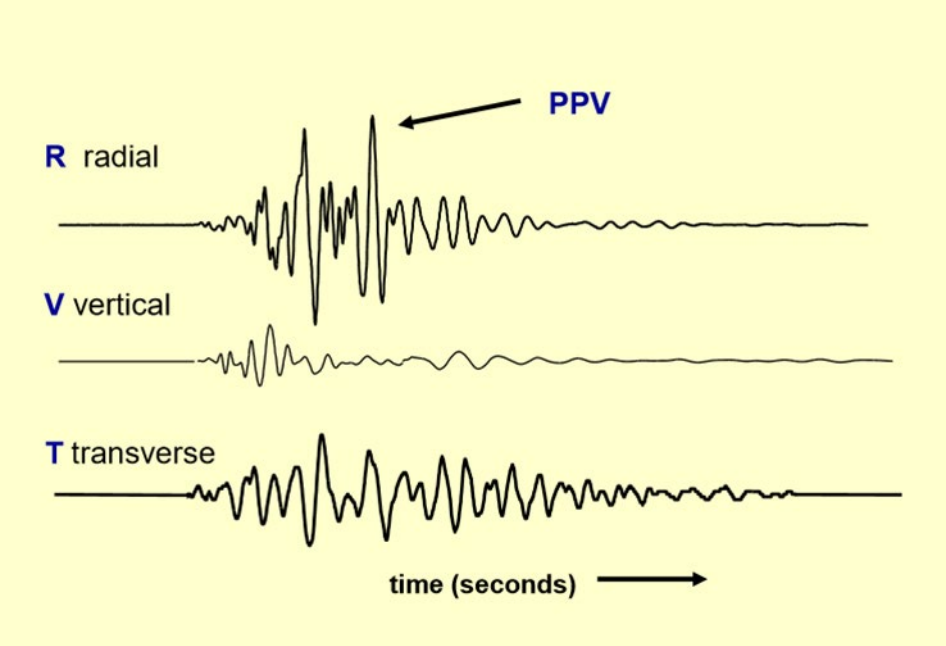

Figure 2.1: Waveform Peak Particle Velocity

2.1.2 *Frequency*

Frequency is the number of cycles or oscillations that a wave completes over 1 second and is measured in cycles per second or Hertz (Hz). Frequency is calculated by the time interval of one complete cycle. Equation one shows the calculation for the frequency of one cycle of the time increment (p).

$$f = 1/p \quad [1]$$

Figure 2.2 from (OSMRE) shows an example of a cycle of 1 over a 0.2 second interval producing a frequency of 5 Hz.

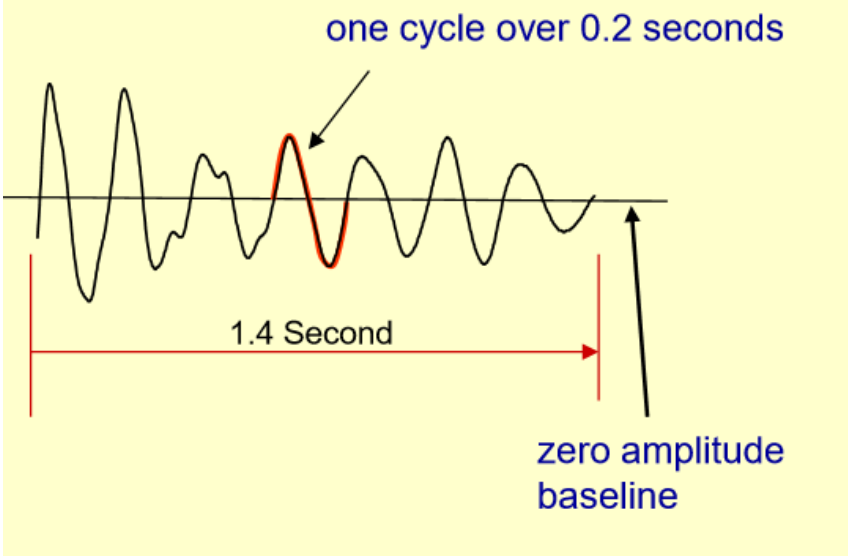

Figure 2.2: Waveform Frequency Cycle

2.1.3 *Duration*

The duration of a ground vibration event is simply the time interval in which the ground is displaced from its original position. It is important to note for ground vibrations that duration increases as the wave disperses. Duration will increase as the measurement distance increases from the source of the blast as frequency and amplitude decrease.

In summary, the amplitude is the strength of the event, frequency is the rate of vibrations, and duration is the length of the event. Each of these characteristics will impact the measurement planning for a blast event and will be covered in more detail in the following literature review.

2.2 Blast Vibration Generation

When preparing to study ground vibrations produced from blasting, it is important to understand the energy distribution produced by the explosive material. Within the generation zone of the blast the main energy of the explosive contributes to fracturing and moving the geologic material. This generation zone is within the inelastic interface of the blast and this movement is what propagates to the elastic zone producing seismic waves (Bollinger 1971). Outside of the elastic-inelastic interface the seismic waves travel through the medium experiencing exponential decay with increasing distance from the blast. This elastic zone and seismic propagation will be the focus of this study. A discussion of the inelastic zone during an explosive event can be referenced in (Cook 1958), (Kisslinger 1963), or (Leet 1960). The principal factors and resulting output ranges will be outlined in this section.

The seismic waves generated from a surface mine blast that propagate through the earth are divided into two types. The first type, body waves, are comprised of two types,

compressive waves (P-waves) and shear waves (S-waves). Figure 2.2 and Figure 2.4 adapted from (Dowding 1985) show these two types of waves and their propagation direction.

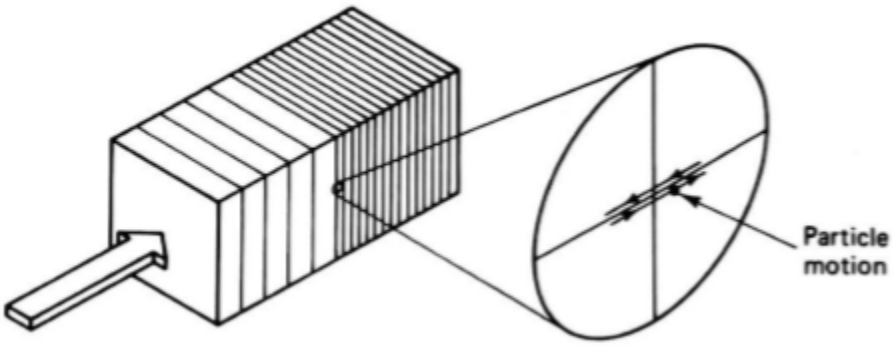

Figure 2.3: Compressive Wave Propagation

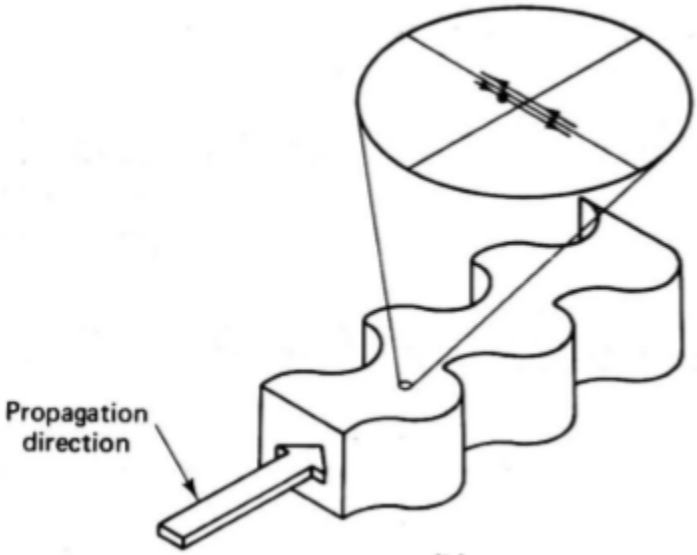

Figure 2.4: Shear Wave Propagation

Body waves, S-waves and P-waves propagate through the media, and the second of the two types of waves, Rayleigh waves (R-waves), travel along the surface of the earth media. Figure 2.5 shows this type of wave and the propagation direction.

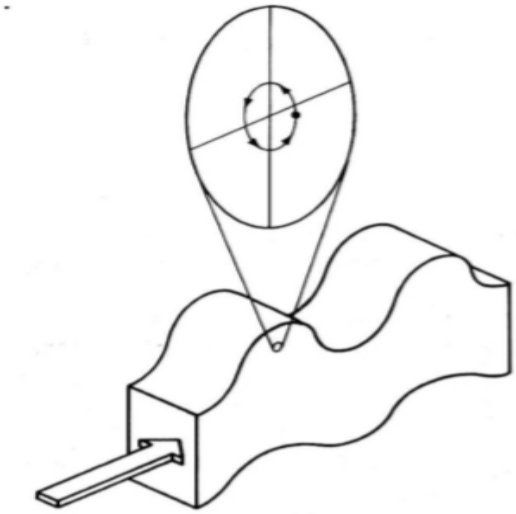

Figure 2.5: Raleigh Wave Propagation

R-waves become more important at larger distances as reflection and refraction waves have time to develop (Dowding 1985). Most blast phenomena are measured at a distance outside the direct pulse region and therefore experience a combination of direct transmission, reflection, and refraction. This combination is illustrated in Figure 2.6 adapted from (Dowding 1985).

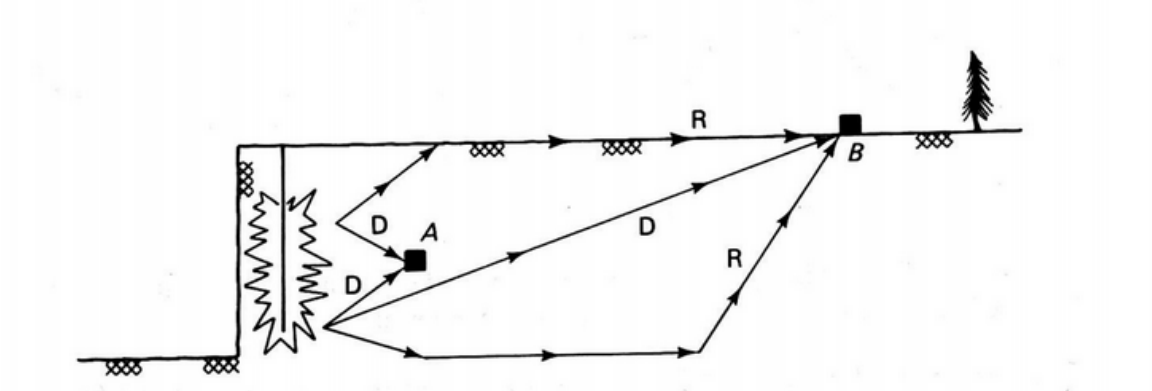

Figure 2.6: Waveform Reflection and Refraction

In Figure 2.6, A represents a monitoring location within the inelastic zone of the blast, B represents a monitoring location in the elastic zone of the blast, D are the direct vibration waves, and R are the is reflected vibration waves.

Several principle factors can affect the ground motion seen during a blast including energy source, shot geometry, geology, and recording distance. When developing an instrument to study ground motion, it is important to understand these factors and their effect on the amplitude and frequency ranges produced during mine blasting.

2.2.1 *Explosive Characteristic*

The type of explosive used in blasting influences the amplitude and frequency of the vibration. Two categories are used to explain detonation type, ideal and non-ideal. Non-

ideal detonations result in a longer duration explosion with a slow rise and fall time. During ideal detonations the pressure rise time is short in comparison and the pressure drop curve is steep (Saharan and Mitri 2008). The density of explosives also affects the generation of vibration waveforms. Explosives with lower density and lower detonation velocity produce lower ground vibration levels (Hunter et. al. 1993).

2.2.2 *Timing and Shot Geometry*

The degree of confinement of charges in a mine blast affects the vibrations levels. A higher degree of confinement will generate higher vibration levels. Six variables are defined in shot geometry and affect the confinement of the blast and the resulting vibration waveforms. These variables are the diameter of the hole, burden, spacing, length, stemming, and sub-drilling (Ash 1973). The shot timing also affects the wave vibrations through constructive or destructive interference. Depending on the blast timing, the delays can create destructive interference to reduce ground vibrations levels.

2.2.3 *Monitoring Distance*

As vibrations travel through the media, the various waveform types travel at different speeds. As the distance from the blast increases, these wave types separate and increase the duration of the event. As the waveform travels, some of the energy is also lost to the medium. In the case of body waves (p and s waves), the amplitude decreases according to the relations (1/R) where R is the distance to source measurement. For surface waves (Rayleigh waves), the decrement relation is ($1/R^{0.5}$). As the medium absorbs energy, the amplitude of ground motion decreases exponentially with R (Kramer 1996)

2.2.4 *Geology*

The vibration waves following a blast event reflect and refract at every boundary in the medium. As this phenomenon occurs new waves can be generated at the discontinuities in the rock structure. The different dynamic properties of the materials making up the travel medium change the amplitude and frequency of the waves. These occurrences explain why each unique monitoring location will produce a unique waveform because of the geologic features encountered while traveling to the monitoring point.

2.3 Blast Vibration Characteristics

Many studies have been produced to study and determine the typical blast vibration characteristics experienced during different types of blasting events including (Cording et al. 1975), (Duvall 1961), and (Kisslinger, Mateker, and McEvilly 1963). Kisslinger, Mateker, and McEvilly conducted a series of explosions in natural media. The three-year research project included 160 charges ranging from 0.25 to 15 pounds. The ground motion was measured at a distance from 0 to 820 feet from detonation. The observed frequency data can be seen in Figure 2.7.

SEISMIC EVENT	MEDIUM					
	CLAY		SANDSTONE		LIMESTONE	
	Velocity fps	Freq. Hz	Velocity fps	Freq. Hz	Velocity fps	Freq. Hz
Direct P	1000	25	3900	30	14,000	50
Refracted P	--	--	8200	40	--	--
Direct S	--	--	2600	40	7900	80-100
Refracted S	--	50	5600	--	--	--
Rayleigh	590-690	6-10	3000-4300	12-20	6900	25
Prograde Rayleigh	1150	10-12	4600	20	--	--
Love	670-850	5-10	3600-5300	15±	--	--

Figure 2.7: Differing Medium Frequency Data

In (Duvall 1961), a Bureau of Mines research program studied the generation and propagation of vibrations from quarry blasting, the effect these vibrations have on structures, and calibration characteristics for seismographs. From these studies, a specific range of frequencies and the expected displacement and its time derivations were complied. The range of these quantities is important in determining the capabilities of a seismograph used to study vibrations produced by blasting. The research produced a frequency range of 1 to 500 Hz, a displacement range of 0.0001 to 0.5 inches, a velocity range of 0.01 to 10 inches/sec, and an acceleration range of 0.005 to 2 g.

As seen in the previous studies, vibrations from mine blasting have frequency content less than 200 Hz (Spathis 2010). In normal blasting operations for surface mining the ranges seen in Figure 2.8 are a good representation of expected outputs and are used as defining parameters for this research. The resulting amplitude ranges of surface blasting events will be covered more thoroughly in future sections of the report when peak particle motion is discussed.

Displacement	10^{-4} to 10 mm
Particle velocity	10^{-4} to 10^{3} mm/s
Particle acceleration	10 to 10^{5} mm/s^{2}
Pulse duration	0.5 to 2 s
Wavelength	30.0 to 1500 m
Frequency	0.5 to 200 Hz
Strain	3.0 to 5000 μ in./in.

Figure 2.8: Vibration Ranges from Typical Mining Operation (adapted from Cording)

Another important characteristic of blast vibration is the duration of the event. Duration of event or decay of vibrations is crucial in determining sampling time when studying blast events. The duration of the event increases with distance to the monitoring point. The pulse duration range is given as 0.5 to 2 seconds. A duration of 1 second for every 1100 feet from the blast can be accounted for to add a safety factor to the recording time.

2.4 Blast Vibration Typical Measurement and Regulations

When designing a seismograph or any system to study blast vibrations, the specific parameters to be measured will depend on the application of the project. For seismographs used in the explosives industry, most products are developed to record the characteristics of blasts that are the limiting factors in vibrations regulations. A major problem with this line of thinking is the non-standardization of vibration regulations throughout the world. The European Federation of Explosive Engineers (EFEE) completed a study to aid in the understanding of similarities and differences between national legislation, standards, and guidelines for vibration monitoring. Several key findings were outlined in this study. The study found that most of the standards include frequency, where higher frequencies allow a higher vibration level. Most countries included in the study also use the maximum value of the three monitored directions as the considering factor in blast vibration (Gjodvad 2020). Figure 2.9 shows the standards and regulations used in the different countries covered in the study.

Country	National standard	National regulations	Other countries standard
Austria	Austrian Standard S 9020 - 2015		
Belgium			DIN4150
Bulgaria			DIN 4150
Czech Republic	ČSN 730040		
Denmark			DIN 4150 for hard rock, SS 460 4866 is used
Estonia		National regulation	
Finland		Tärinänormit/ Finnish Vibration normes	
FRANCE		Decree of 22 September 1994 Circulaire du 23/07/86	
Germany	DIN 4150		
Greece		Greek Mining Regulation	
Hungary			DIN and some inner std. (ex. customer, authority)
Hong Kong		Limits by Authorities	
India			Australian standards
Ireland			British Standards
Italy	UNI 9916		(UNI 9916 refers to both DIN 4150 and BS 7385)
Israel			DIN 4150
Netherlands			DIN 4150
Nigeria			Use of consultants
Norway	NS8141, 2. Ed., 2001, NS8141-3, 2014		
Poland	PN-B-02170:2016		
Portugal	NP 2074:2015		
Saudi Arabia			BS7385:2, USBM RI8507
Slovakia	STN EN 1998-1/NA/Z1 STN ISO 4866+Amd 1+Amd Euro 8		
Spain	UNE 22-381-93		
Sweden	SS 4604866:2011		
UAE		Ministerial Dec. 567: 2014	
United Kingdom	BS 5228; BS 6472; BS 7385		
USA	USBM RI 8507		

Figure 2.9: Vibration Regulations from Across the World (Gjodvad 2020)

Similarly, Figure 2.10 and Figure 2.11 showing frequency ranges and monitoring locations were included in the paper by Gjodvad.

Country	Standard	Frequency range
Austria	ÖNORM S 9020	2-250 Hz
France	Circulaire du 23/07/86	4-150 Hz
Germany	DIN 4150-3	1-315 Hz
Italy	UNI 9916-2004	1-300 Hz
Norway	NS 8141-1:2012	3-400 Hz
Poland	PN-B-02170:2016	1-100 Hz
Portugal	NP-2074	3-80 Hz
Schweiz	SN 640 312a	5-150 Hz
Spain	UNE 22381:1993	2-200 Hz
Sweden	SS 460 48 66	5-300 Hz
UK	BS 7385-1:1990	1-300 Hz
USA	ISEE	2-250 Hz

Figure 2.10: Allowed Frequency Ranges in Corresponding Countries

Country	Position of Monitor
Austria	Basement
France	Basement, parallel to the wall
Hungary	Define direction at front of the building
Ireland	Placed at base of building facing the source of vibration. Refer to BS 7385-2:1993
Norway	Sensor on the foundation or near the foundation, where vibrations enter into the structure
Poland	Using the SWD scale, one should use vibrations of horizontal vibrations, i.e. in x and y directions recorded at the source point of vibrations, in a rigid structural node —at the intersection of load-bearing walls in two directions —located on the foundation of the building or in a rigid node on the wall underground level in the ground level.
Portugal	Transducer must be fixed to the base of structure or foundation according ISO 5348, max up to 0.5 m from the level of the ground
Slovakia	The sensors must be stored at the reference point on the foundations of the building.
Spain	On the ground, near to the structures
Sweden	Vibrations should be measured at a point where they enter a building or structure. The sensor should be attached to the load bearing part of the foundation.
USA	Monitors should be buried in undisturbed soil or bolted to rock

Figure 2.11: Monitoring Locations used in the Corresponding Countries

As seen in Figure 2.9 the regulatory legislation for ground vibrations from blasting in the United States is USBM RI 8507. This is adapted from a study done by the United States Department of Interior's Bureau of Mines (USBM) to evaluated damage caused by blast vibrations (Siskind et. al. 1980). The blast vibrations limits outlined by the study are based mainly on particle velocity and frequency content. The research studied houses ranging from modern homes with drywall interiors to older houses with plaster and wood interior. The damage, either threshold, minor, or major, was graphed from 200 blast events. The damage plot produced the "Z" curve seen in Figure 2.12, which is currently used in the United States as the regulator guideline for vibrations produced by blasting.

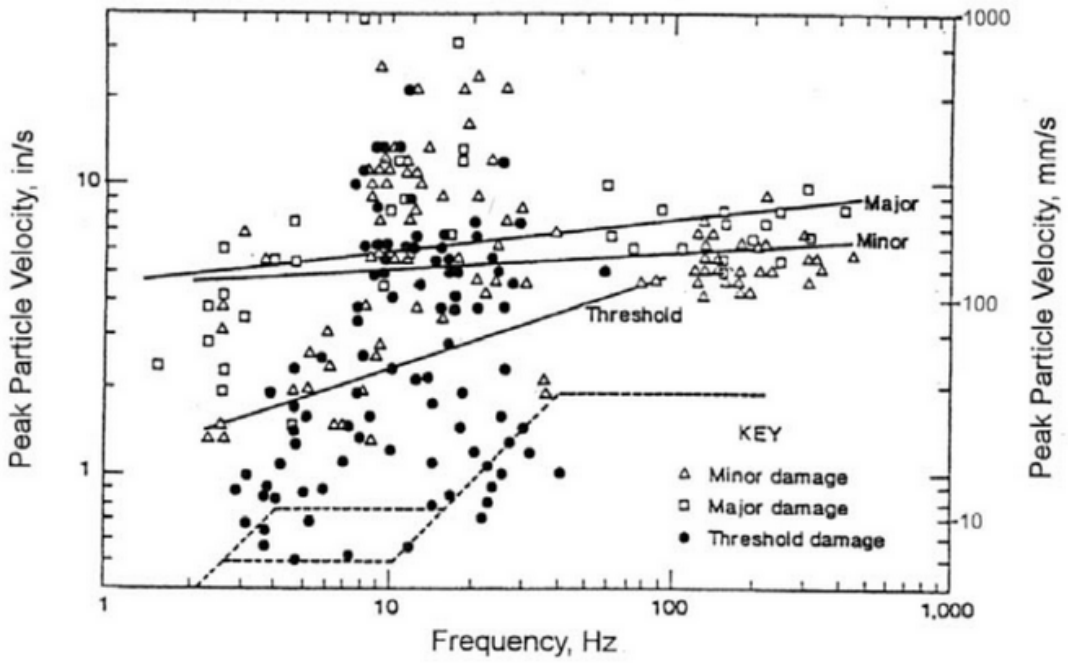

Figure 2.12: The United States "Z-curve" (Siskind et. al. 1980)

The Z curve represents safe limits of blast vibrations to produce no damage to surrounding houses. Some shortcomings of the study should be noted. All the blast events studied at that time had a hole delay minimum of 8-ms. This was because of the capabilities of detonators at the time of the study. The study was also limited to one- and two-story typical homes and no other structure types were analyzed.

2.5 Measurement Techniques and Seismograph Types

Seismograph installation and recording settings will be laid out in this section in accordance with the ISEE blast vibration and seismograph section guidelines. Proper installation and sensor design are crucial in obtaining accurate and precise vibration readings. In conjunction with the proper installation, a review of the most common seismograph types used in the mining industry are explained and reviewed.

In 1997, the Blast Vibration and Seismograph Section was created to answer questions raised about the accuracy, reproducibility and defensibility of data from blasting seismographs (ISEE 2015)

2.5.1 *Sensor Placement:*

The sensor should be placed on or in the ground on the side of the structure towards the blast. The location relative to the structure should be less than 10% of the distance from the blast. When placing the sensor, the longitudinal channel should be directed at the blast at a perpendicular angle.

2.5.2 *Sensor coupling:*
If the acceleration is to exceed 0.2 g, slippage may occur.
If the acceleration is expected to be:

a. less than 0.2 g, no burial or attachment is necessary
b. between 0.2 and 1.0 g, burial or attachment is preferred. Spiking may be acceptable.
c. greater than 1.0 g, burial or firm attachment is required (USBM RI 8506).

If the sensor is to be buried the hole must be no less than three times the height of the sensor. The sensor should be firmly compacted with soil around and above the sensor.

2.5.3 *Programming considerations:*
The trigger level should be set low enough to trigger the unit from blast vibration while minimizing the potential for false triggers. The level should, therefore, be set slightly above the expected background vibrations in the area. A starting point of 0.05 in/s is recommended. An appropriate dynamic range should be used to allow the resolution to verify a blast event upon inspection of the report. Lastly, the recording duration should be set to 2 seconds longer than the blast duration plus 1 second for every 1100 feet from the blast.

Following the standard vibration regulations and ISEE guidelines most of the blasting industry uses a mass and spring type geophone to monitor blast vibrations. There are no uniform guidelines for the system type or data processing of the actual vibration data. This leads to much ambiguity in the selection of seismographs and the processing methodologies of the data. The differences seen in the output of vibration data from different units were outlined in-depth in a comparison study and can be reviewed in (Aimone-Martin 2016). For the purpose of this report the mechanics behind the typical system will be outlined but for specific industry specifications the before mentioned study can be referenced.

A typical seismograph consists of three parts – a transducer, a recorder, and a timing system (Bollinger 1980). The transducer is responsible for producing a signal that is proportional to the response motion. The recorder then accepts this signal and produces an analog recording. The timing is superposed on the analog signal to provide timing information. Seismographs are usually single-degree-of-freedom systems and thus require three sensors to record 3-degree ground motions. Since the seismometers are to provide a relatively steady point in space, the arrangement is made for the inertial member to tend not to participate in the vibratory motion, and signal measurement is made of the relative motion between this inertial member and the vibrating earth (Bollinger 1980). In order to obtain this equilibrium, position a restoring force comprising of elasticity, and gravity is usually used along with some type of damping, normally electromagnetic damping. The system is modeled by a single-degree-of-freedom system as seen in Figure 2.13.

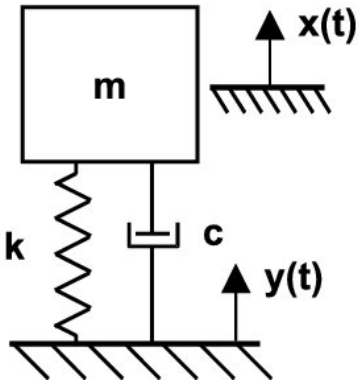

Figure 2.13: Mass, Spring, and Damper System

$$Z(t) = y(t) - x(t) \quad [2]$$

As technology has improved and changed, a new type of sensor is beginning to be used to measure acceleration. Such new devices are used in many industries, automotive, aeronautical, etc. Methodologies have also been changing in vibration analysis. The use of piezoelectric materials has been changing the sensors for vibrations. A piezoelectric accelerometer uses solid-state materials that are electrically responsive to mechanical forces to measure motion. Piezoelectric material produces electrical responses proportional to the stress being applied. There are several advantages to piezo accelerometer transducers: the sensors have a wider frequency response; they can be used to measure low frequency and high frequencies simultaneously. These types of sensors are temperature stable, rugged, and, most important, adaptable to different applications. This theory of piezoelectric transducer can be seen in Figure 2.14.

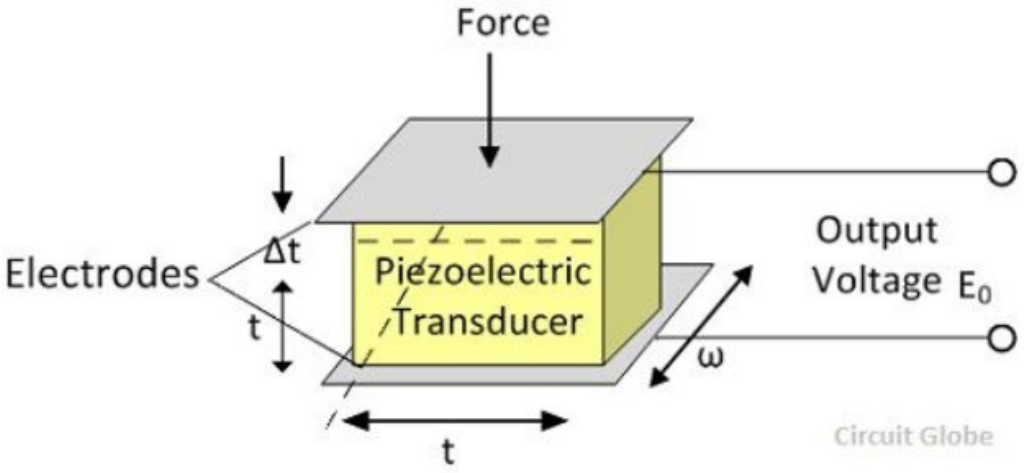

Figure 2.14: Piezoelectric Theory (Circuit Globe...)

The direction of the applied force changes the polarity of the charge following the constraints of Equation 3.

$$Q = d * F \; coulomb \quad [3]$$

Where Q is the charge, d is the sensitivity of the material, and F is the force applied in Newtons.
The thickness of the material is changed with force following equation 4,

$$F = \frac{AE}{t}\Delta t \; Newton \quad [4]$$

Where A is the area of the material (m^2), t is the thickness of the material (m), and E is the young's modulus.
The young's modulus is,

$$E = \frac{stress}{strain} = \left(\frac{F}{A}\right) * \frac{1}{\Delta t/t} \quad [5]$$

$$E = \frac{Ft}{A\Delta t} N/m^2 \quad [6]$$

$$A = wl \quad [7]$$

Where w is the width of the material (m), and l is the length (m).
Substituting the value of force into the charge equation,

$$Q = dAE\left(\frac{\Delta t}{t}\right) \quad [8]$$

The output voltage is dependent on the electrode charges,

$$E_0 = \frac{dF}{\varepsilon_r \varepsilon_0 A/t} \quad [9]$$

$$E_0 = \frac{d}{\varepsilon_r \varepsilon_0} tp \quad [10]$$

$$E_0 = gtP \quad [11]$$

$$g = \frac{d}{\varepsilon_r \varepsilon_0} \quad [12]$$

Where E_0 is the electric field strength. The voltage sensitivity is expressed by the ratio of the electric field intensity and the pressure. (Circuit Globe 2020). This sensitivity relationship allowed for a much more sensitive device than the original mass, spring, and damper system used for vibrations studies. The materials are much more customizable to meet the specifications of the events being studied and can closely follow and more precisely convert the actual ground motion levels.

The development of micro-electrotechnical systems (MEMS) has revolutionized the accelerometer application. MEMS is a process technology used to create tiny integrated devices or systems that combine mechanical and electrical components (Prime Faraday 2002). These systems can range in size from a few micrometers to millimeters. These systems can sense on a micro-scale and can generate effects on the macro scale. These

devices have a wide range of applications, from airbag sensors to phone accelerometers and are commonplace in recent technology.

MEMS technology has allowed for smaller, low powered, and more accurate affordable accelerometers. When these accelerometers are coupled with microcontrollers to store and treat data, a usable and affordable product can be created for blast vibration monitoring.

2.6 Comparison Techniques for Ground Vibration Sensor

In 2015, Edward Sheehan et al. performed a side-by-side comparison of blasting seismographs. During the test, six blasts were monitored using seven different makes of seismograph used for blast monitoring. The seismographs were set up using two different deployment techniques, linear and clustered.

Figure 2.15: Seismograph Comparison Deployments (Sheehan et al. 2015)

At the time of the study, the Seismographs Standards group within the ISEE expected the amplitudes would fall within the range of ±5% of the median value for particle velocities. The actual % deviation can be seen in Table 1, from the paper written following the study.

Table 1: Side-by-side Seismograph Data Summary (Sheehan et. al. 2015)

	Acoustic		Radial			Vertical			Transverse			VS	
Seismograph	dB	Hz	mm/s	in/s	Hz	mm/s	in/s	Hz	mm/s	in/s		mm/s	in/s
A1a	124	6.3	24	0.93	6.3	8	0.33	34	9	0.37	7.2	24	0.93
A2a	124	6.3	27	1.06	3.5	7	0.29	7.1	11	0.43	6.3	27	1.06
B1a	125	6.2	21	0.82	6.4	9	0.34	25.6	10	0.39	6.8	21	0.83
B1d	125	6.3	19	0.76	6.4	8	0.33	10.4	10	0.40	6.8	21	0.82
B1e	126	6.2	20	0.78	6.4	10	0.41	25.6	12	0.48	6.6	21	0.84
C1a	124	NA	21	0.81	9.3	9	0.37	26.3	10	0.40	6.7	21	0.82
C2a	122	NA	20	0.80	3.6	8	0.31	27.8	9	0.37	6.5	20	0.80
D1a	124	7.0	24	0.95	6.0	8	0.33	11	9	0.37	6.0	24	0.96
E1a	123	6.4	20	0.79	8.9	8	0.33	26.9	10	0.40	6.6	21	0.82
Median	124.0		20.57	0.81		8.38	0.33		10.03	0.40		21.08	0.83
Max Deviation from Median	2		6.35	0.25		2.03	0.08		2.03	0.08		5.84	0.23
% Deviation	NA		30.9%	30.9%		24.2%	24.2%		20.3%	20.3%		27.7%	27.7%

The percentage of deviation from the median recorded for the max deviation in peak particle velocity ranged from 20.3% to 30.9%. Of the 138 PPVs recorded during the six field tests 50 or 36% fell outside the expected ±5% of median values. Of the 46 maximum PPV's recorded during the six tests, 18, or 39% fell outside the expected range.

This study reinforced the need for more comparative studies using vibration monitoring equipment in the industry. It also reinforced the need to practice good field installation to minimize variability in data.

Ultimately, it can be concluded that a need for more standardized data processing and equipment is needed to perform blast vibration research where these variabilities in data can have catastrophic effects on a research project.

CHAPTER 3. VIBRATION MONITORING SYSTEM

This chapter will outline the sensor system developed for the ground vibrations project. The system contains three main components: the accelerometer, micro-controller, and microprocessor. The developed system was created to effectively and accurately gather ground vibrations data from surface mine blast events. A sensor was produced to be economically feasible in large scale blast vibration research projects requiring many monitoring locations. Along with the system electronics, the optimized settings and specifications are discussed.

3.1 Accelerometer

During the project several sensors were tested for vibration analysis feasibility. The sensor chosen to fit the specific ground vibration needs best was the ICM-20948 developed by InvenSense. The ICM-20948 is the world's lowest power 9-axis motion tracking device. The sensor is equipped with a 3-axis gyroscope, a 3-axis accelerometer, 3-axis compass, and a Digital Motion Processor. ICM-20948 supports an auxiliary I^2C interface to external sensors, programmable digital filters, and an embedded temperature sensor. Communication ports include I^2C and high-speed SPI. The main component of interest for the project is the 3-axis accelerometer with a programmable force-sensing resistor (FSR) of ±2g, ±4g, ±8g, and ±16g. The sensor operating circuit produced from InvenSense and the accelerometer component specification can be seen in Figure 3.1 and Figure 3.2.

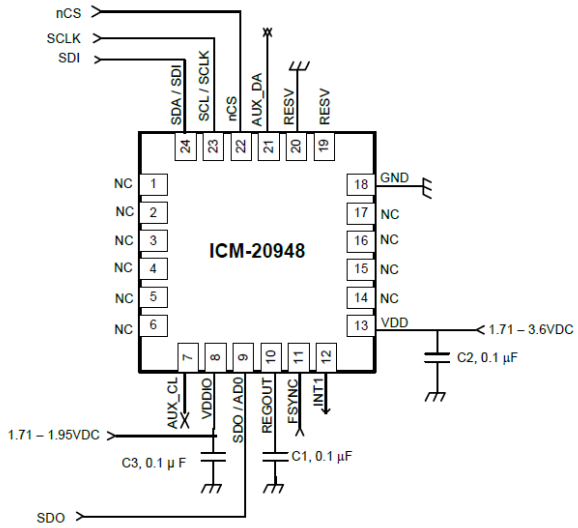

Figure 3.1: ICM-20948 Typical Operating Circuit

PARAMETER	CONDITIONS	MIN	TYP	MAX	UNITS	NOTES
ACCELEROMETER SENSITIVITY						
Full-Scale Range	ACCEL_FS=0		±2		*G*	1
	ACCEL_FS=1		±4		*G*	1
	ACCEL_FS=2		±8		*G*	1
	ACCEL_FS=3		±16		*G*	1
ADC Word Length	Output in two's complement format		16		Bits	1
Sensitivity Scale Factor	ACCEL_FS=0		16,384		LSB/*g*	1
	ACCEL_FS=1		8,192		LSB/*g*	1
	ACCEL_FS=2		4,096		LSB/*g*	1
	ACCEL_FS=3		2,048		LSB/*g*	1
Initial Tolerance	Component-level		±0.5		%	2
Sensitivity Change vs. Temperature	-40°C to +85°C ACCEL_FS=0		±0.026		%/ºC	2
Nonlinearity	Best Fit Straight Line		±0.5		%	2, 3
Cross-Axis Sensitivity			±2		%	2, 3
ZERO-G OUTPUT						
Initial Tolerance	Component-level, all axes		±25		mg	2
Initial Tolerance	Board-level, all axes		±50		mg	2
Zero-G Level Change vs. Temperature	0°C to +85°C		±0.80		mg/°C	2
ACCELEROMETER NOISE PERFORMANCE						
Noise Spectral Density	Based on Noise Bandwidth = 10 Hz		230		µg/VHz	2
LOW PASS FILTER RESPONSE	Programmable Range	5.7		246	Hz	1, 3
ACCELEROMETER STARTUP TIME	From Sleep mode		20		ms	2, 3
	From Cold Start, 1 ms V_{DD} ramp		30		ms	2, 3
OUTPUT DATA RATE	Low-Power Mode	0.27		562.5	Hz	1
	Low-Noise Mode ACCEL_FCHOICE=1; ACCEL_DLPFCFG=x	4.5		1.125k	Hz	
	Low-Noise Mode ACCEL_FCHOICE=0; ACCEL_DLPFCFG=x			4.5k	Hz	

Figure 3.2: Accelerometer Specifications

The typical blast vibration ranges are below ±2g so the ACCEL_FS=0 setting was used to obtain the largest sensitivity scale factor of 16,384 LSB/g seen in the specifications shown in Table 3.1. As discussed in the introduction chapter, the industry-standard used for the seismograph sampling rate is 1024. For comparison purposes, the sampling rate for the

sensor was 1024 or higher. To obtain higher sampling rates sent to the micro-processor a SPI connection was used for signal transfer.

To connect the accelerometer to the microcontroller a breakout board was required. The chosen breakout board was manufactured by SparkFun and is pictured in Figure 3.3. Figure 3.3 also shows the breakout pins for SPI configuration.

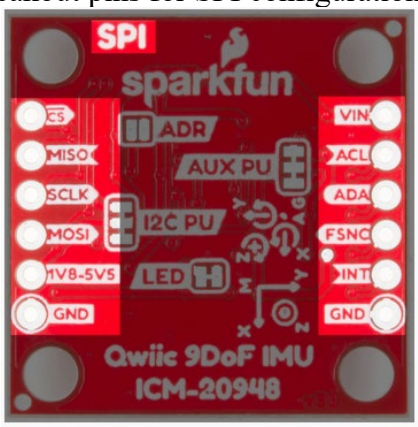

Figure 3.3: SPI-SparkFun Pin Configuration

For the SPI Connection outlined the pin layout to connect to the breakout board to the micro-controller is listed in Figure 3.4.

Breakout Board Pin Functions (SPI)			
Breakout Pin	**Arduino Uno**	**Esp32 Thing Plus**	**Microcontroller Pin Requirements**
MOSI	11	18	Data output of chosen SPI port
SCLK	13	5	Clock output of chosen SPI port
MISO	12	19	Data input of chosen SPI port
CS	2	2	An output pin to select the ICM for SPI

Figure 3.4: Breakout Board Pin Configuration

The breakout board for the accelerometer sensor was connected to a microcontroller to control the sensor programming.

3.2 Arduino

A microcontroller is a computer containing a central processing unit (CPU) that executes programs. The CPU loads the program to be used to control the sensor, stored in the read-only memory (ROM), and has random-access memory (RAM) to store variables. Microcontrollers are low-powered devices used for one task and run one specific program. In the case of the assembled system the microcontroller used was the Arduino Uno and is used to store and run the specific accelerometer sensor programming. The advantage of this system for the application is a small size and the low-cost nature of the Arduino Uno.

The Arduino Uno Pinout Diagram can be referenced in Figure 3.5 for connection and operation.

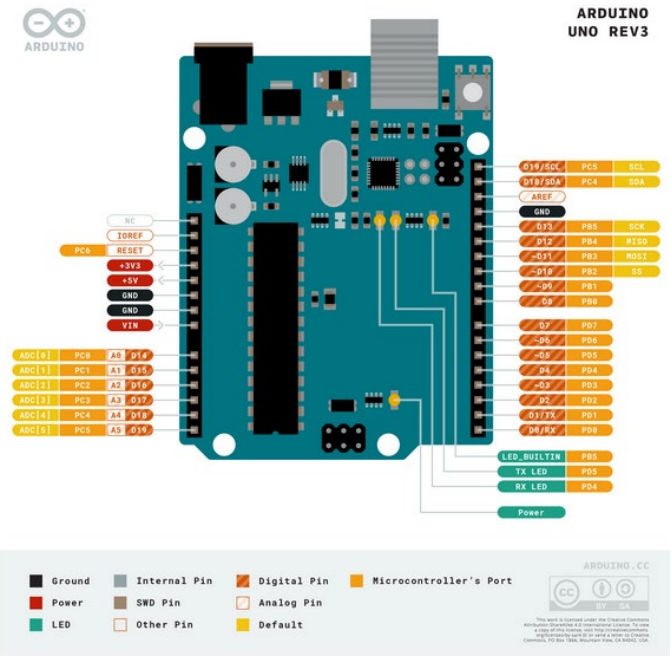

Figure 3.5: Arduino Uno Rev3 Pinout Diagram

The ICM-20948 breakout board was connected to the Arduino Uno using pin cables and a breadboard. The actual system configuration can be seen in Figure 3.6. The system is 69 mm by 54 mm and weighs 25g, which allows it to be housed in a small casing and buried for ideal vibration monitoring installation outlined by ISEE. The operating voltage is 5V and can be easily integrated into a common power supply system used for remote data collection.

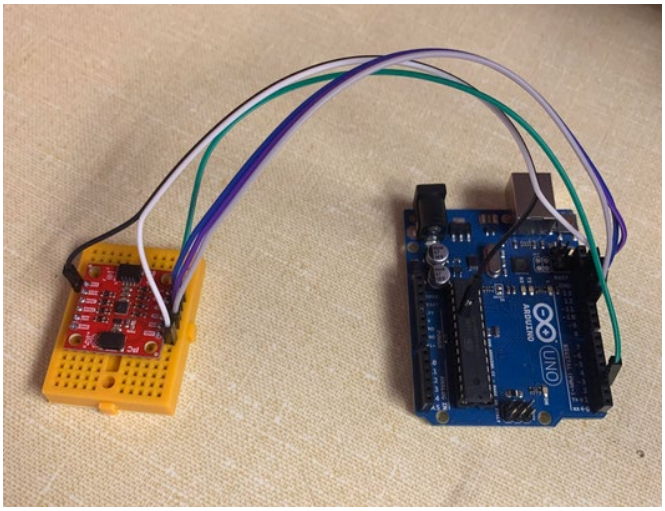

Figure 3.6: Breakout to Microcontroller Wiring

The Arduino Uno was used to run the sensor program for data collection but because of the limitations of the microcontroller, a data logging micro-computer was used for logging and storing data during vibration collection periods. Standard serial communication was utilized between the Arduino and the chosen micro-computer, the Raspberry Pi 4. The Raspberry Pi 4 and its specification will be outlined in the following section.

3.3 Raspberry Pi

The data logging entity used for the storage and control of the data stream for this project was the Raspberry Pi 4. The Raspberry Pi is a single-board computer, as the entire computer is on one board and operates as a complete system. The product is shown in Figure 3.7.

Figure 3.7: Raspberry Pi 4

The key features include a 64-bit quad-core processor, dual-display output via two micro HDMI ports, and 4GB of RAM. For the project the Raspberry Pi was used for logging the continuous data stream collected by the Arduino Uno. The analysis of the continuous data stream was used to determine and save each vibration event recorded by the accelerometer. The trigger, sample size of events saved, and event storage are all performed from the Raspberry Pi 4.

CHAPTER 4. EXPERIMENTAL SETUP

The ground vibration information was collected in a surface coal mine operation and is part of ongoing research regarding the structural response of farm buildings subjected to ground vibrations from blasting. The description of the structural response project, the mining operation, the monitoring locations, the different sensor types used for comparison, and the specifics of the events recorded and analyzed are discussed in the following sections.

4.1 Structural Response of Farm Buildings Project

The sensor system being developed is part of an ongoing research project conducted by the University of Kentucky Explosives Research Team (UKERT). The objectives of the research project are included in this subsection of the experimental chapter of this report.

4.1.1 *Statement of Work*

The last intensive and detailed study to analyze the effects of vibrations in structures, RI 8507 "Structure Response and Damage Produced by Ground Vibration from Surface Mine Blasting", was published in 1989, almost 30 years ago. New technologies and methodologies to collect and analyze data have been developed since the publication of this report. Peabody's Bear Run Mine has three structures that will be demolished in the next two years in accordance with the mine development. The structures are typical farm structures and include a brick house, a garage, and two silos, Figure 4.1 shows the structures.

Figure 4.1: Structures being studied by UKERT

UKERT is interested in collecting vibration data generated by the surface mine operation in those structures as well as the surrounding ground. The data will be used to produce papers and reports relating to the parameters of the blast to its effects observed in the structures.

4.1.2 *Objective of the Structural Response Project*

Study the structure response produced by ground vibrations from surface mine blasting using modern tools. A primary goal of this project is to be completely non- disruptive to normal mine operations, with zero personnel or equipment requirements from Bear Run Mine.

4.1.3 *Data Collection*

UKERT will install a network of regular seismographs used to record ground vibrations generated from blast events. Also, instrumentation for the structures will be installed. The systems utilized at the buildings will be accelerometers, crack displacement detectors, and similar devices. All the instrumentation will be provided by UKERT.

4.1.4 *Tasks of the Project*

Task 1- Installation of the devices. This task is expected to have a duration of one week. Task 2- Collection of data. UKERT is developing a ground vibration recording system. However, periodic visits to the mine are expected at the beginning of the project. Task 3- Analysis of data. The collected data will be processed and analyzed according to the most recent methodologies. Task 4- Reports and papers. The findings will be published in reports and peer-review publications. Also, technical information will be presented at various conferences.

4.1.5 *Required Collaboration*

Communication with site personnel to schedule any necessary pre -study site visits for training and identification of necessary procedures, – Access to the structure sites, – Mapping (topographic information) of the blasting site and the area of the structures, – Blast logs of the shots relevant to the data collected.

The developed sensor will be applicable to several tasks outlined by the research project and has, therefore, been developed to fit the needs of the project. Several specifications of the sensor have been set to match these individual requirements. As seen in the data collection and tasks section of the structural response project, several accelerometers are needed for data collection. It was decided that the best way to obtain raw data for the project was the development of the sensor system, which is the focus of this research project.

The specific testing and comparison experimental set up will be outlined in the remaining sections of this chapter.

4.2 Location of the Structural Response Project and Blasting Parameters

The structures outlined in the project parameters are located at Bear Run Coal Co LLC in Southern IN. Bear Run Mine is a subsidiary of Peabody Energy. The mine operates in the Illinois coal basin and is a surface coal mining operation. The location of the mine can be seen in Figure 4.2

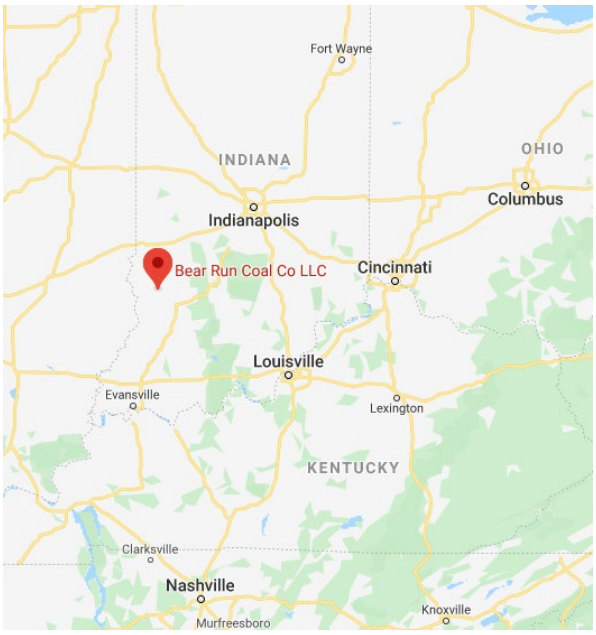

Figure 4.2: Testing Mine Location

In Figure 4.3, part of the active working bench is shown in red for reference, and the locations of the structures are shown in blue with a star indicating the locations of the sensors. The sensors were oriented toward the closest point to the working face. The perpendicular line of the mining working face direct or y-axis is denoted as the radial waveform in the data. The parallel direction of the working face or x-axis is denoted as the transverse waveform in the data. The vertical direction of the working face or z-axis is denoted as the vertical waveform in the data.

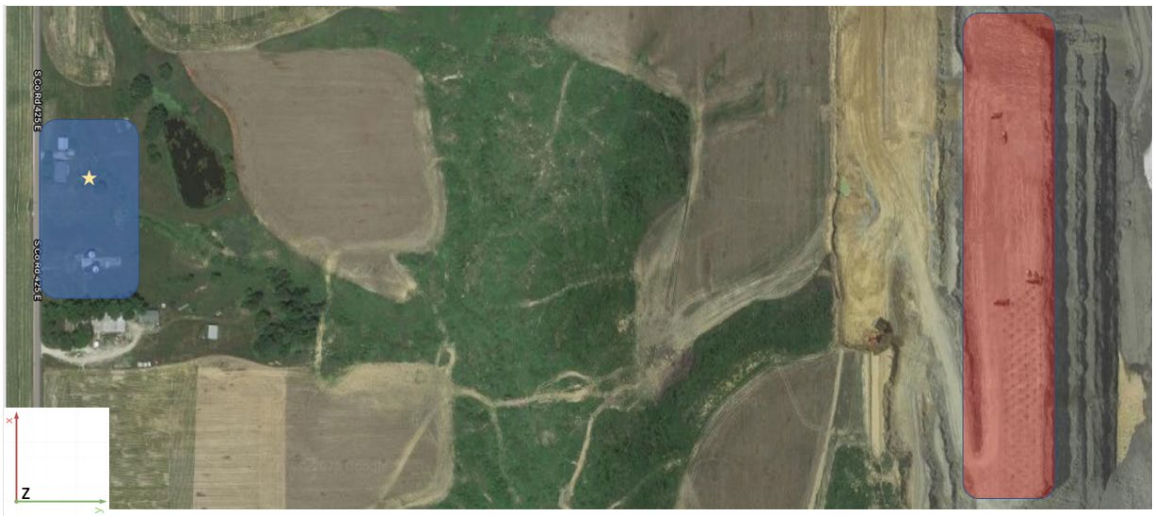

Figure 4.3: Sensor Location Oriented to the Working Face

Three blast events were studied for data comparison between devices. One event each day from the dates 01/20/2020, 01/21/2020, and 01/22/2020. The shot numbers designated by the mine for the events studied were #12278, #12284, and #12287, respectively. The blasting reports for the three events are included in Appendix A. The map in Figure 4.4 can

be used to reference the specific locations of each of the blast events compared to the location of the house.

Shot #12278 (event 1):

The shot type for this event was a corner blast consisting of 78 holes with an average depth of 44 ft. The burden was 24 ft. and the spacing was 25 ft. The explosives used were 72,352 lbs. of bulk ANFO and 31,008 lbs. of Bulk Emulsions.

Shot #12284 (event 2):

The shot type for this event was a cast blast consisting of 60 holes with an average depth of 93 ft. The burden was 23 ft. and the spacing was 32 ft. The explosives used were 146,016 lbs. of Bulk ANFO and 26,504 lbs. of Bulk Emulsion.

Shot # 12287 (event 3):

The shot type for this event was a corner blast consisting of 88 holes with an average depth of 64 ft. The burden was 24 ft. and the spacing was 26 ft. The explosives used were 101,486 lbs. of bulk ANFO and 43,494 lbs. of Bulk Emulsion.

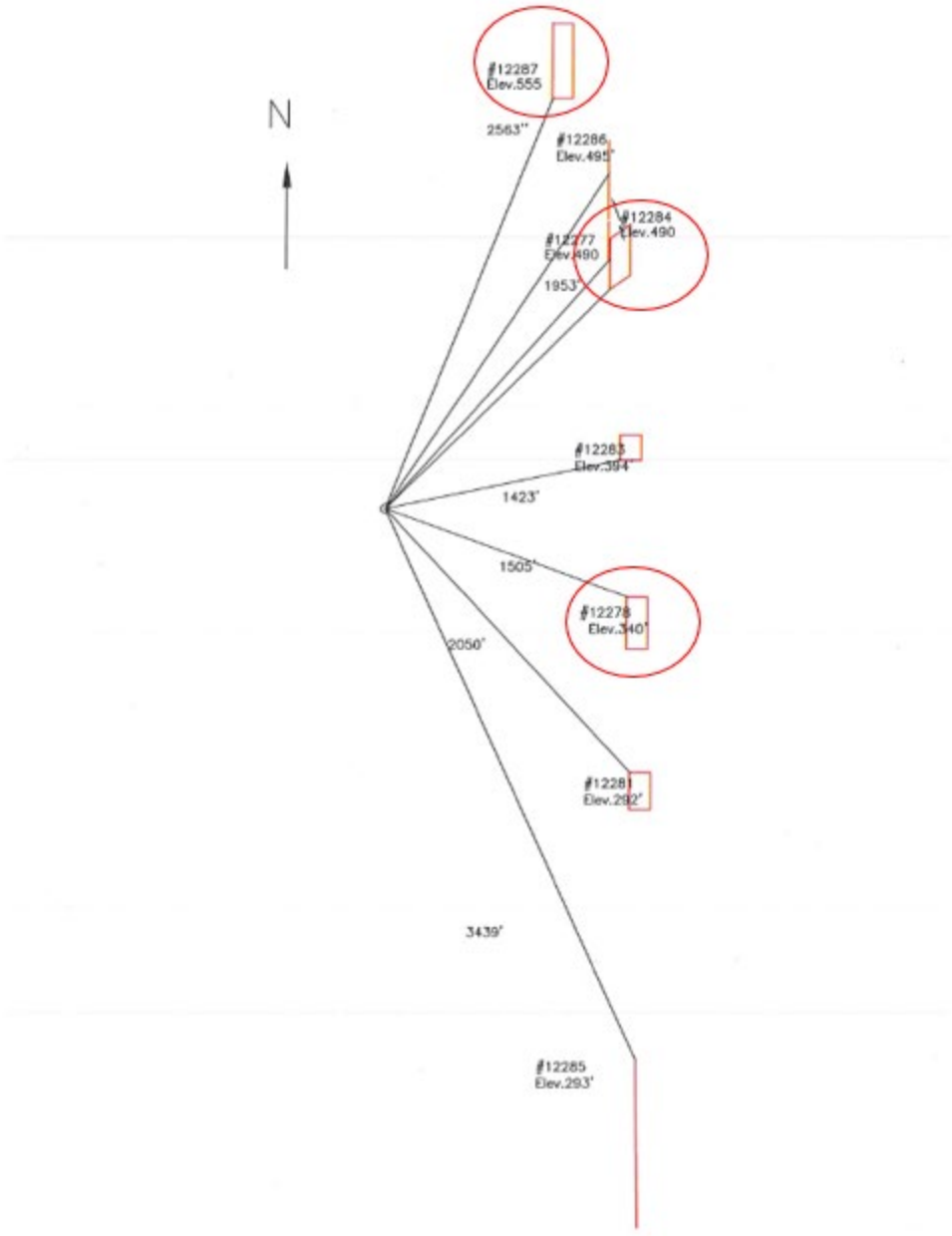

Figure 4.4: Blast Event Locations (provided by Andrew Alano with Peabody Energy)

Both the distance from the shot and the elevation changes are shown in Figure 4.4. In order to study the blast events and validate the data recorded with the system under development, two additional systems were used. The two additional systems considered were a typical commercial seismograph used in the mining industry, and an accelerometer used for measuring seismic activity (Geophysics studies) and borrowed from the United States Kentucky Geological Survey (USKGS). The specific sensor types, installation specifics, and specifications of the three sensors are outlined in the following sections of this chapter.

4.3 System Under Development

The developed prototype sensor electronics were explained in chapter three. For installing the developed system device below the ground to record the blast vibration waveforms, a PVC pipe housing was created. This prototype housing was assembled to orient the sensor and protect it from environmental damage. The PVC housing can be seen in

Figure 4.5 and Figure 4.6.

Figure 4.5: Electronic Positioning within the PVC Housing

Figure 4.6: PVC Sensor Housing

Both the sensor and the microcontroller were housed within the component underground, while the Raspberry Pi being used for data logging remained above ground in a weatherproof casing. A schematic of the housing with sensor and Arduino installed can be seen in Figure 4.7.

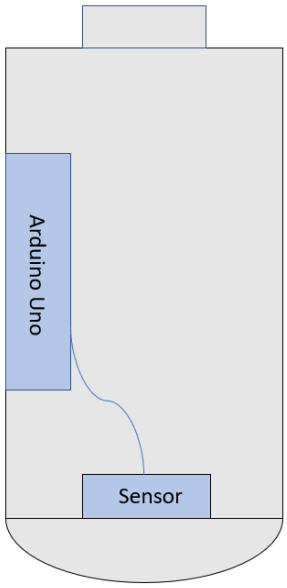

Figure 4.7: PVC Housing Unit

The Arduino was screwed to the side of the housing unit to not interfere with the sensor element. The sensor was mounted to the bottom of the housing unit using a strong adhesive. The two components were connected by a rubber encased serial cable. The PVC housing was installed in a post hole with a diameter of 6 inches at the bottom of a 2x2x1 foot opening in the ground. The device was firmly compacted with dirt in the 6-inch circular hole and then covered with sand in the remainder of the square opening. The installation area and the installed device are pictured in Figure 4.8 and Figure 4.9, respectively.

Figure 4.8: Ground Prepped for Sensor Installation

Figure 4.9: Installed Sensor Before Full Burial

Before being buried completely, the sensor was connected, and the instantaneous G's readout was monitored to level the device. Before the device was armed, an average running trigger was set to monitor for a 2% rise or fall in average data readings in order to capture the events. The sampling rate was set to 1024 samples (variation was seen in the sampling rate and will be discussed further in the data collection chapter). When triggered, the device was set to read 10,000 samples or roughly ten seconds of data. After the specifications were programmed into the device, it was armed, and the Raspberry Pi was installed inside the weatherproof container powered by a 12v battery with a power converter to monitor the output.

4.4 Commercial Seismograph

The commercial seismograph used in the experiment was a Mini-seis digital seismograph produced by White Industrial Seismology, Inc. The sensor, in the form of a geophone, was

installed similarly to the developed system. The device was installed at the bottom of a 2x2x2 hole and compacted back with the original dirt. The seismograph data logging computer was installed on the surface in a White Industrial Seismograph box equipped with a 12v battery for power and a solar panel for extended use. The prepped hole and the installation box for the commercial seismograph are shown in Figure 4.10.

Figure 4.10: Seismograph Installation

The seismograph was set with a 0.1 in/sec trigger to capture the events. When triggered 0.5 seconds prior to the event and 10 seconds following the event are recorded at a sampling rate of 1024 samples/sec. The seismograph utilized a mass and spring geophone, so the sampling units are in/sec. A level was used to prep the ground to ensure that the device was level and the recording was accurate.

4.5 Accelerometer Used for Geophysics Applications

The final device used to measure the ground vibrations from the three events was a geology industry accelerometer used for geophysics studies. The device was a Nanometrics Titan 4g accelerometer utilizing a Nanometrics Centaur 2 data logger. The device was installed similarly to the developed prototype sensor. A 6inch diameter hole was dug at the bottom

of a 2x2x1 foot hole, and the device was seated firmly to the bottom, as shown in Figure 4.11.

Figure 4.11: Nanometrics Titan

The device was packed firmly with sand per the manufacturer's instruction and was connected to the data logger being powered by a 12v battery inside the provided weatherproof encloser. The final setup can be viewed in Figure 4.12.

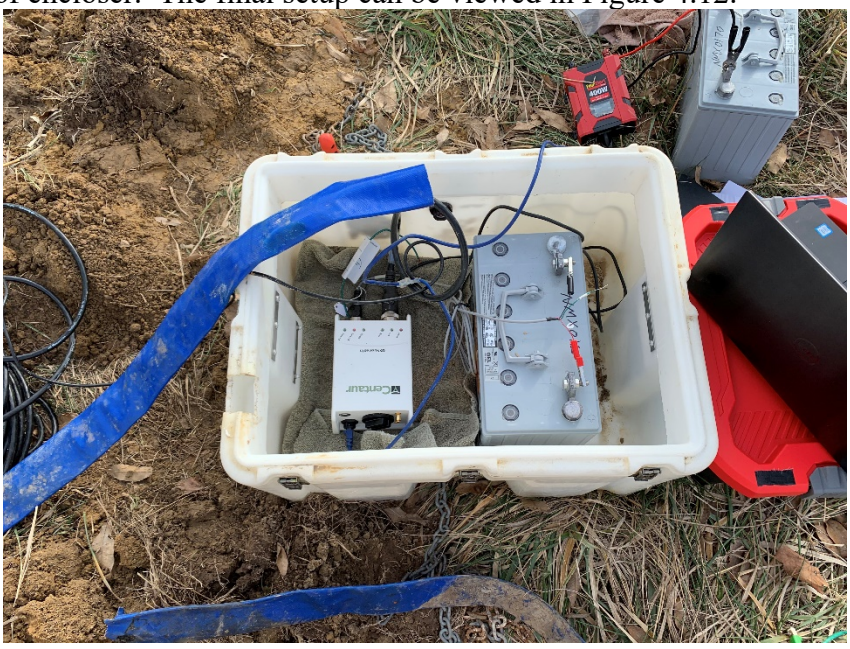

Figure 4.12: Data Logger Connection to Titan Accelerometer

The accelerometer was configured to trigger at a 10% change in continuous data. When the device was trigger 1 second prior to the trigger and 10 seconds after the trigger was recorded. All three devices listed above were oriented with the radial component, or y-

axis depending on the system's utilized coordinate system, facing the closest point to the working face to ensure uniformity in each components data.

4.6 System Installation Map

Two different system installation setups were used during data collection for the three systems. Event 1 and Event 3 used the same system configuration and the positioning of the systems are shown in Figure 4.13

Figure 4.13: Event 1 and Event 3 Map of Installed Monitoring Systems

Event 2 used a similar setup, but the assembled system was installed in the back row closer to the seismograph as seen in Figure 4.14.

Figure 4.14: Event 2 Map of Installed Monitoring Systems

As seen in Figure 4.13, the assembled system and the Titan Accelerometer were installed together at 3 feet for Event 1 and Event 3. The seismograph was installed behind the other two devices at 20 feet for Event 1 and Event 3. When the systems were installed, it was considered that the distance between the seismograph (A) and the other two systems (B and C) would not impact the collected data. However, this setup caused some discrepancies between the two systems (B and C), and the seismograph (A) for Event 1 and Event 3. Such discrepancies are discussed in detail following the data comparison section of this document.

Likewise, for Event 2 seen in Figure 4.14, the assembled system and seismograph were installed together at 3 feet, while the Titan Accelerometer was installed in front of the two systems at a distance of 20 feet. In the results chapter of this report, the discrepancies in data caused by the differing distances is discussed and outlined.

CHAPTER 5. DATA COLLECTED

As mentioned in the previous chapter, in order to compare the performance of the assembled system, two additional ground vibrations recording systems were used. The data collected corresponds with three blast events in a surface coal mine operation. In this chapter, the details of the raw data and its post-processing procedure is included. Due to clarity in the document, the details are included for one of the events. The results and details of the other two events are included in the following chapters and the appendices. The event selected for presentation in this chapter is the event number two or event #12284 on 01/21/2020 This event was selected because of a complete triggering of the assembled system. During the other two events the triggering specifications on the assembled system did not save the 1 second of data prior to the triggering. Around 5% of the initial waveform was lost during event 1 and event 2. In order to directly compare the waveforms, it was required to use several data processing techniques. The main aim of the pre-processing data was to be able to normalize the data sampling rates and time shift the signals for analysis. The focus of the chapter will be the processing of the assembled system. However, the raw seismograph and Titan Accelerometer data will be shown in its original form in this chapter.

5.1 Assembled System Data

The raw output of the assembled system was measured using Least Significant Bit units (LSB) and was the starting point for the data analysis. The three-axis accelerometer is denoted by an x, y, and z coordinate system. The system was aligned so that the y-axis represents the radial, the x-axis represents the transverse, and the z-axis represents the vertical component of the measured vibration waveform. Figure 5.1shows the raw output data from the event for the three components downloaded directly from the data logging Raspberry Pi in its original form.

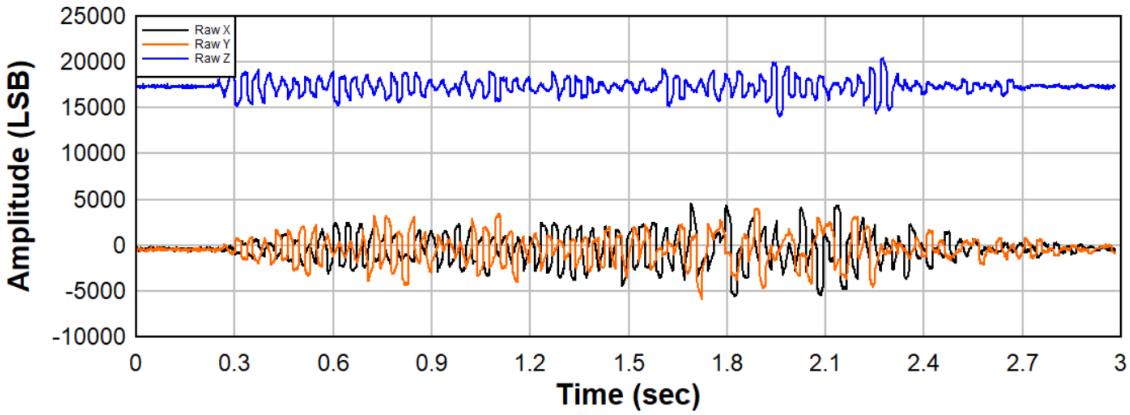

Figure 5.1: Raw LSB Data from Developed System

According to the specifications of the electronic components, the sensitivity of the assembled system is 16384 LSB/g. The sensitivity of the device was used to convert the raw data to Gals or g's. Once the three waveforms are in g units, a value of 1 g was

subtracted from the z component to account for the insitu gravitational force exerted on the sensor. After this operation, all the data is now using the same zero reference axis and only contains the output of the vibration waveform in units of g's, as seen in Figure 5.2

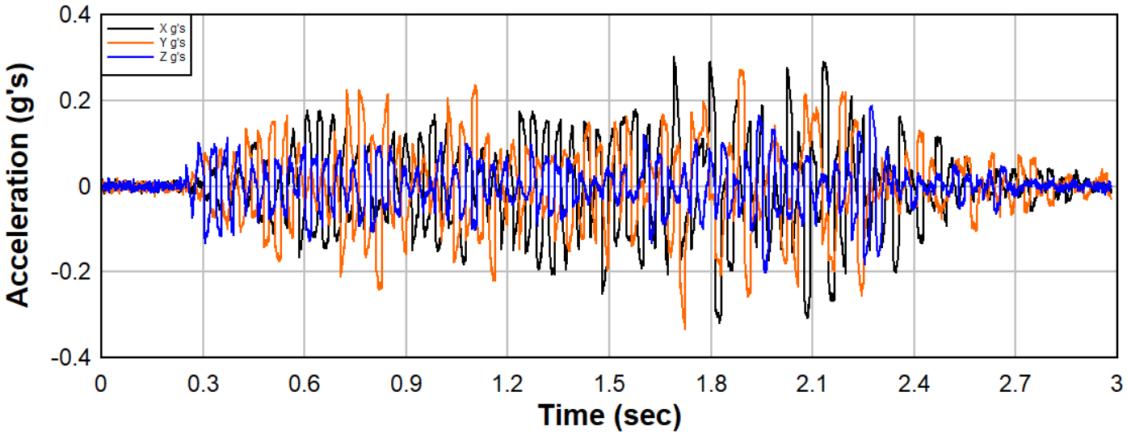

Figure 5.2: Raw Acceleration Waveform in g's from Assembled System

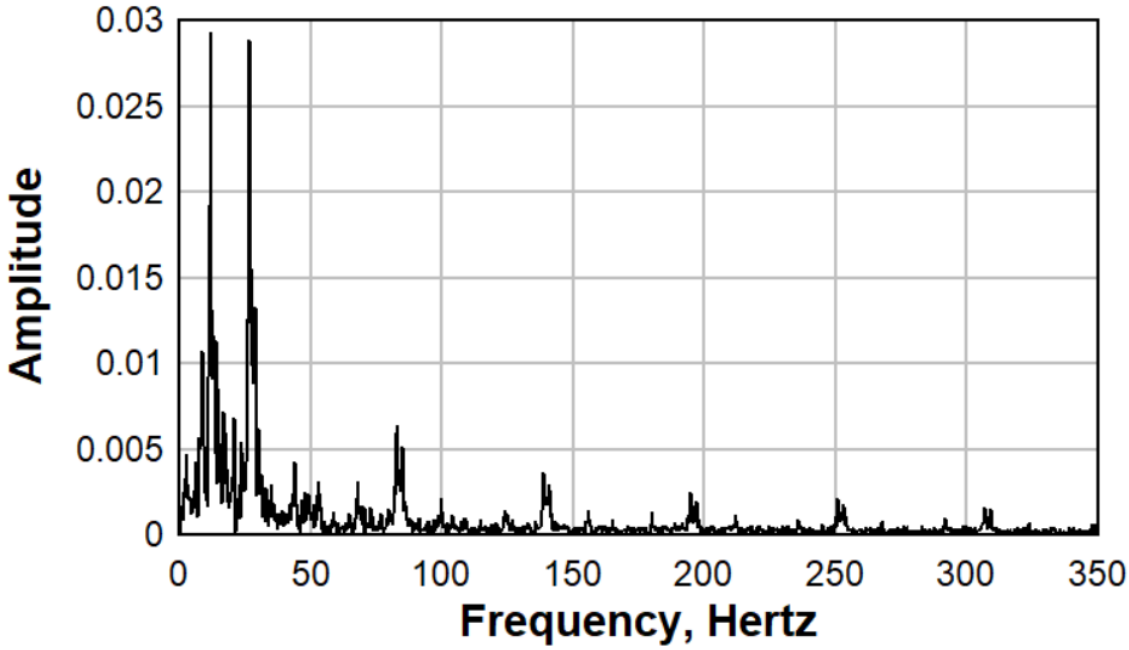

Figure 5.3: Frequency Content of Signal Experiencing Noise

As seen in Figure 5.3. The assembled system experienced a considerable amount of high-frequency information in the form of noise. In order to filter out this noise, a bandpass filter was utilized to obtain a "clean" vibration waveform. For each component of the vibration waveform, a bandpass filter was utilized. The bandpass filter cutoffs were determined using the three decibels rule (3dB) that uses Equations 1,2, and 3. Cutoff frequencies include a lower limit and an upper limit creating a range of frequency allowed to pass through the filter as illustrated by Figure 5.4.

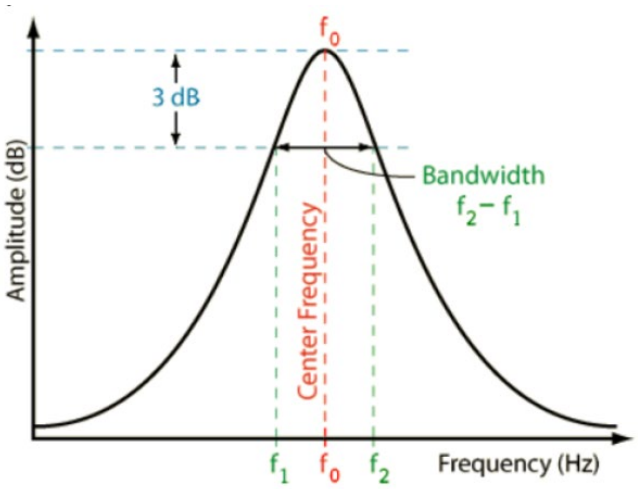

Figure 5.4: Bandpass Filter

The variables in Figure 5.4 are governed by the following equations.

$$Q = \frac{f_0}{f_2 - f_1} \quad [13]$$

Where Q is the signal quality factor, this quality factor measures the selectiveness of the bandpass filter. The lower the value of Q, the wider the bandwidth, and consequently, the higher the Q factor, the narrower and more selective the filter.

$$b_m = f_2 - f_1 = \frac{f_0}{Q} \quad [14]$$

Where b_m is the bandwidth

$$f_1 = f_0\left(\sqrt{1 + \frac{1}{4Q^2}} - \frac{1}{2Q^2}\right) \quad [15]$$

Where f_1 is the lower cutoff frequency and f_0 is the central frequency

$$f_2 = f_0\left(\sqrt{1 + \frac{1}{4Q^2}} + \frac{1}{2Q^2}\right) \quad [16]$$

Where f_2 is the upper cutoff frequency

In order to determine the upper and lower frequency cutoff using the process shown in Figure 5.4, a 3dB loss must be represented by a decay in the amplitude of the signal. Using Equation 7, the decay in amplitude can be calculated to represent such loss.

$$L = 20 * \log\left(\frac{amplitude\ after\ loss}{initial\ amplitude}\right) \quad [17]$$

In Equation 7, L is the loss in decibels, so a 3-decibel loss would correspond to a 30% loss in the signal amplitude. When applying these equations to the signals, it was found that the quality factor of the filter to be much to low and was filtering at too small an interval to pass the entire frequency content of the blast event. In order to correct the bandpass filter, the quality factor was lowered until the bandpass encompassed the typical range of frequency seen in similar surface coal mine blasts. A quality factor of 1.25 was determined and applied to the waveforms.

Once the cutoffs were determined following the previous procedure, the bandpass filter was applied to each waveform signal.

The bandpass filtered of the waveforms are shown in the table below.

Table 2: Bandpass Filters for Event 2

Waveform	Bandpass	Units
X Component	5.3-47.7	Hz
Y Component	1.8-16.2	Hz
Z Component	5.3-47.6	Hz

The resulting waveforms are shown in Figure 5.5

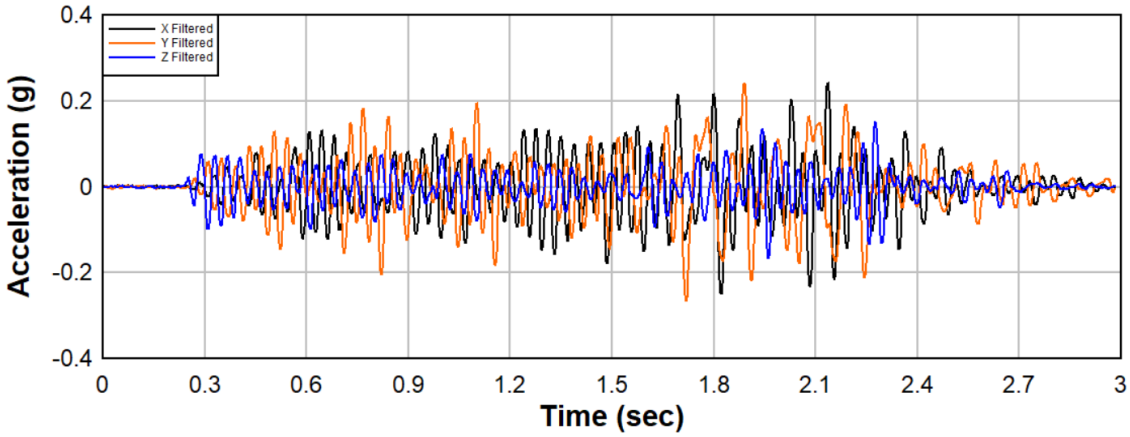

Figure 5.5: Filtered Acceleration Waveforms

In order to obtain the particle velocity waveform in (in/sec), which is the unit of measure used in the United States' vibration regulation, the acceleration in g's must be converted to (in/sec^2) using the conversion factor of 1g = 386.08 in/sec^2. The following figure shows the individual waveforms in acceleration. The acceleration graphs that follow are also shifted to orient the front of the vibration waveform arrival with time stamp zero.

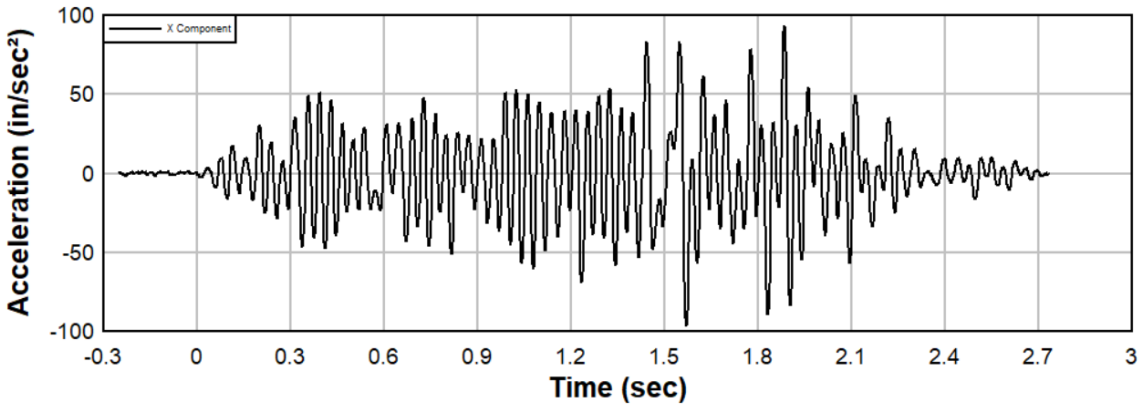

Figure 5.6: Transverse Component Acceleration

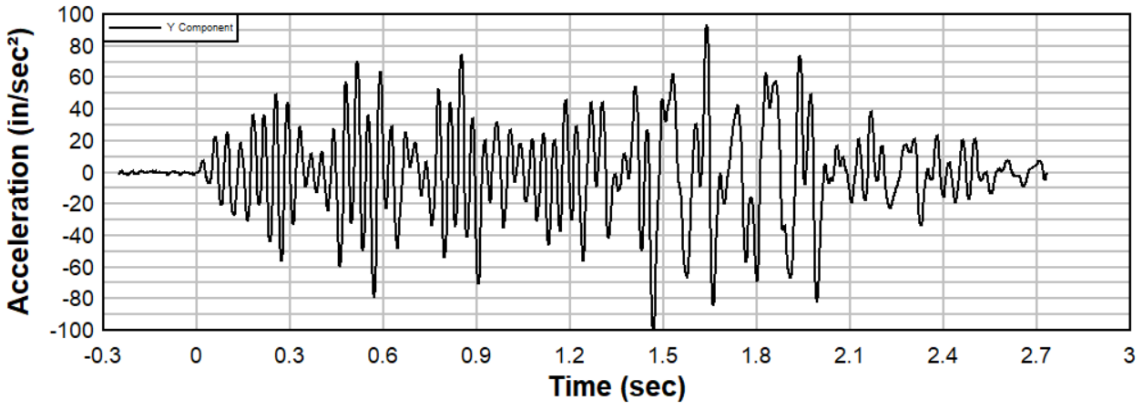

Figure 5.7: Radial Component Acceleration

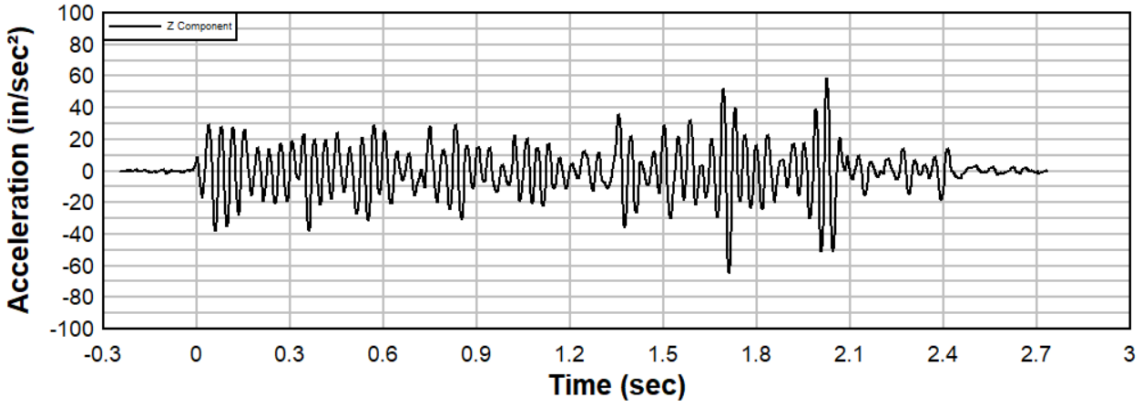

Figure 5.8: Vertical Component Acceleration

In order to integrate the acceleration waveforms to obtain the velocity curves needed for data comparison, the trapezoid rule was used. The trapezoid rule is a technique for approximating the definite integral as follows

$$\int_a^b f(x)dx \approx (b-a) * \left(\frac{f(a)+f(b)}{2}\right) \quad [18]$$

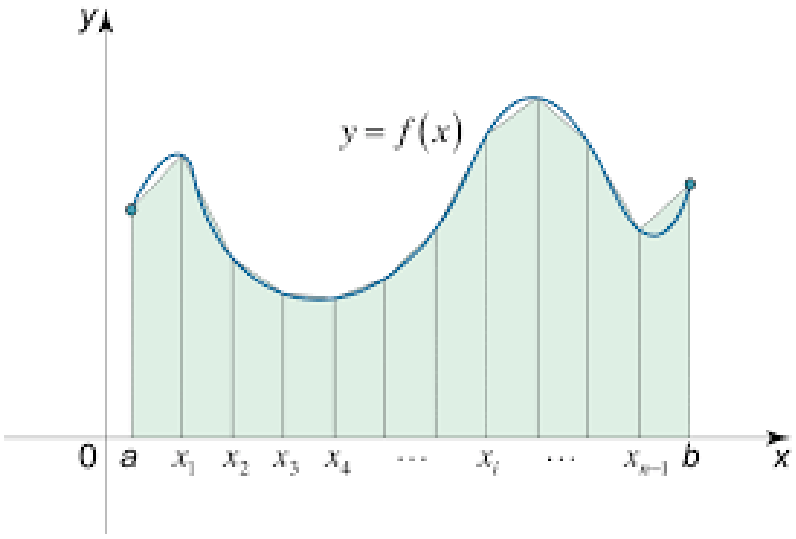

Figure 5.9: Trapezoidal Rule Representation

Thus, the rule works by approximating the region under the graph of function $f(x)$ as a trapezoid and calculating the area as indicated in Figure 5.9. Using this basic technique, the particle velocity curves for each component were determined and are included in Figure 5.10 to Figure 5.12.

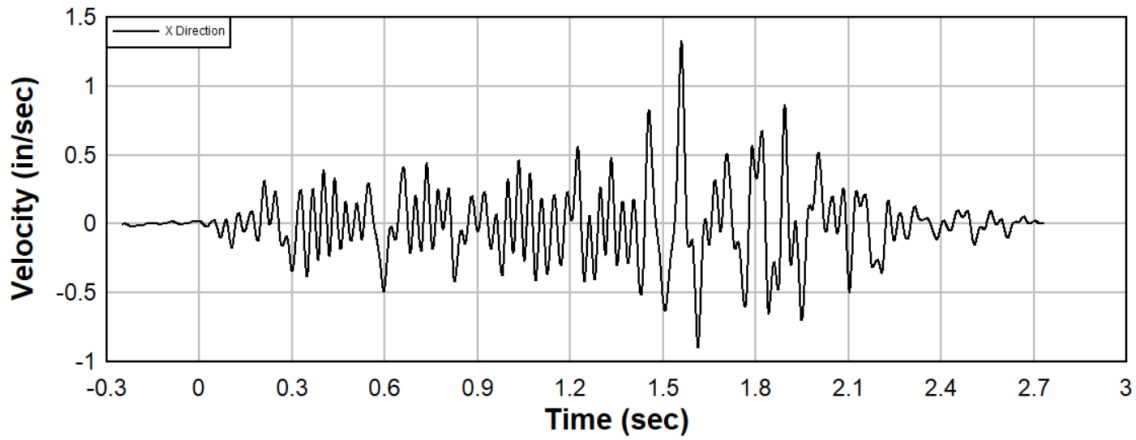

Figure 5.10: Transverse Component Velocity Waveform, Assembled Sensor

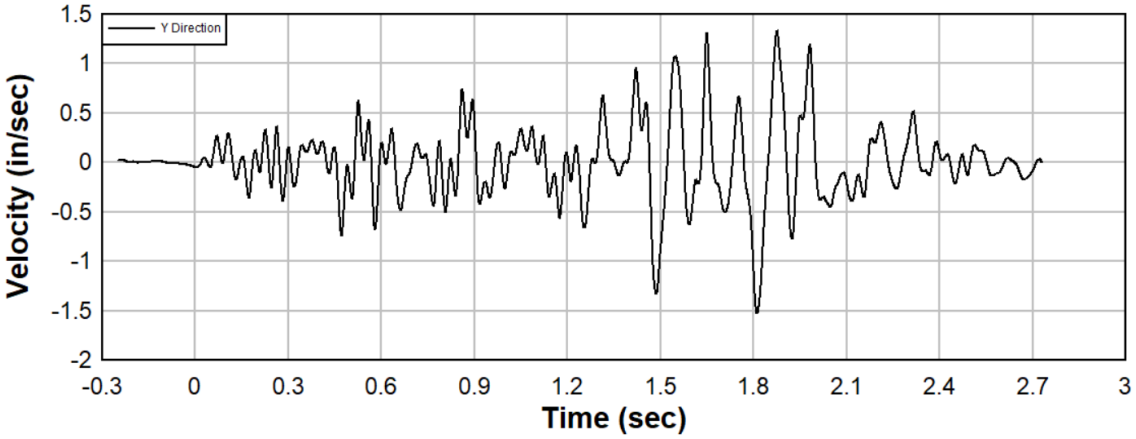

Figure 5.11: Radial Component Velocity Waveform, Assembled Sensor

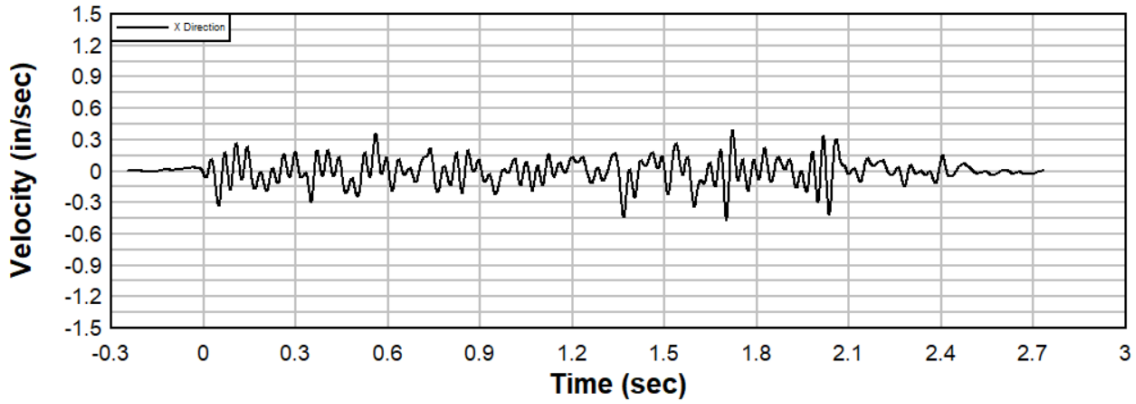

Figure 5.12: Vertical Component Velocity Waveform, Assembled Sensor

Lastly, the frequency content will be needed to analyze the similarity between waveforms in the following chapters. A Fast Fourier Transform was performed on the three velocity components in order to produce frequency content spectrums for the collected data in each direction. The following figure shows the frequency content of the individual components of the vibration waveform.

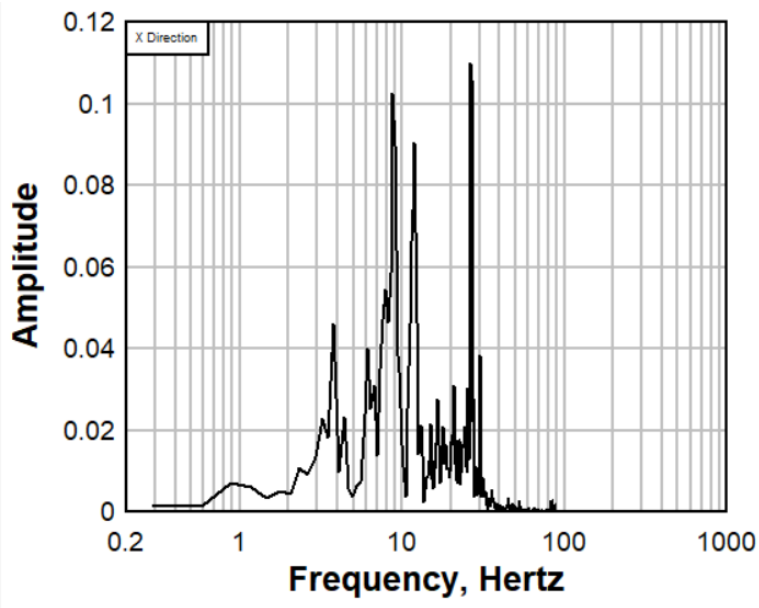

Figure 5.13: Frequency Content of Transverse Waveform, Assembled Sensor

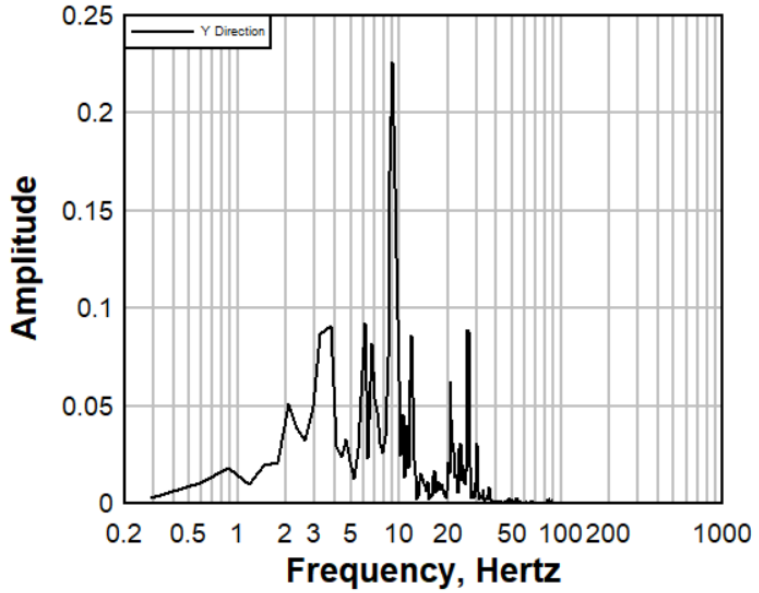

Figure 5.14: Frequency Content of Radial Waveform, Assembled Sensor

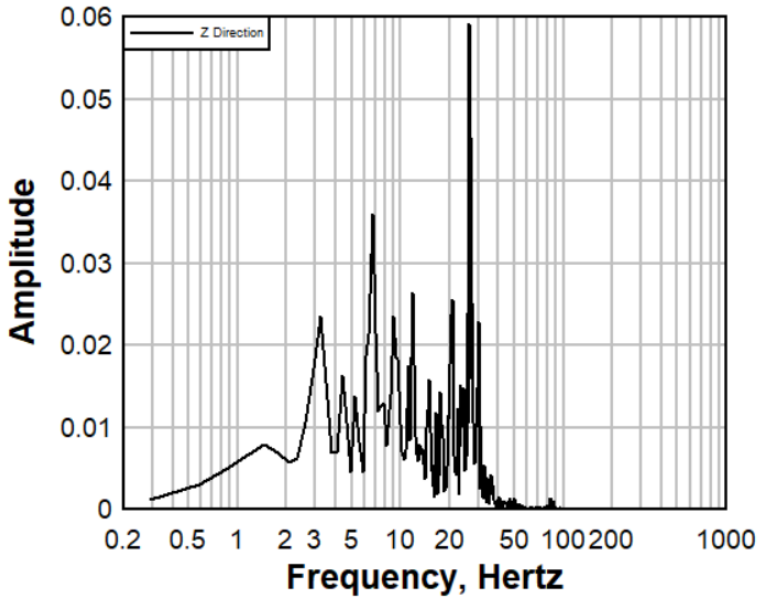

Figure 5.15: Frequency Content of Vertical Waveform, Assembled Sensor

5.2 Commercial Seismograph Data

The White Industrial Seismograph ® comes with a manufacturer's data processing tool for viewing and analyzing the data. The velocity waveforms and the frequency spectrums in the form of FFT's are displayed in the following figures. These images are straight from the manufacturer's software. The data was then exported to txt files for the comparison with the other sensor waveforms in the following chapters. Figure 5.16shows time in seconds on the x-axis and velocity in (in/sec) on the y-axis. As discussed previously in this chapter, the components of transverse, radial and vertical directions match the x, y, and z directions of the assembled prototype system, respectively.

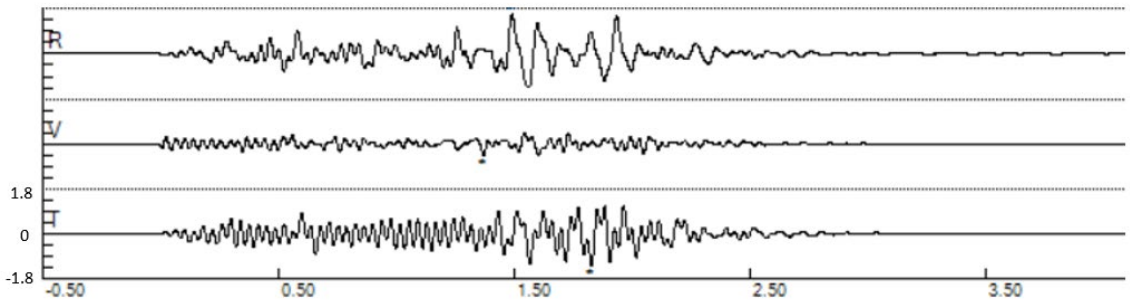

Figure 5.16: Waveform for Each Component Taken from Seismograph Software

Figure 5.17shows the FFT amplitude spectrums of the velocity curves.

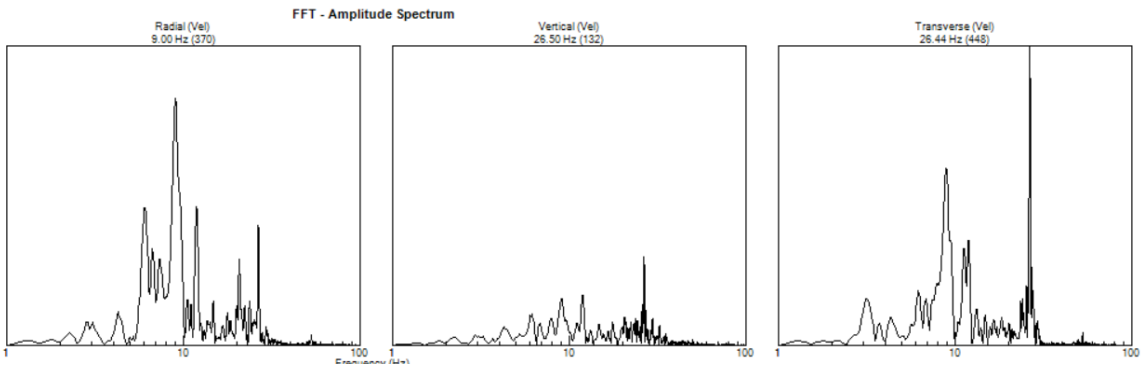

Figure 5.17: Frequency Content for Each Component Taken from Seismograph Software

5.3 Accelerometer for Geophysical Studies Data (Titan Accelerometer)

The raw accelerometer data was measured in counts and required the readings to be converted using the companies provided sensitivity and conversion rates to obtain the velocity curves in (in/sec). The following graphs provide a visual representation of the velocity data with their corresponding frequency contents. The recorded data contains one (1) second prior to the blast and 5 seconds following the trigger of the device.

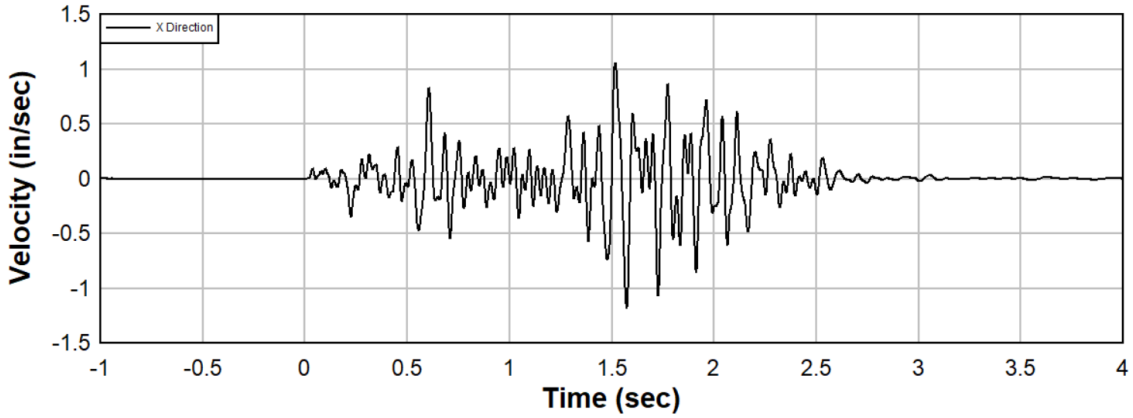

Figure 5.18: Transverse Component Velocity Waveform, Titan Accelerometer

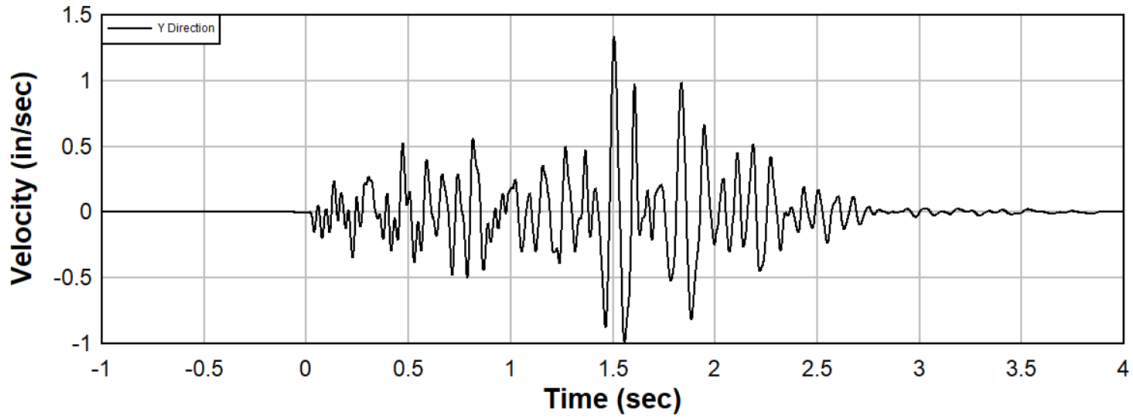

Figure 5.19: Radial Component Velocity Waveform, Titan Accelerometer

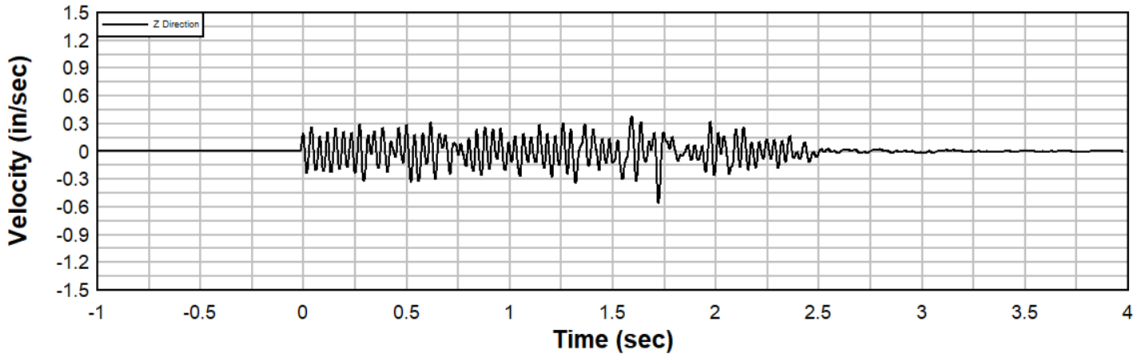

Figure 5.20: Vertical Component Velocity Waveform, Titan Accelerometer

Using the velocity curves, the frequency content (FFT) was calculated for each signal.

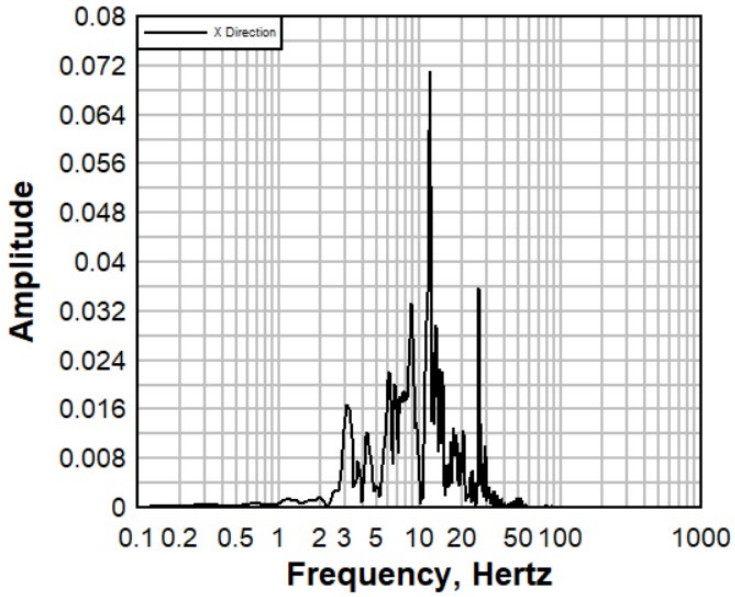

Figure 5.21: Frequency Content of Transverse Waveform, Titan Accelerometer

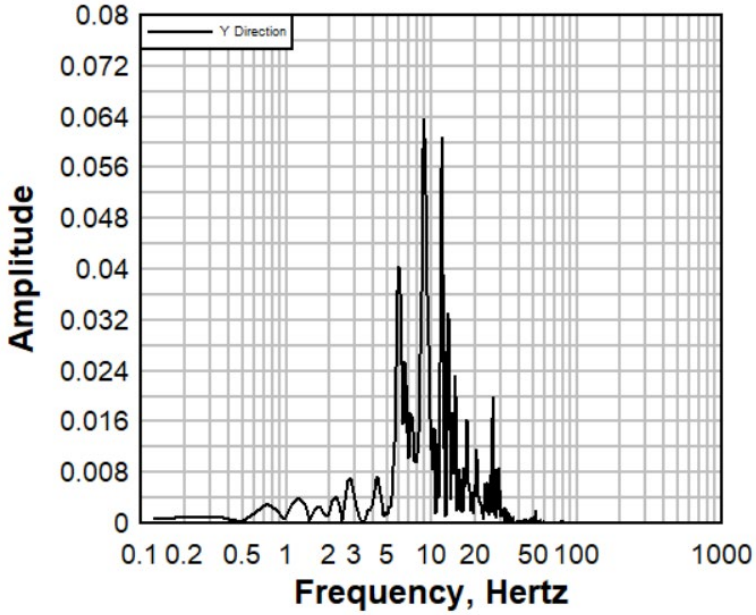

Figure 5.22: Frequency Content of Radial Waveform, Titan Accelerometer

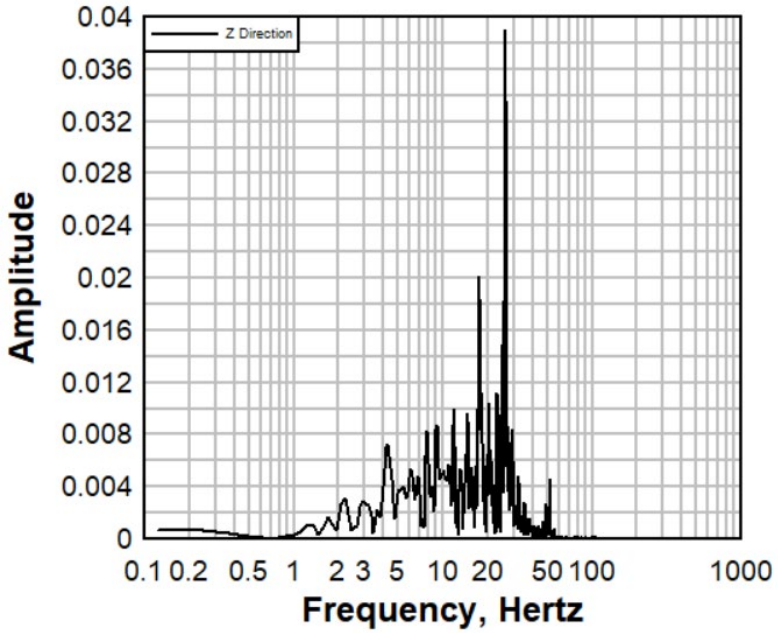

Figure 5.23: Frequency Content of Vertical Waveform, Titan Accelerometer

The processed data in velocity for the three devices will be used for comparison in the following chapter along with the frequency content of the vibration waveforms.

The waveforms from each device were compared both visually and by utilizing cross-correlation to compare waveform similarity. Frequency content is an important component to understand vibration events, therefor the frequency contents of the vibration's waveforms will be compared both visual and by conducting spectral coherence on the waveforms. The focus of this study is the feasibility of the developed monitoring system, so the developed system data will be compared directly with the seismograph waveforms in the first section of the chapter and then the comparison between the developed sensor and the seismology sensor will follow. Similar to chapter 5, the report event 2 will be outlined in detail in this chapter and the subsequent data from event 1 and event 2 will be included for reference in the appendices of the document.

6.1 Developed Sensor vs. Seismograph

In order to establish understanding of the waveforms being compared in the following sections a visual comparison of the waveforms is provided below. The transverse, radial, and vertical components are shown below from the developed sensor and the seismograph. In cases where sampling rates differed, a rational factor of the sampling rates was used to resample the data with the lower of the two sampling rates.

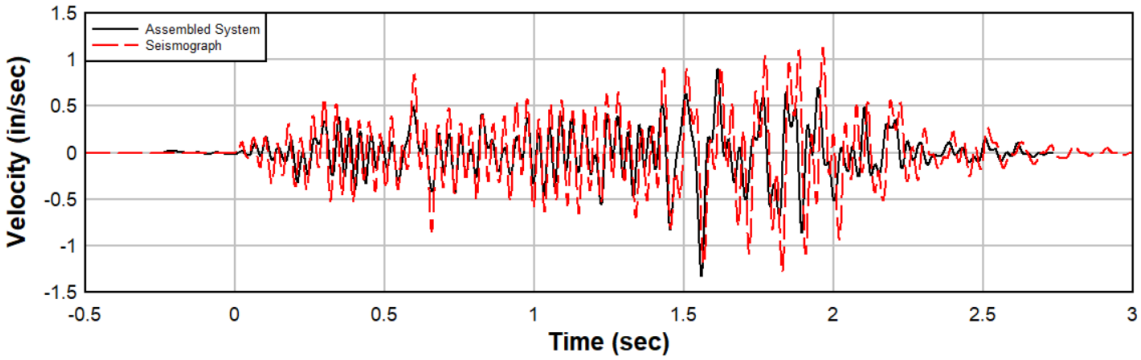

Figure 6.1: Transverse Velocity Assembled Sensor vs. Seismograph

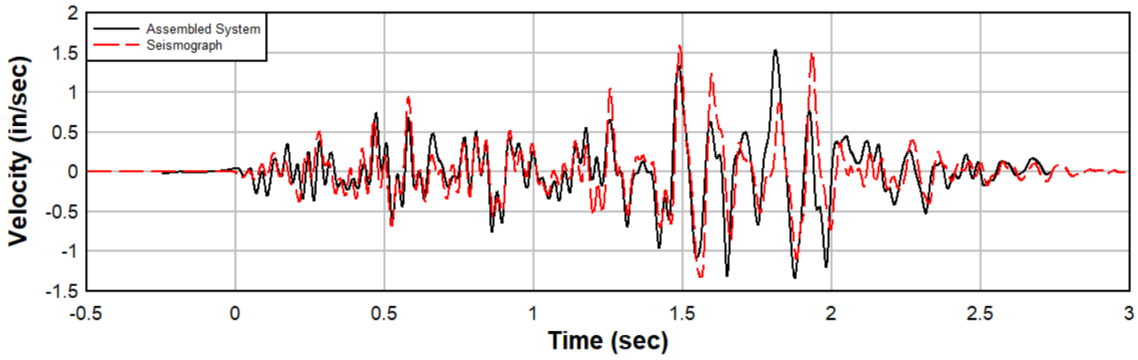

Figure 6.2: Radial Velocity Assembled Sensor vs. Seismograph

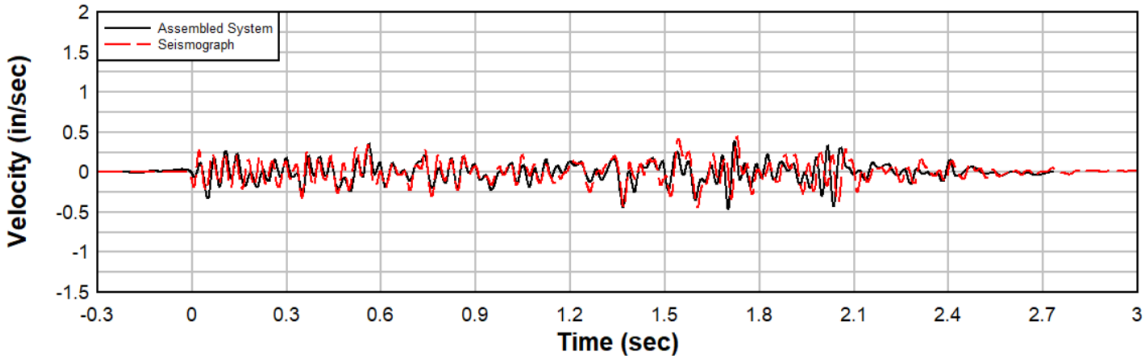

Figure 6.3: Vertical Velocity Assembled Sensor vs. Seismograph

Cross-correlation was performed on the previous three waveforms from the developed sensor and the seismograph. Cross-correlation measures the similarity between a time series and lagged versions of another time series as a function of the lag. The cross-correlation graphs that follow show correlation with respect to the measured lag correlation. Cross correlation starts with an estimate of the sample cross-covariance function. Consider the time series y_{1t} and y_{2t} and lags k= 0,±1,±2,… for data pairs $(y_{11}, y_{21}), (y_{12}, y_{22}), \ldots, (y_{1T}, y_{2T})$, an estimate of the lag k cross-covariance is

$$c_{y1y2}{}^{(k)} = \begin{cases} \frac{1}{T}\sum_{t=1}^{T-k}(y_{1t} - \bar{y}_1)(y_{2,t+k} - \bar{y}_2); k = 0,1,2,\ldots \\ \frac{1}{T}\sum_{t=1}^{T+k}(y_{2t} - \bar{y}_2)(y_{1,t-k} - \bar{y}_1); k = 0,-1,-2,\ldots \end{cases} \quad [19]$$

Where $\bar{y}_1$ and $\bar{y}_2$ are the sample means of the series. The sample standard deviations of the series are:

$$s_{y1} = \sqrt{c_{y1y1}(0)} \quad [20]$$

$$s_{y2} = \sqrt{c_{y2y2}(0)} \quad [21]$$

Where

$$c_{y1y1}(0) = Var(y_1) \quad [22]$$

$$c_{y2y2}(0) = Var(y_2) \quad [23]$$

The estimate of the cross-correlation is

$$r_{y1y2}{}^{(k)} = \frac{c_{y1y2}{}^{(k)}}{s_{y1}s_{y2}}; k = 0, \pm 1, \pm 2, \ldots \quad [24]$$

The cross-correlation outputs a value with a range of -1 to 1 correlation. The peak of the correlations is provided and a value of 0.75 or higher shows a strong correlation between waveforms.

The following figures show the cross-correlation for the three vibration waveform components between the assembled system and the seismograph.

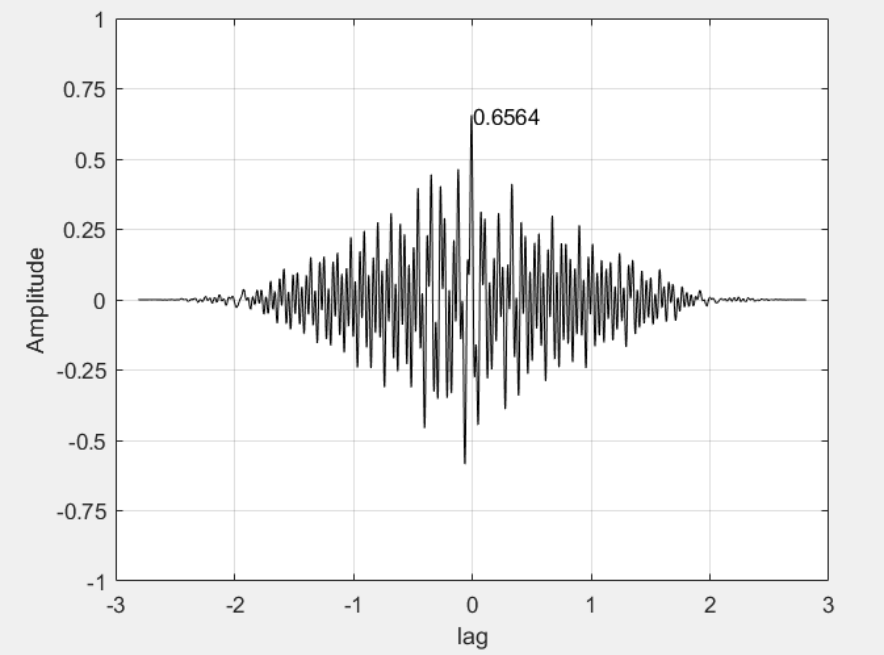

Figure 6.4: Cross-Correlation Transverse Waveform Comparison

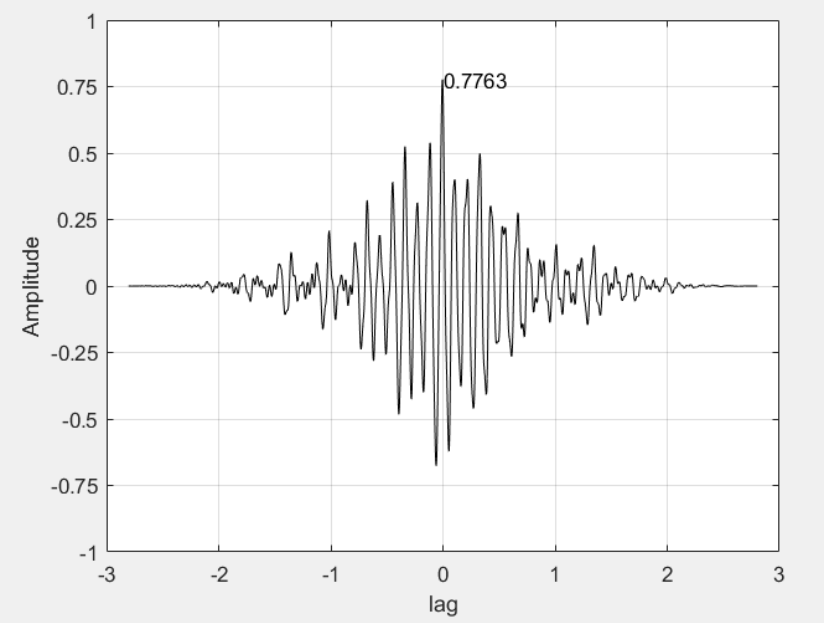

Figure 6.5: Cross-Correlation Radial Waveform Comparison

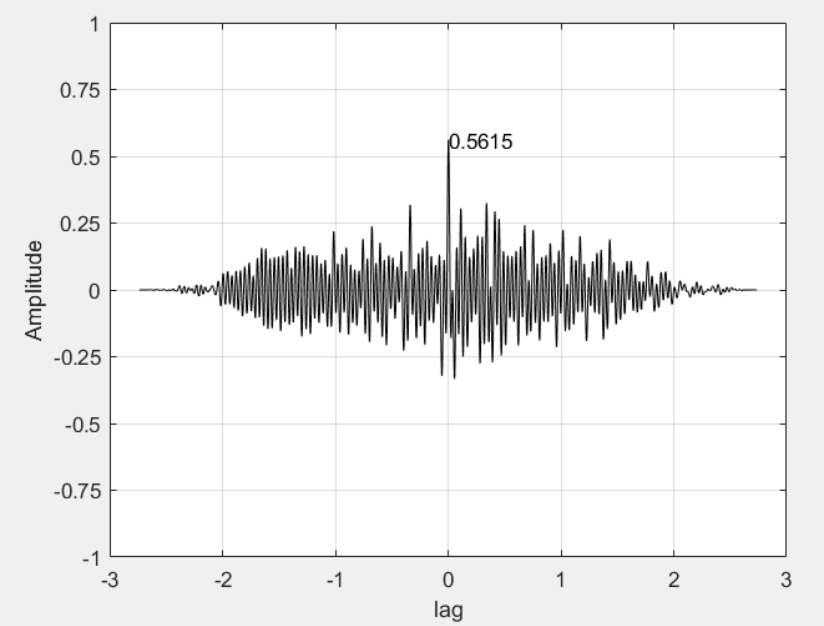

Figure 6.6: Cross-Correlation Vertical Waveform Comparison

The high peaks in the graphs indicate a high correlation between all three components of the vibration waveform. To determine the feasibility of the prototype system, not only the waveforms in time need to be compared, but also the frequency of the signals. Spectral coherence was used to compare the signals in the frequency domain. Coherence values tending toward 0 indicate that the corresponding frequency components are uncorrelated while values tending towards 1 indicate that the corresponding frequency components are correlated. Values above 0.75 are marked as showing a high coherence between data. These values express how x values correspond to y values at each frequency. This estimate is a

function of the power spectral densities. $P_{xx}(f)$ and $P_{yy}(f)$, and the cross power spectral density, $P_{xy}(f)$, of x and y:

$$C_{xy}(f) = \frac{|P_{xy}(f)|^2}{P_{xx}(f)P_{yy}(f)} \quad [25]$$

The following figures display the spectral coherence and the corresponding frequency content components with a high correlated value.

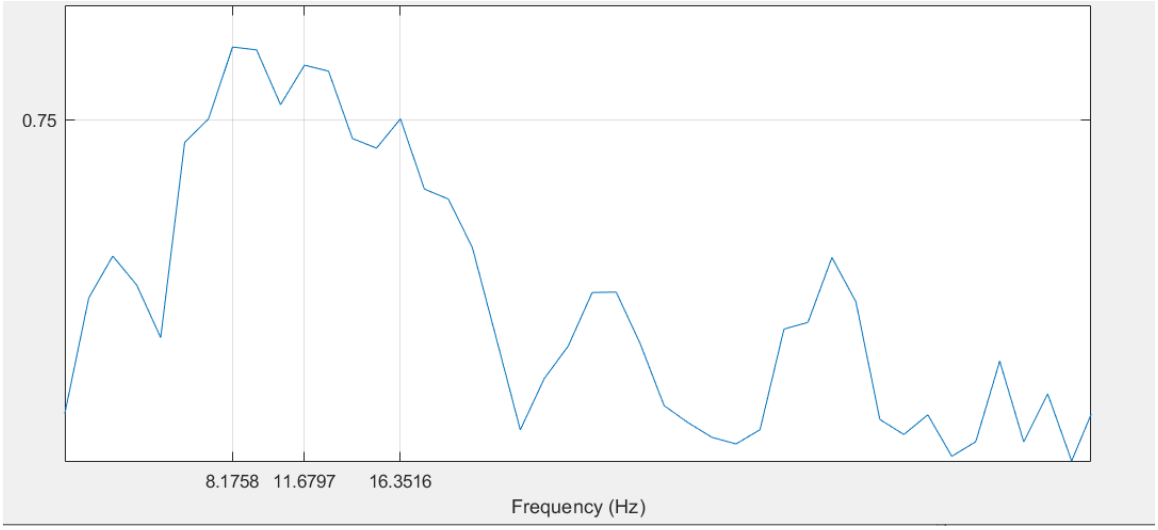

Figure 6.7: Spectral Coherence Transverse Component Comparison

Figure 6.7 shows levels of correlation above 0.75 at frequencies of 8.17, 11.67, and 16.35 Hz.

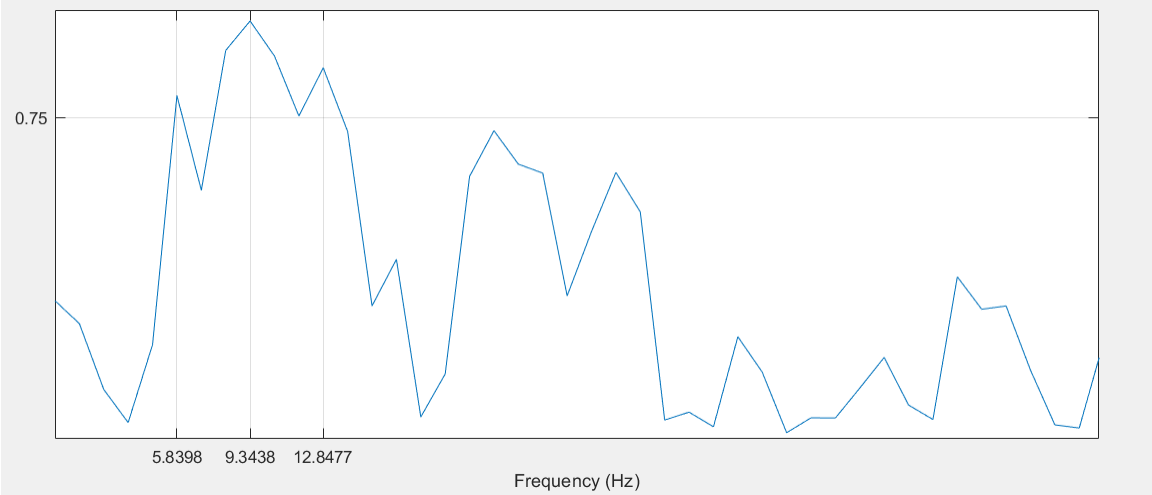

Figure 6.8: Spectral Coherence Radial Component Comparison

Figure 6.8 shows levels of correlation above 0.75 at frequencies of 5.89,9.34, and 12.84 Hz.

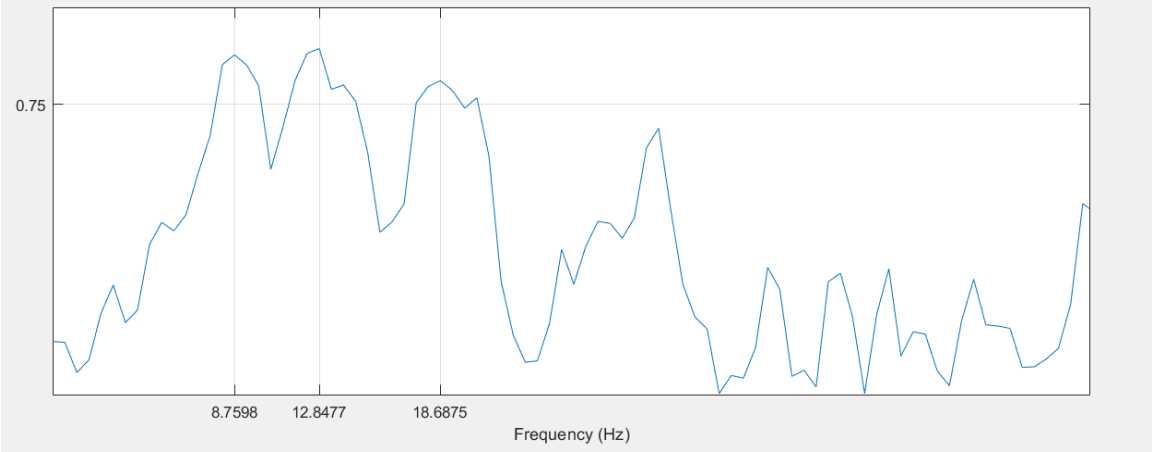

Figure 6.9: Spectral Coherence Vertical Component Comparison

Figure 6.9 shows levels of correlation above 0.75 at frequencies of 8.75, 12.85, and 18.69 Hz.

6.2 Assembled System vs. Accelerometer for Geophysical Studies

The same procedure was used to compare the vibration waveforms with the seismology sensor. The waveforms were show first as a visual comparison and analyzed using cross-correlation and spectral coherence.

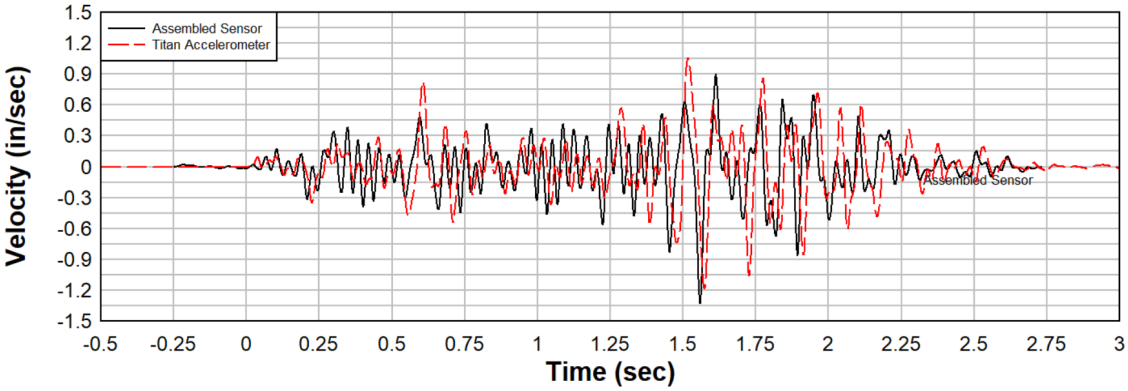

Figure 6.10: Transverse Velocity Assembled System vs. Titan Accelerometer

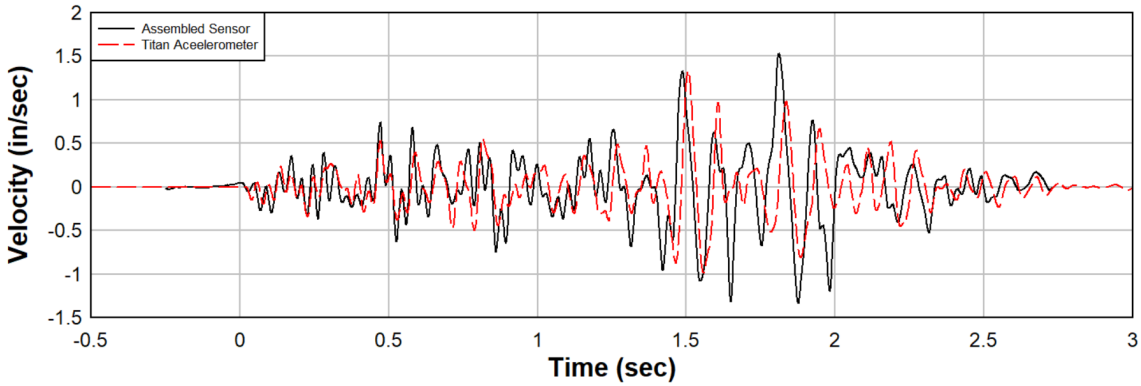

Figure 6.11: Radial Velocity Assembled System vs. Titan Accelerometer

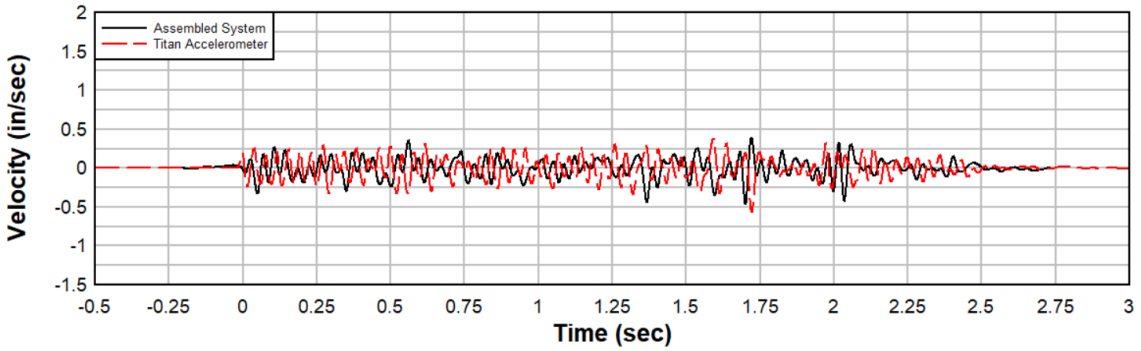

Figure 6.12: Vertical Velocity Assembled System vs. Titan Accelerometer

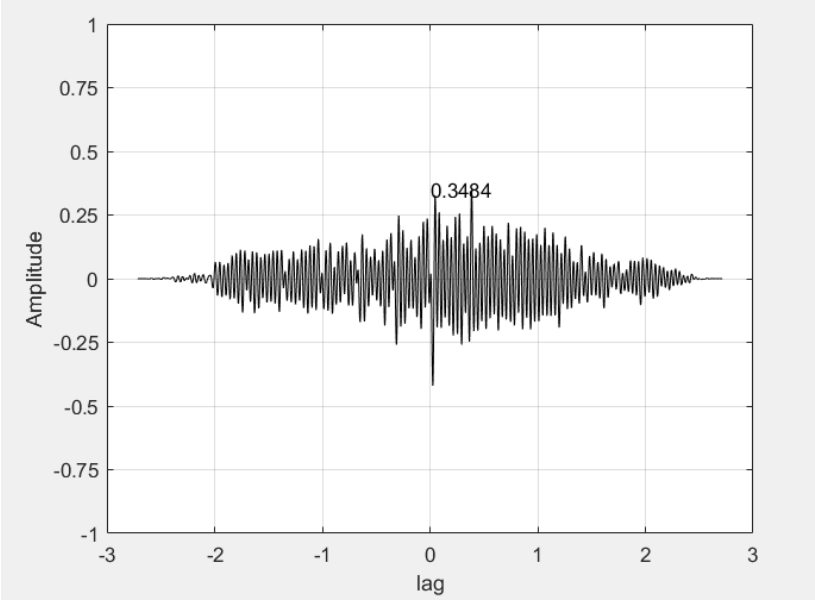

Figure 6.13: Cross-Correlation Transverse Waveform Comparison

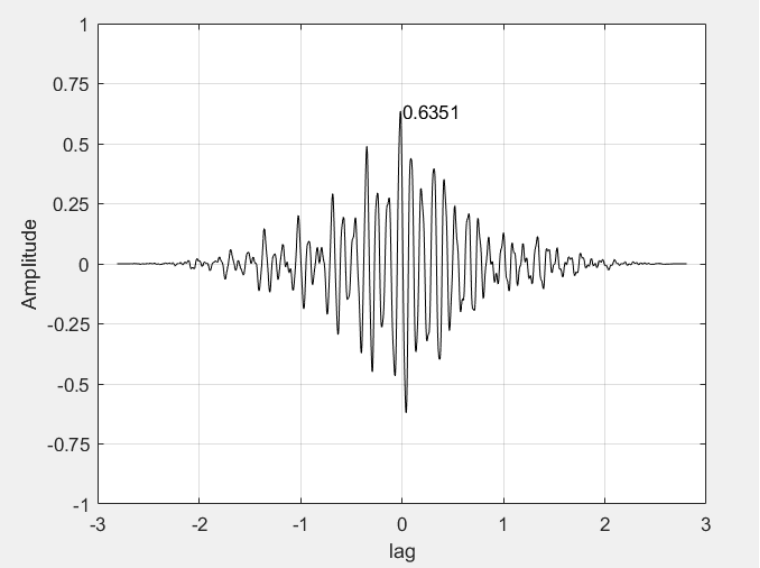

Figure 6.14: Cross-Correlation Radial Waveform Comparison

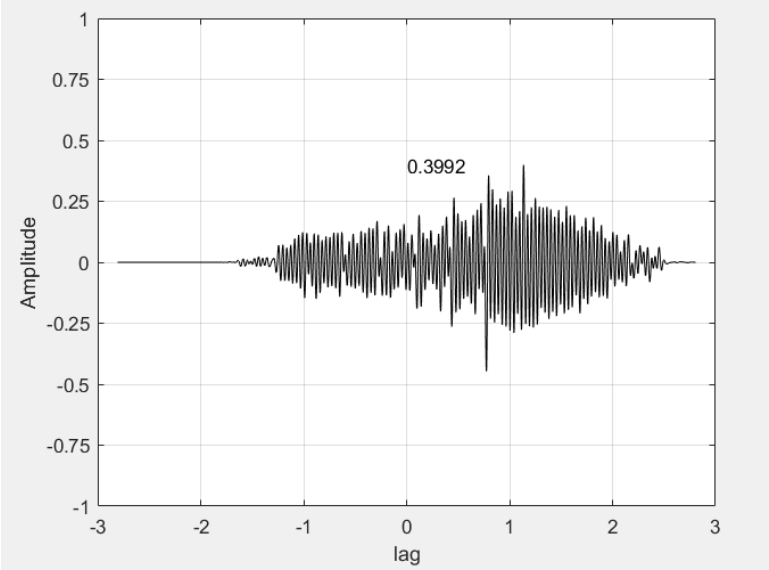

Figure 6.15: Cross-Correlation Vertical Waveform Comparison

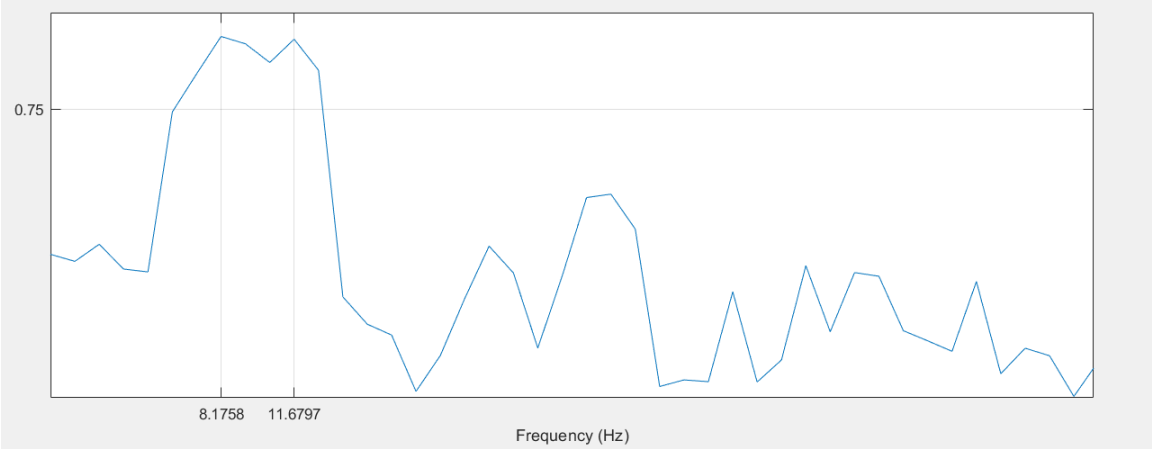

Figure 6.16: Spectral Coherence Transverse Component Comparison

Figure 6.16 shows levels of correlation above 0.75 at frequencies of 8.18 and 11.68 Hz.

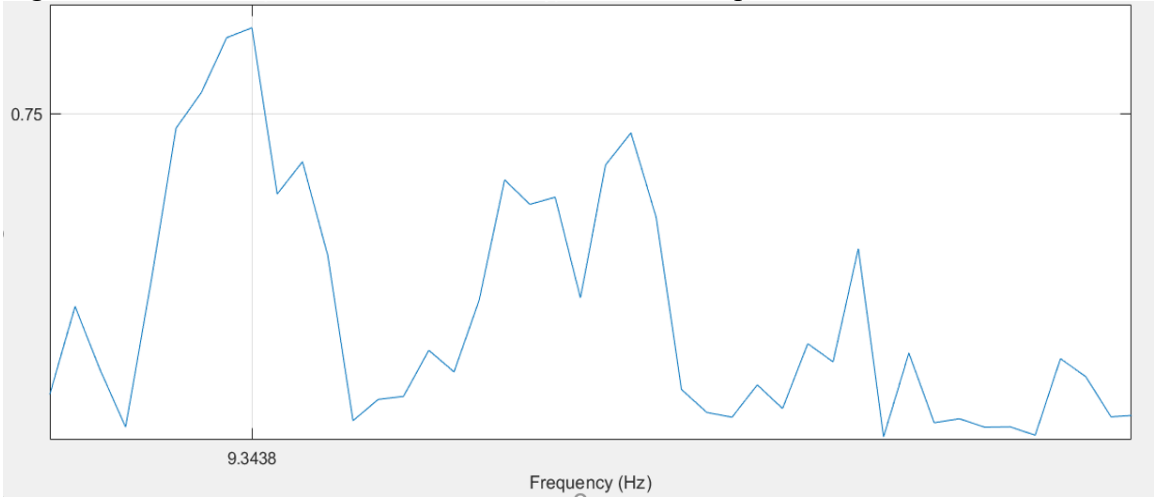

Figure 6.17: Spectral Coherence Radial Component Comparison

Figure 6.17 shows levels of correlation above 0.75 at frequency of 9.35 Hz.

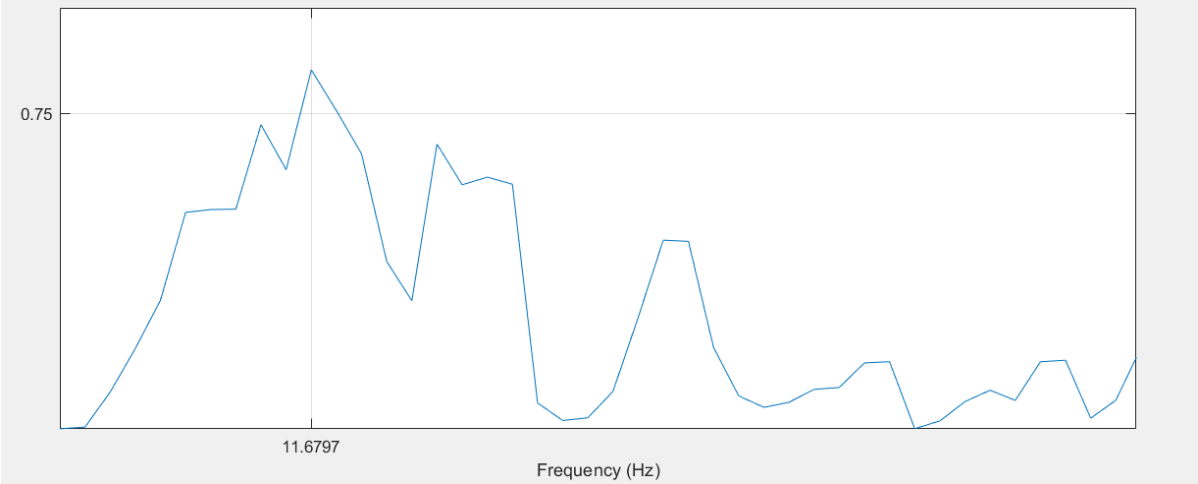

Figure 6.18: Spectral Coherence Vertical Component Comparison

Figure 6.18 shows levels of correlation above 0.75 at frequency 11.68 Hz.

6.3 PPV Comparison and Frequency Summary

The peak particle velocities (PPVs) were obtained from the waveforms for each monitoring device and listed according to the component in Table 3.

Table 3: PPVs and Deviations for Event 2

Component/System	Transverse PPV (in/sec)	Radial PPV (in/sec)	Vertical PPV (in/sec)
Assembled Sensor	-1.33	1.53	-0.46
Seismograph	-1.28	1.60	-0.44
Titan Accelerometer	-1.18	1.33	-0.56
Assembled System Deviation from Seismograph	0.05	0.07	0.02
Assembled System Deviation from Titan Accelerometer	0.15	0.19	0.10
Assembled System % Deviation from Seismograph	3.91	4.44	4.55
Assembled System % Deviation from Titan Accelerometer	12.71	14.58	17.86

The percent deviations of the assembled system from the other two monitoring devices for each component are listed in the final two rows of Table 3.

A summary of the spectral coherence values above 0.75, showing strong relationships, are provided in Table 4.

Table 4: Frequencies with Spectral Coherence Values Above 0.75

Spectral Coherence Frequencies	Transverse	Radial	Vertical
Assembled System vs. Seismograph	8.17	5.84	8.76
	11.68	9.34	12.85
	16.35	12.85	18.69
Assembled System vs. Titan Accelerometer	8.17	9.34	11.68

The values that corresponded across the two coherency tests are highlighted in Table 4. These values show the frequencies present in all the vibration waveforms and correspond to the peak frequencies of the signals. The vertical component has no matching frequencies above the 0.75 coherency value.

Event 1:

In the data comparison of Event 1 each of the three components, transverse, radial, and vertical were compared visually. Each of the waveforms seemed to follow the general waveform of the ground vibration with similar amplitude values. When cross-correlation was performed each of the waveform comparisons showed a spike in correlation around the origin of the lag. It can be inferred from these graphs that all the waveforms from Event 1 were aligned properly with respect to time and each waveform showed a significant correlation with respect to the ground vibration from the blast event. The assembled system's PPV percent deviation from the seismograph for each component was 19.5%, 53.13%, ad 28.21%, respectively. The assembled system's PPV percent deviation from the Titan Accelerometer was 15.76%, 10.58%, and 0.08%, respectively. These values show a much lower percent deviation from the Titan accelerometer than from the seismograph. When comparing the frequency content of the signal, the coherence values were above 0.75 for the spikes or the main frequency content of the ground vibrations. The characteristic values above 0.75 coherence for the Transverse waveform was 5.93 Hz. The characteristic values above 0.75 coherence for the Radial waveform were 8.29 Hz and 18.69 Hz. No frequencies found for the vertical waveform matched from the spectral coherency tests.

Event 2:

In the data comparison of Event 2 each of the three components, transverse, radial, and vertical were compared visually. Each of the waveforms seemed to follow the general waveform of the ground vibration with similar amplitude values. When cross-correlation was performed each of the waveform comparisons showed a spike in correlation around the origin of the lag. It can be inferred from these graphs that all the waveforms from Event 2 were aligned properly with respect to time and each waveform showed a significant correlation with respect to the ground vibration from the blast event. The assembled system's PPV percent deviation from the seismograph for each component was 3.9%, 4.44%, ad 4.55%, respectively. The assembled system's PPV percent deviation from the Titan Accelerometer was 12.71%, 14.58%, and 17.86%, respectively. These values show a much lower percent deviation from the Titan accelerometer than from the seismograph. When comparing the frequency content of the signal, the coherence values were above 0.75 for the spikes or the main frequency content of the ground vibrations. The characteristic values above 0.75 coherence for the Transverse waveform was 8.17 Hz. The characteristic values above 0.75 coherence for the Radial waveform was 9.34 Hz. No frequencies found for the vertical waveform matched from the spectral coherency tests.

Event 3:

In the data comparison of Event 3 each of the three components, transverse, radial, and vertical were compared visually. Each of the waveforms seemed to follow the general waveform of the ground vibration with similar amplitude values. When cross-correlation was performed each of the waveform comparisons showed a spike in correlation around

the origin of the lag. It can be inferred from these graphs that all the waveforms from Event 3 were aligned properly with respect to time and each waveform showed a significant correlation with respect to the ground vibration from the blast event. The assembled system's PPV percent deviation from the seismograph for each component was 6%, 35.56%, and 54.24%, respectively. The assembled system's PPV percent deviation from the Titan Accelerometer was 17.54%, 3.39%, and 15.63%, respectively. These values show a much lower percent deviation from the Titan accelerometer than from the seismograph. When comparing the frequency content of the signal, the coherence values were above 0.75 for the spikes or the main frequency content of the ground vibrations. No frequencies found for the transverse waveform matched from the spectral coherency tests. The characteristic values above 0.75 coherence for the Radial waveform were 3.58 Hz and 8.36 Hz. No frequencies found for the vertical waveform matched from the spectral coherency tests.

In summary, for all three events the visual comparisons showed a similarity between the waveforms. Some of the visual comparisons were at the level needed to mark the assembled system as feasible, while others lacked a continuous similarity between the two waveforms. The assembled system percent deviation from the comparison devices ranged from 0.08% to 53%. The seismograph had a very wide range of percent deviation while the Titan accelerometer percentages remained around 15% for all three events. As expected, the spectral coherencies show coherence values about 0.75 percent for most of the peak frequencies of the signal.

As outlined in the experimental setup chapter of the report, the differing distances between systems has a significant impact on the comparisons between the waveforms. Table 5 shows the correlations between the systems with respect to the distance between them for each waveform component.

Table 5: Correlation Between Systems with Respect to Distance

	Distance Between Systems	Transverse	Radial	Vertical
Event 1				
Correlation between Assembled System and Seismograph	20 feet	0.48	0.56	0.47
Correlation between Assembled System and Titan Accelerometer	3 feet	0.84	0.81	0.63
Event 2				
Correlation between Assembled System and Seismograph	3 feet	0.66	0.78	0.56
Correlation between Assembled System and Titan Accelerometer	20 feet	0.3484	0.6351	0.3992
Event 3				
Correlation between Assembled System and Seismograph	20 feet	0.6943	0.5279	0.5909
Correlation between Assembled System and Titan Accelerometer	3 feet	0.8834	0.8443	0.6783
Average correlation for a distance of 3 feet between systems		0.79	0.81	0.62
Average correlation for a distance of 20 feet between systems		0.51	0.57	0.49

A summary of the percent deviations between PPV values for the systems with respect to distance is provided in Table 6.

Table 6: PPV % Deviation Between Systems with Respect to Distance

	Distance Between Systems	Transverse PPV	Radial PPV	Vertical PPV
Event 1				
Assembled System % Deviation from Seismograph	20 feet	19.50	53.13	28.21
Assembled System % Deviation from Titan Accelerometer	3 feet	15.76	10.58	0.80
Event 2				
Assembled System % Deviation from Seismograph	3 feet	3.91	4.44	4.55
Assembled System % Deviation from Titan Accelerometer	20 feet	12.71	14.58	17.86
Event 3				
Assembled System % Deviation from Seismograph	20 feet	6.00	35.56	54.24
Assembled System % Deviation from Titan Accelerometer	3 feet	17.54	3.39	15.63
Average % deviation for a distance of 3 feet between systems		12.40	6.14	6.99
Average % deviation for a distance of 20 feet between systems		12.74	34.42	33.43

CHAPTER 8. CONCLUSIONS AND FUTURE WORK

The two research questions posed at the beginning of the research are listed again below.

1. Is the developed system capable of measuring and recording blast vibrations from a surface mining operation?
2. Is the acquired data accurate and precise enough to be used in research projects moving forward in the field of mining?

At the beginning of the research conducted for this report, it was not known whether the assembled system would be capable of measuring and recording the ground vibrations from a surface mine blast. Through the testing done on the three events, it is clear the system is capable of performing these actions. The waveform durations and sampling rates of the system closely matched those of the seismograph and Titan accelerometer. For the preliminary testing for the feasibility of the device, the waveforms were visually similar and provided accurate frequency content for the events. However, there are some issues with the data that need to be outlined before a decision on the feasibility of the system can be determined.

There were noticeable variations in the waveforms from the assembled system versus the seismograph. The wide range of deviation from the seismograph in Event 1 and Event 3 is believed to be linked to the monitoring location of the seismograph. As shown in the experimental setup, the seismograph was placed 20 feet from the assembled system as opposed to 3 feet for the Titan accelerometer. Likewise, in Event 2 the deviation of the Titan Accelerometer is believed to be linked to this same discrepancy in distance. This distance likely led to the deviations in the vibration waveforms seen for those devices in the respective events. It is not certain whether this is the cause of the differences in the waveforms because of the limited tests done on the system. In order to prove this hypothesis, further testing would need to be done.

This difference in seismograph data is again outlined when the PPVs are analyzed, with the exception of event 2 the deviations of the assembled system PPVs are high compared to the seismograph. However, the assembled system PPV deviation from the Titan Accelerometer was within the range of 30% maximum deviation outlined by the side-by-side comparison of industry seismographs performed by Sheehan et al. The assembled system PPC deviation from the seismograph fell outside the 30% range on both Event 1 and Event 2.

When the data was analyzed with respect to distances between the device, a connection between similarity of waveforms and distance became apparent. The average correlation of devices placed three feet apart was 0.79, 0.81, and 0.62 for the transverse, radial, and vertical components respectively. The average correlation of devices placed 20 feet apart were 0.54, 0.57, and 0.62 for the transverse, radial and vertical components respectively. These values show a stronger correlation when the systems were placed in close proximity to one another. When placed together the systems shows a strong correlation (above 0.75). The percent deviation of the PPVs showed a similar trend. The percent deviation average

for systems placed 3 feet apart were 12.4, 6.14, and 6.99 for the transverse, radial, and vertical components respectively. The percent deviation average for systems placed 20 feet apart were 12.74, 34.42, and 33.42 for the transverse, radial, and vertical components respectively. When the systems were within 3 feet proximity to one another the deviations fell well within the 30% range outlined by the Sheehan et al. side-by-side comparison test. The lower vertical component correlation could be linked to the installation of the device. As outlined by the ISEE installation guide, the sensor should be buried at a minimum of three times its height. The assembled system was buried at the same depth as the other two systems which equated to two times the height of the sensor.

To answer the second research question, the assembled system shows hopeful results. If being compared solely to the Titan Accelerometer the values would be within the range for feasibility of this system for future research at the University of Kentucky. However, with the limited events studied and the issued with the distances outlined, it is recommended that future tests be performed to inexplicable prove that the assembled sensor is a valuable tool for vibrations research.

The research conducted in this report was the initial testing of the assembled system, although it is not a finished product the results show that new piezoelectric technologies have allowed for the development of a better vibration monitoring system. The creation of a low-cost alternative to the monitoring devices available on the market is feasible and will allow for the collection of raw ground vibration data for the University of Kentucky Explosives Research Team's projects moving forward.

8.1 Future Work

While each of the research questions has been addressed in this thesis, there are recommendations for future work to advance the research. As stated above more testing needs to be done before this initial system can be accepted as a research tool. The following aspects need to be considered in future tests of this system.

1. As outlined in the procedure during a side-by-side comparison paper published in 2015 by Sheehan et al., the comparison needs to be performed with the systems in the same hole as opposed to several holes used in this research.
2. The system should be compared with more than two other systems to establish a better baseline for the ground vibration readings.
3. Coordination with the surface mine to allow for better oriented systems for the specific blast events, instead of a single deployment for a multitude of events

Along with these recommendations for future testing of the sensor, in order to use this as a research tool at the University of Kentucky, more rugged and permanent housing for the system needs to be produced.

Similarly, a program needs to be developed to more easily run the scripts controlling the system and to more precisely set the specifications of the systems.

The assembled system was planned to be tested on a shaking table at a certified seismograph calibration testing facility, but scheduling conflicts prevented such calibration. In the future, once a more complete system is established calibration and validation will be preformed at a similar site. Along with this testing an analysis of the frequency resolution needs to be performed. In order to insure the assembled system is collecting the most accurate frequency content, an adequate frequency resolution is needed.

The assembled system remains in ongoing development at the University of Kentucky. Other sensors are planned to be added to the system including air pressure, humidity, and gps, in order to better understand the factors affecting ground vibration levels.

APPENDICES

Peabody

Peabody Bear Run Mining, LLC

DAILY BLASTING REPORT

Shot # 12278 Date 1-20-20

Pit # 4 Time 4:42 P.M.

Shot Type Corner Mine Bear-Run

Location of Shot SWCN55 3997 E431665 1676 ft NE of S. Gasline

Name of Owner, Distance & Direction to Nearest Building 5400 ft NE of Taylor

Reasons and Conditions for Unscheduled Detonation

EXPLOSIVES USED

Quantity	Type
72352	lbs of Bulk Anfo Dyno Nobel
	lbs 50# Bags
	lbs of Wethole
	lbs of Slurry
	lbs of Emulsion
31006	lbs of Bulk Emulsion Dyno Nobel
	lbs of
78	each, Cast Primers 1 lb
	each, Cast Primers
78	each, Primadets 80 ft MS Det Cord
	each, Primadets
	each, Primadets
	each, Primadets
	each, Primadets
	each, Primadets
	each, Primadets
	each, Primadets
	each
	each
	each
	each Nonels ft ms
	each Nonels ft ms
	each Nonels ft ms
	each Nonels ft ms
	each
	each, Electric Caps
	each, Plastic Spacers
	feet, Detonating Cord
1000	feet, Bulk Lead In Line

Remarks: Also 4WD from 1" allowed WT= 11299.5 lbs 2" allowed WT= 5129.9 lbs

Number of Holes 78

Avg Hole Depth 44 ft

Hole Diameter 10 5/8 in

Burden 24 Spacing 25

Area of Shot sq ft

Cu Yds Shot yds

Total Weight Explosives 103438 lbs

Holes per Delay 1

Max Weight per Delay 1372 lbs

Stemming Type D. C

Avg Stemming Length 12-13 ft

Coal Seam Overburden 5A

Overburden Type Shale

Initiation System Nonel

Det nator Type Shot Shell

Protective Mat Yes No —

Weather Overcast

Wind Direction N

Wind Velocity 6 mph

Temperature 20°

Seismograph Model Mini Mate Plus

Seismograph Number 13698

Seismograph Location Taylor

Seismograph Distance from Shot 5400 ft

Seismograph Calibration Signal .5-0

Seismograph Setting .05 122

Seismograph PPV Reading .13 in/sec

Seismograph Airblast Reading dBs

Blaster In Charge (Print) John Cook

Blaster In Charge (Sign) John Cook

Certification Number I 0117

Seismograph Operator Vibronics

APC FORM # 20082025

Peabody

Peabody Bear Run Mining, LLC

DAILY BLASTING REPORT

Shot # 12284 Date 1-21-20

Pit # 4 Time 4:44 P.M.

Shot Type Cast + Pre-split Mine Bear-Run

Location of Shot NWC N 556290 E 431590 2196ft SE of N. Gasline

Name of Owner, Distance & Direction to Nearest Building 4188ft SE of Mason

Reasons and Conditions for Unscheduled Detonation

EXPLOSIVES USED

Quantity	Type
16016 lbs	of Bulk Anfo Warex
lbs	50# Bags
lbs	of Wethole
lbs	of Slurry
lbs	of Emulsion
16564 lbs	of Bulk Emulsion Warex
lbs	of
126 each	Cast Primers TB
each	Cast Primers
3 each	Primadets 120ft 500ms
3 each	Primadets 60ft 8.2 Dets
each	Primadets
each	Primadets
each	Primadets
each	Primadets
each	Primadets
each	Primadets
61 each	Nigi Shot Plus 60ft
60 each	120ft
each	
each	Nonels ft ms
each	Nonels ft ms
each	Nonels ft ms
each	Nonels ft ms
each	
each	Electric Caps
each	Plastic Spacers
feet	Detonating Cord
feet	Bulk Lead In Line

Remarks: Use WID form
1" allowed WT = 10693.0 lbs
2" allowed WT = 8607.1 lbs

Pre-split
6 - Drilled
3 - Loaded

Number of Holes 60 - Cast

Avg Hole Depth ft

Hole Diameter 10 5/8 in

Burden 23 - 9 Spacing 32 - 13

Area of Shot sq ft

Cu Yds Shot yds

Total Weight Explosives 18264 lbs

Holes per Delay 1

Max Weight per Delay 3073 lbs

Stemming Type D.C

Avg Stemming Length 12-13 ft

Coal Seam Overburden 7

Overburden Type Shale

Initiation System Nonel Elect

Det nator Type "

Protective Mat Yes No ✓

Weather Partly Sunny

Wind Direction SE

Wind Velocity 3mph

Temperature 31°

Seismograph Model Mini Mate Plus

Seismograph Number 14331

Seismograph Location Mason

Seismograph Distance from Shot 4188 ft

Seismograph Calibration Signal .50

Seismograph Setting .05 132

Seismograph PPV Reading .355 in/sec

Seismograph Airblast Reading dBs

Blaster In Charge (Print) John Cook

Blaster In Charge (Sign) John Cook

Certification Number I N117

Seismograph Operator Vibronics

APC FORM # 20082025

Peabody

Peabody Bear Run Mining, LLC

DAILY BLASTING REPORT

Shot # 12287
Pit # 4
Shot Type Corner

Date 1-22-20
Time 4:48 P.M.
Mine Bear-Run

Location of Shot NWC N 557502 E 431253 1249ft SE of N. Gaslini
Name of Owner, Distance & Direction to Nearest Building 2939ft SE of Mason
Reasons and Conditions for Unscheduled Detonation

5

EXPLOSIVES USED

Quantity	Type
101486	lbs of Bulk Anfo Wares
	lbs 50# Bags
	lbs of Wethole
	lbs of Slurry
	lbs of Emulsion
43499	lbs of Bulk Emulsion Wares
	lbs of
88	each, Cast Primers 1 lb
	each, Cast Primers
88	each, Primadets 120 ft EZ-Dets
	each, Primadets
	each, Primadets
	each, Primadets
	each, Primadets
	each, Primadets
	each, Primadets
	each, Primadets
	each
	each
	each
	each Nonels ft ms
	each Nonels ft ms
	each Nonels ft ms
	each Nonels ft ms
	each
	each, Electric Caps
	each, Plastic Spacers
	feet, Detonating Cord
1000	feet, Bulk Lead In Line

Remarks: Also AW 10 form
1" allowed WT= 5266.1 LBS
2" allowed WT= 2849.0 LBS

Number of Holes 88
Avg Hole Depth 64 ft
Hole Diameter 9 in
Burden 24 Spacing 26
Area of Shot sq ft
Cu Yds Shot yds

Total Weight Explosives 145068 lbs
Holes per Delay 1
Max Weight per Delay 1682 lbs

Stemming Type D.C
Avg Stemming Length 12-13 ft

Coal Seam Overburden 7 CAP
Overburden Type Shale

Initiation System Nonel
Det nator Type Shot Shell

Protective Mat Yes No ✓

Weather Sunny
Wind Direction S
Wind Velocity 5 mph
Temperature 34°

Seismograph Model Mini Mate Plus
Seismograph Number 14331
Seismograph Location Mason
Seismograph Distance from Shot 2939 ft
Seismograph Calibration Signal .50
Seismograph Setting .05 1.32
Seismograph PPV Reading .31 in/sec
Seismograph Airblast Reading dBs

Blaster In Charge (Print) John Cook
Blaster In Charge (Sign) John Cook
Certification Number IN117
Seismograph Operator Vibronics

APC FORM # 20082025

APPENDIX 2. EVENT 1 DATA COMPARISON

Assembled System vs. Seismograph

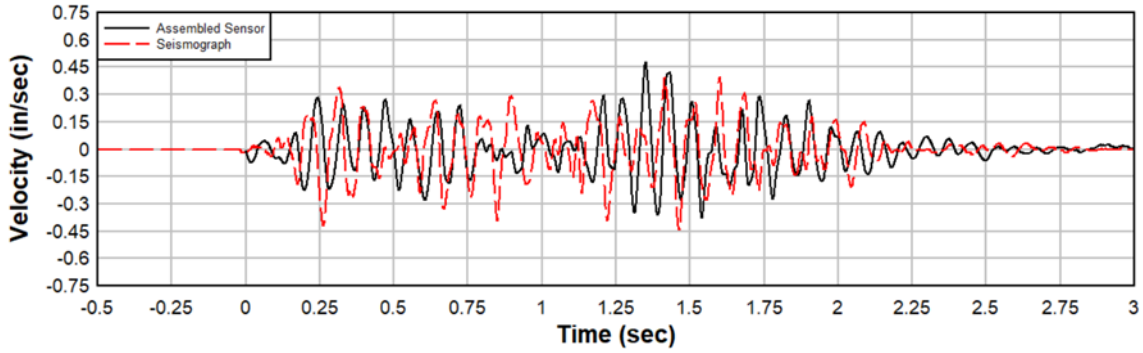

Figure A2. 1: Transverse Waveform Assembled Sensor vs. Seismograph

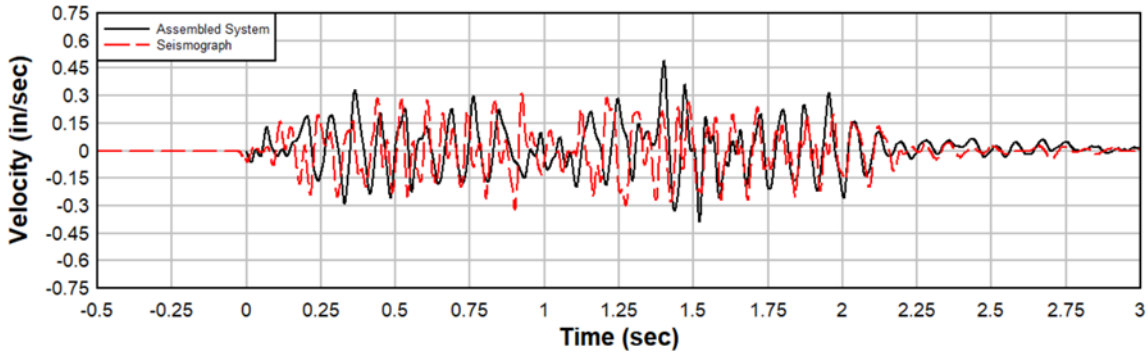

Figure A2. 2: Radial Waveform Assembled Sensor vs. Seismograph

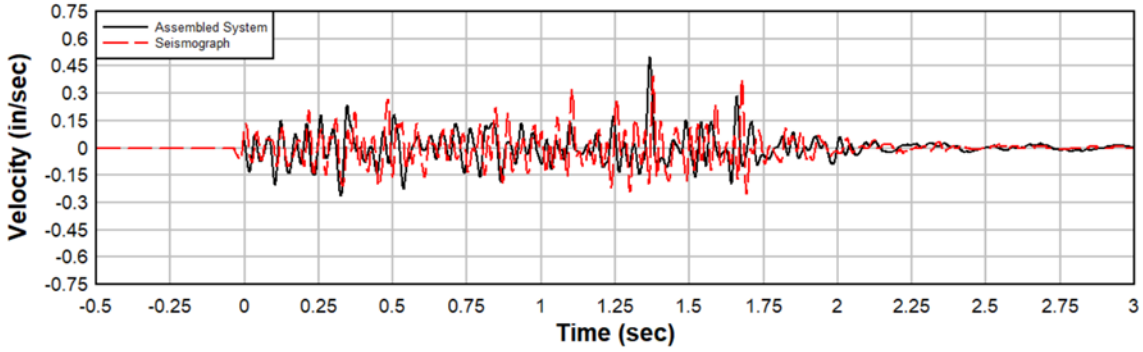

Figure A2. 3: Vertical Waveform Assembled Sensor vs. Seismograph

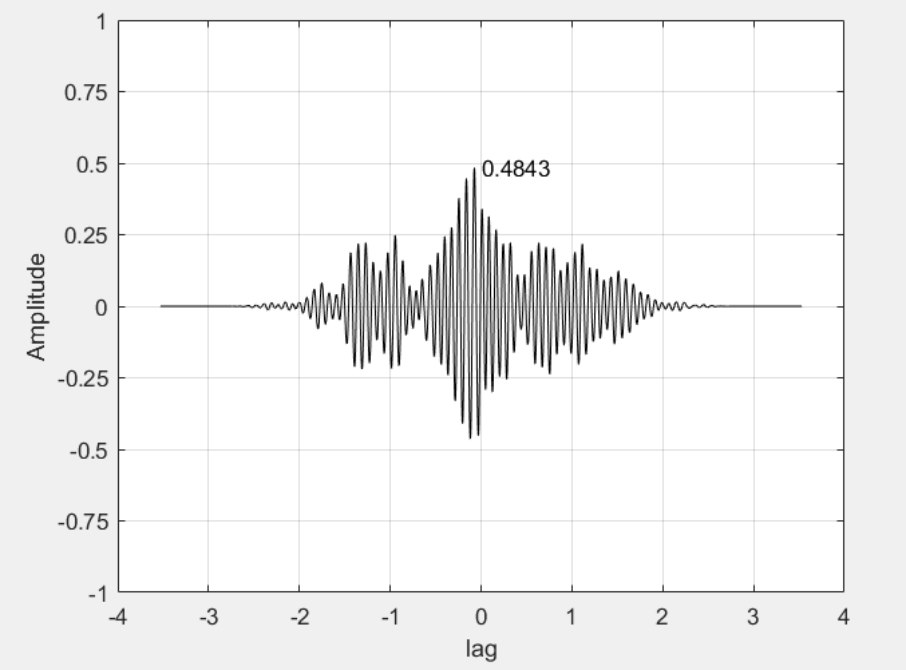

Figure A2. 4: Cross-Correlation Transverse Waveform Assembled System vs. Seismograph

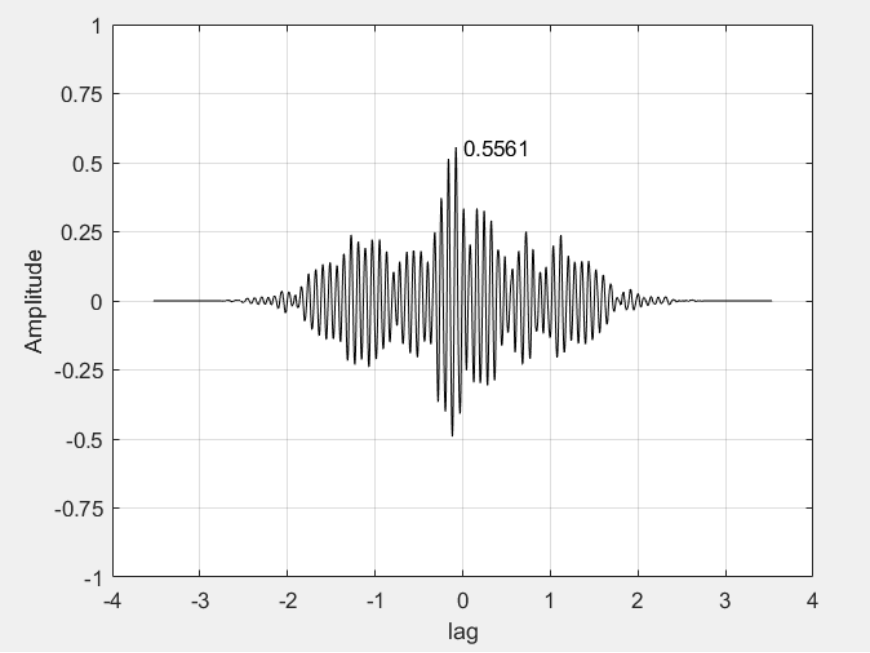

Figure A2. 5: Cross-Correlation Radial Waveform Assembled System vs. Seismograph

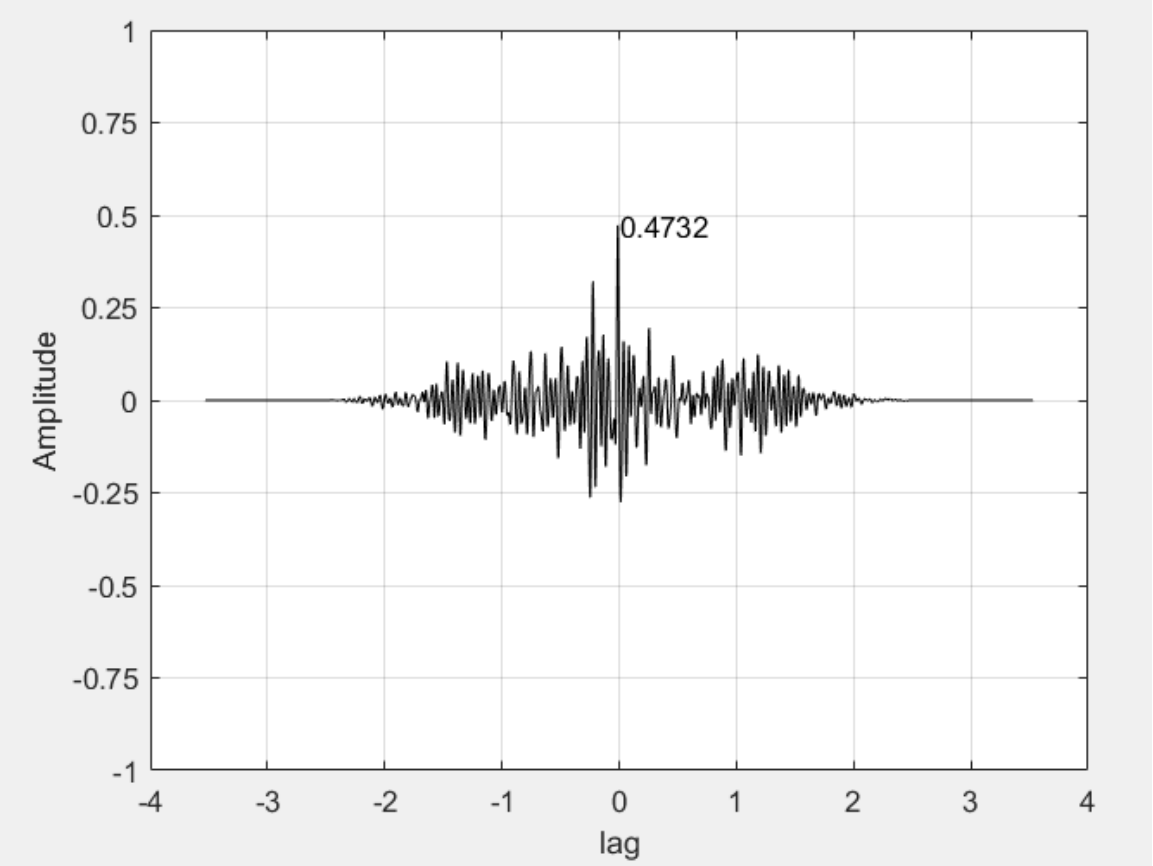

Figure A2. 6: Cross-Correlation Vertical Waveform Assembled System vs. Seismograph

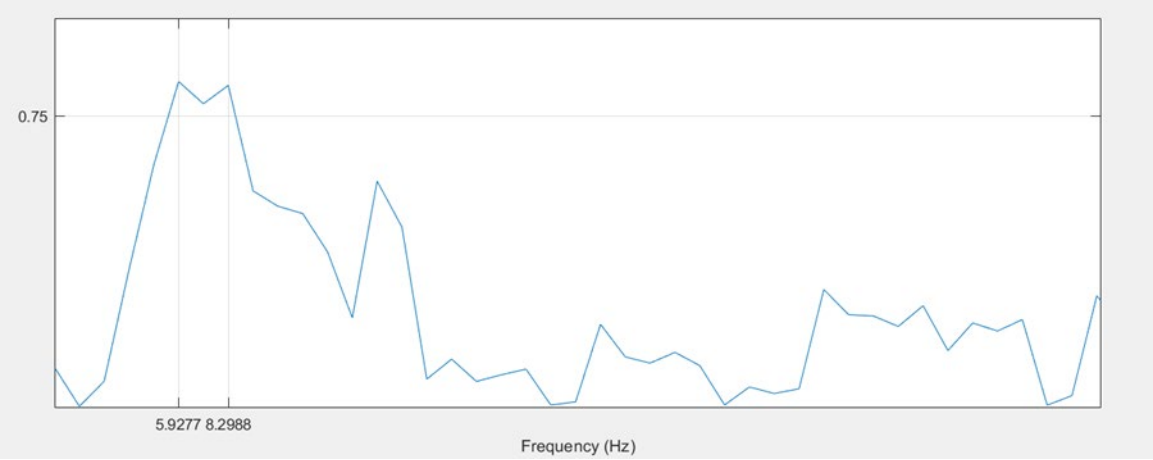

Figure A2. 7: Spectral Coherence Transverse Assembled System vs. Seismograph

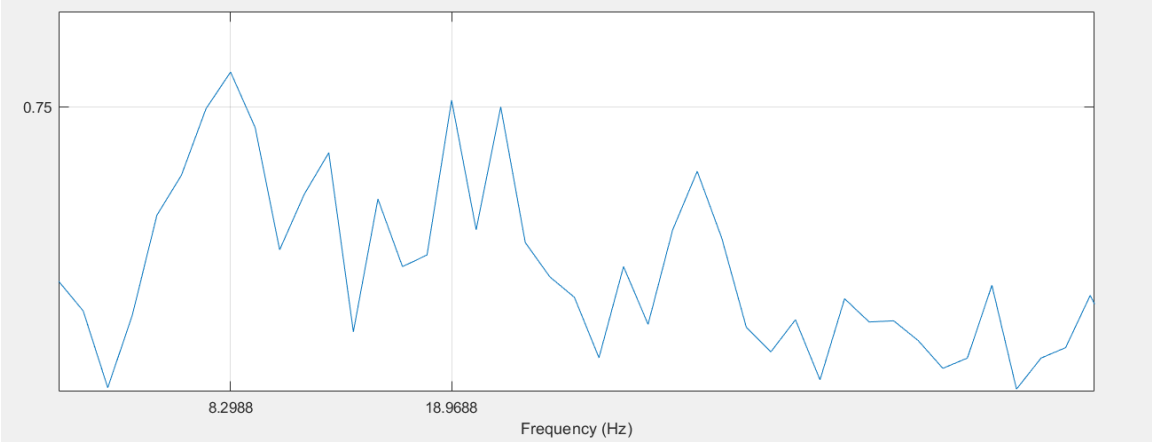

Figure A2. 8: Spectral Coherence Radial Assembled System vs. Seismograph

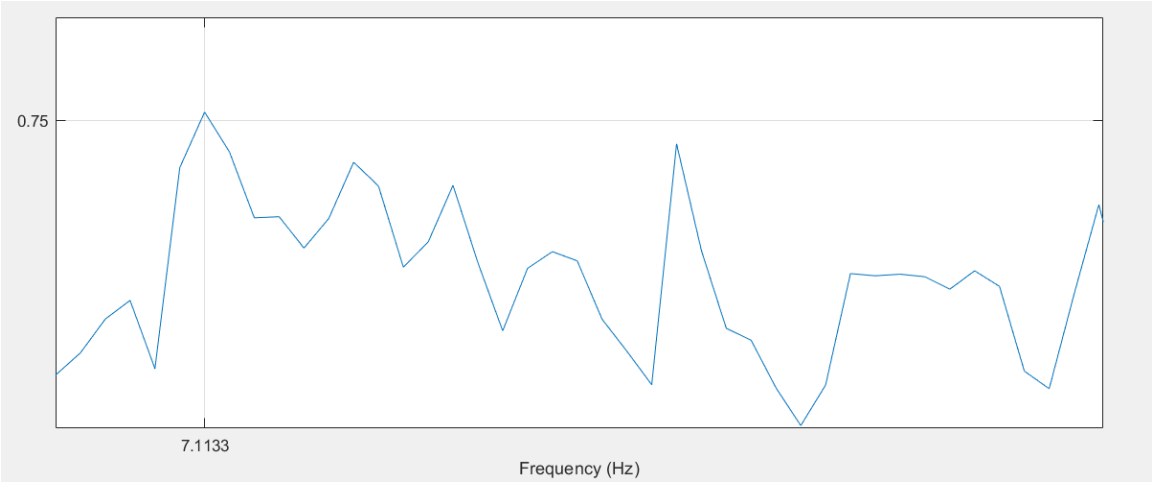

Figure A2. 9: Spectral Coherence Vertical Assembled System vs. Seismograph

Assembled System vs. Geophysics Accelerometer

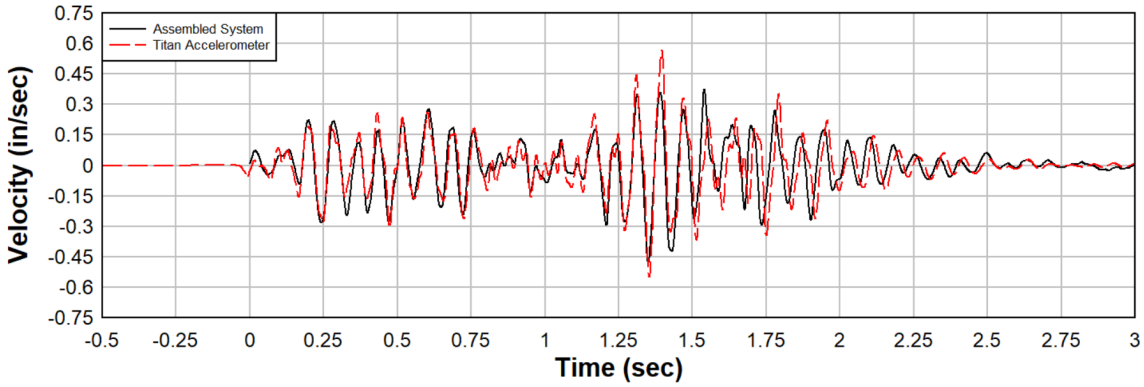

Figure A2. 10: Transverse Waveform Assembled Sensor vs. Titan Accelerometer

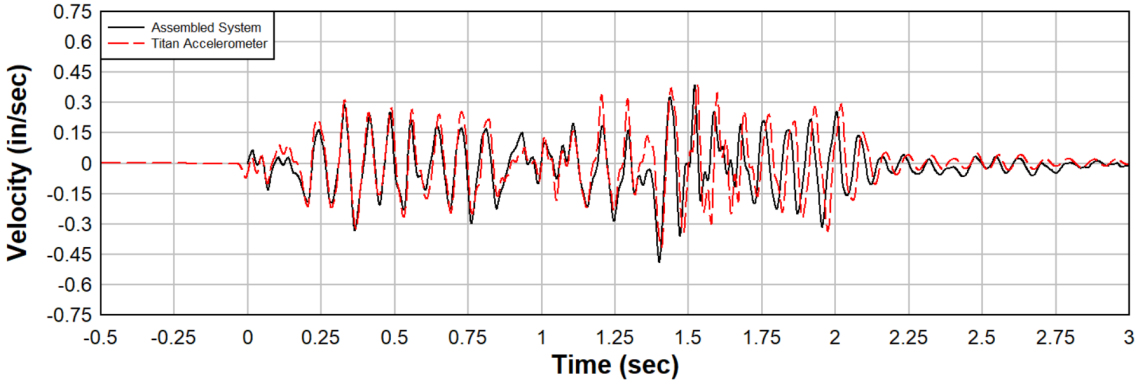

Figure A2. 11: Radial Waveform Assembled Sensor vs. Titan Accelerometer

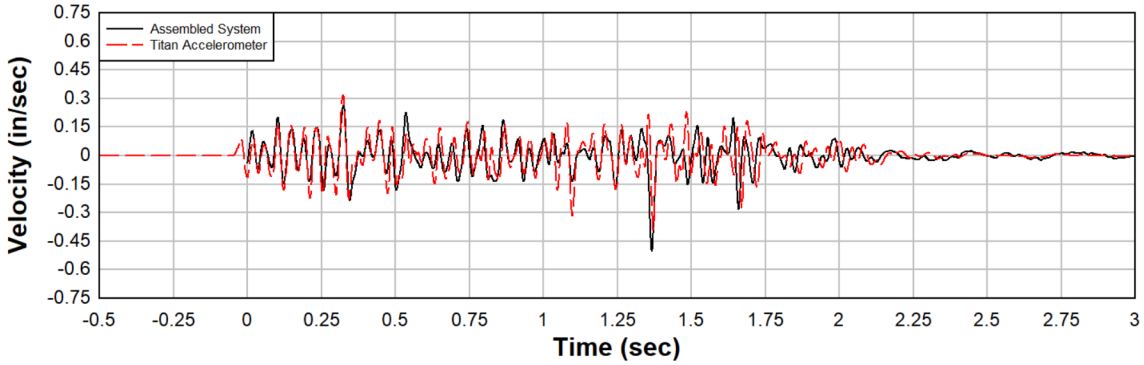

Figure A2. 12: Vertical Waveform Assembled Sensor vs. Titan Accelerometer

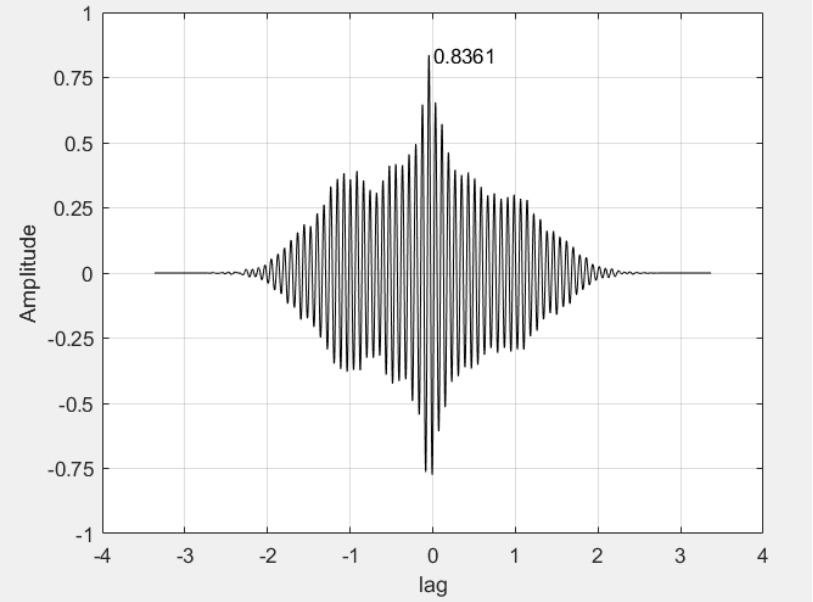

Figure A2. 13: Cross-Correlation Transverse Waveform Assembled System vs. Titan

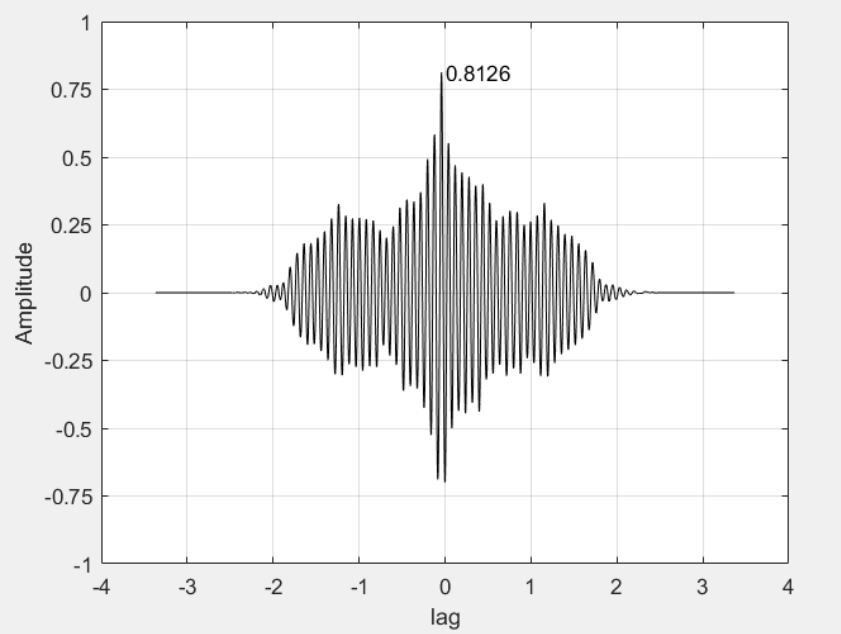

Figure A2. 14: Cross-Correlation Radial Waveform Assembled System vs. Titan

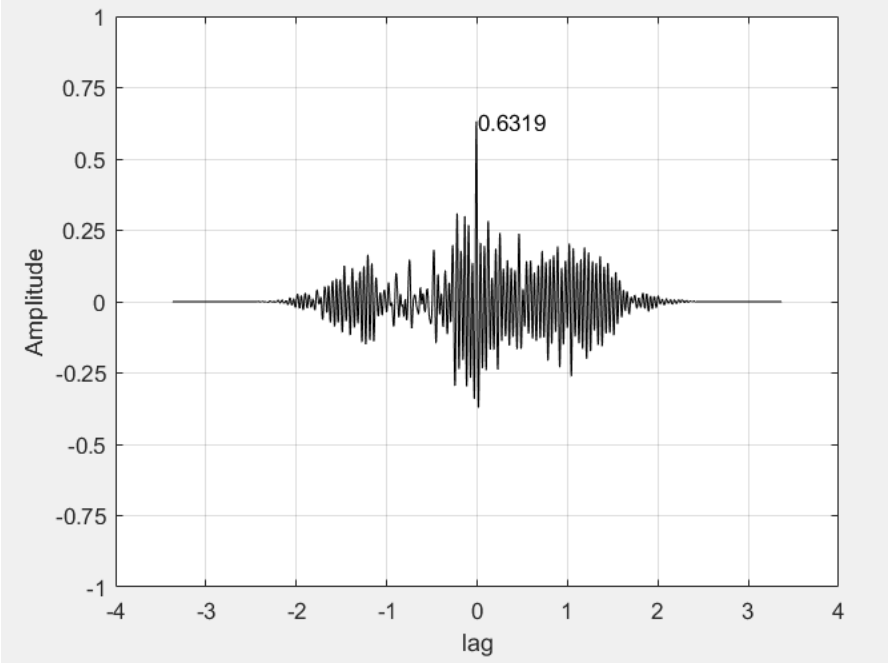

Figure A2. 15: Cross-Correlation Vertical Waveform Assembled System vs. Titan

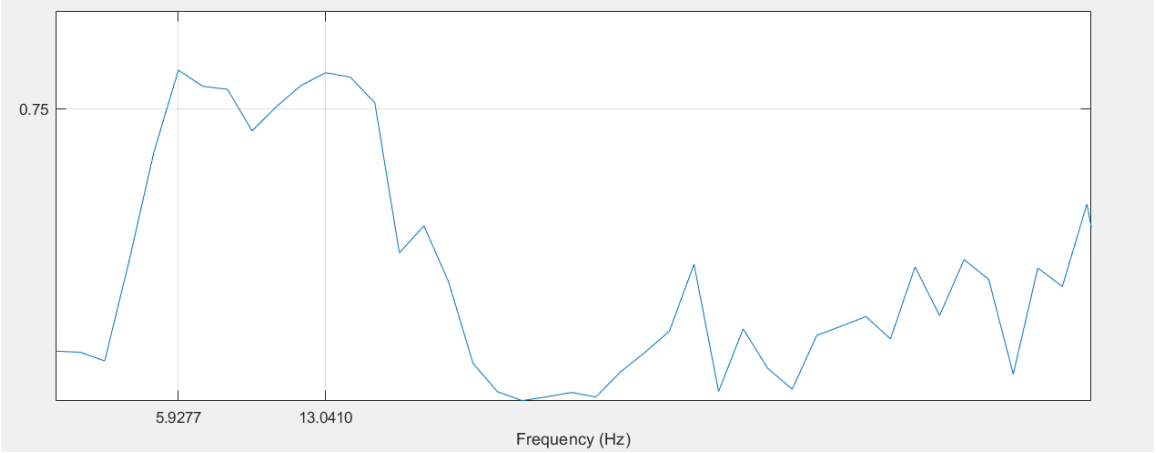

Figure A2. 16: Spectral Coherence Transverse Assembled System vs. Titan

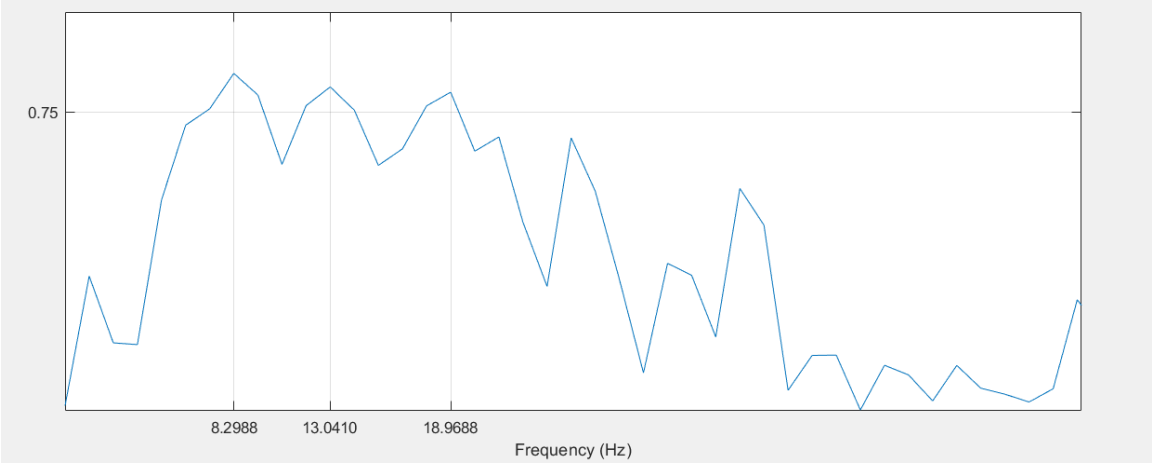

Figure A2. 17: Spectral Coherence Radial Assembled System vs. Titan

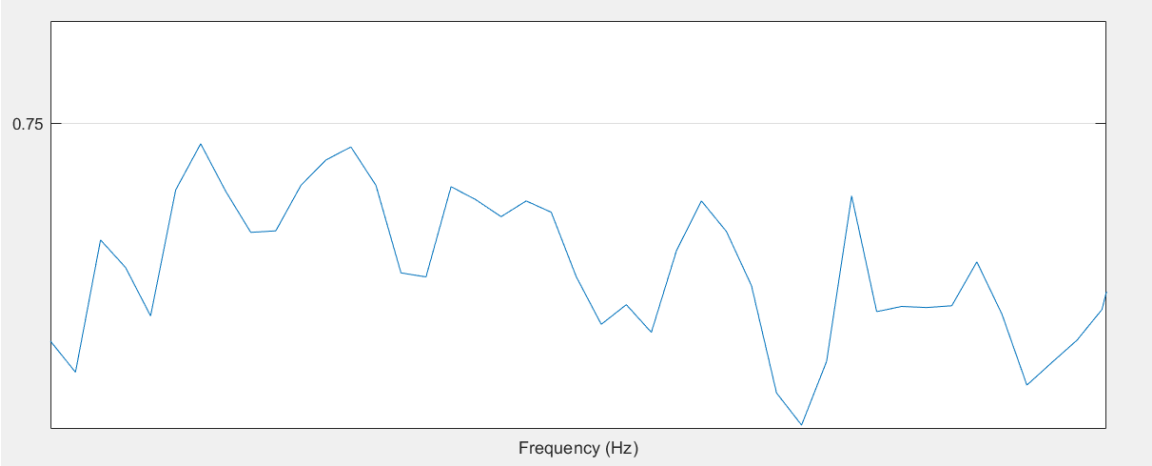

Figure A2. 18: Spectral Coherence Vertical Assembled System vs. Titan

PPV Comparison and Frequency Summary

Table A2. 1: PPVs and Deviations for Event 1

Sensor Type	Transverse PPV (in/sec)	Radial PPV (in/sec)	Vertical PPV (in/sec)
Assembled Sensor	0.48	-0.49	-0.50
Seismograph	0.40	-0.32	-0.39
Titan Accelerometer	0.57	-0.55	-0.39
Assembled System Deviation from Seismograph	0.08	0.17	0.11
Assembled System Deviation from Titan Accelerometer	0.09	0.06	0.00
Assembled System % Deviation from Seismograph	19.50	53.13	28.21
Assembled System % Deviation from Titan Accelerometer	15.76	10.58	0.80

Table A2. 2: Frequencies with Spectral Coherence Values Above 0.75

Spectral Coherence Frequencies	Transverse (Hz)	Radial (Hz)	Vertical (Hz)
Assembled System vs. Seismograph	5.93	8.29	7.11
	8.3	18.96	
Assembled System vs. Titan Accelerometer	5.93	8.29	
	13.04	13.04	
		18.96	

APPENDIX 3. EVENT 3 DATA COMPARISON

Assembled System vs. Seismograph

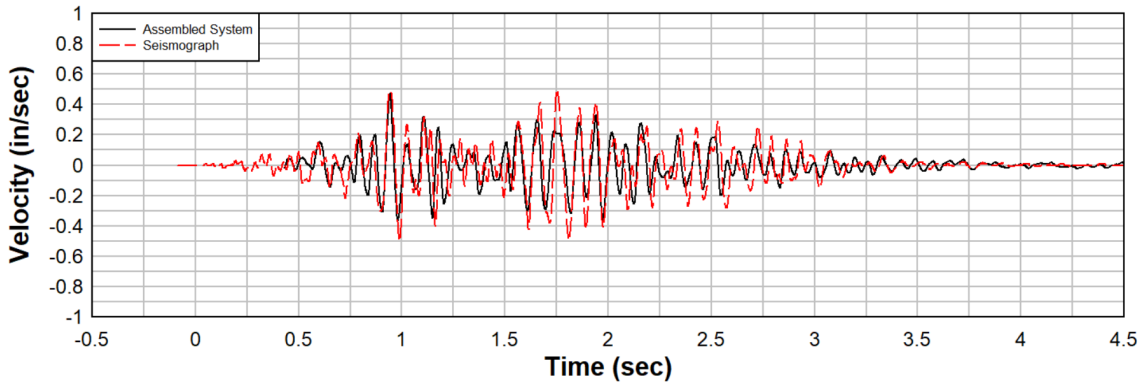

Figure A3. 1: Transverse Waveform Assembled Sensor vs. Seismograph

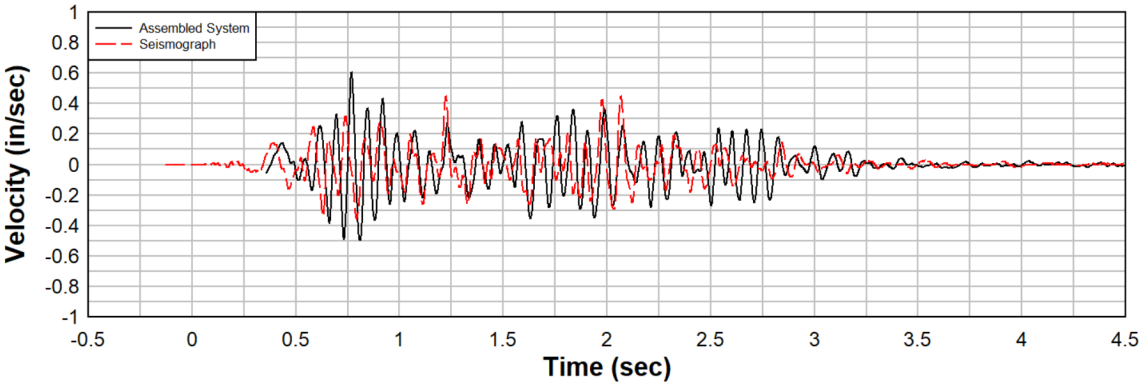

Figure A3. 2: Radial Waveform Assembled Sensor vs. Seismograph

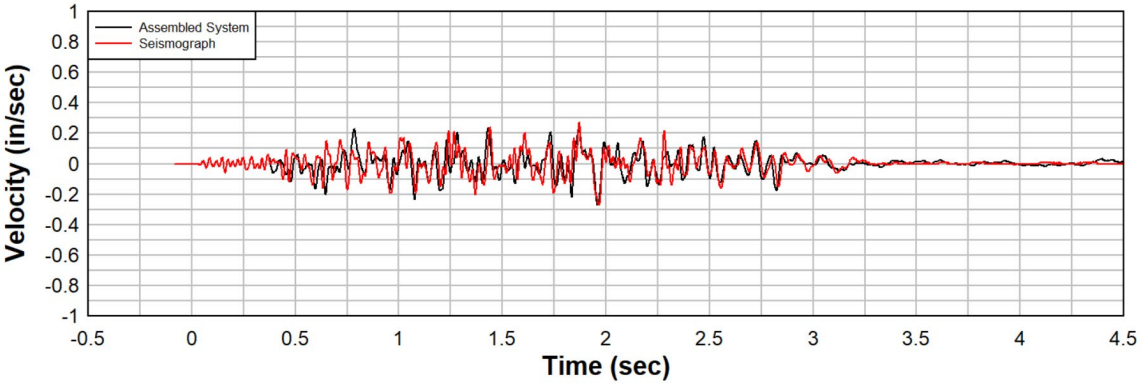

Figure A3. 3: Vertical Waveform Assembled Sensor vs. Seismograph

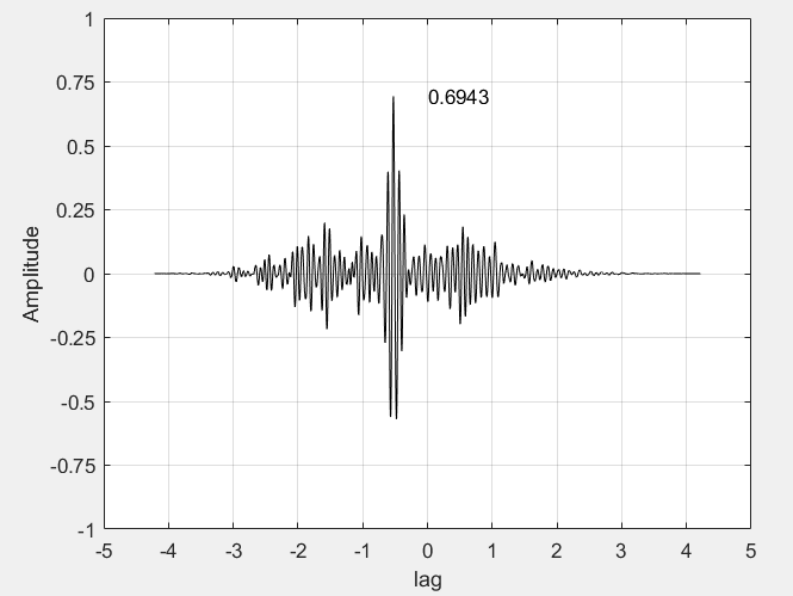

Figure A3. 4: Cross-Correlation Transverse Waveform Assembled System vs. Seismograph

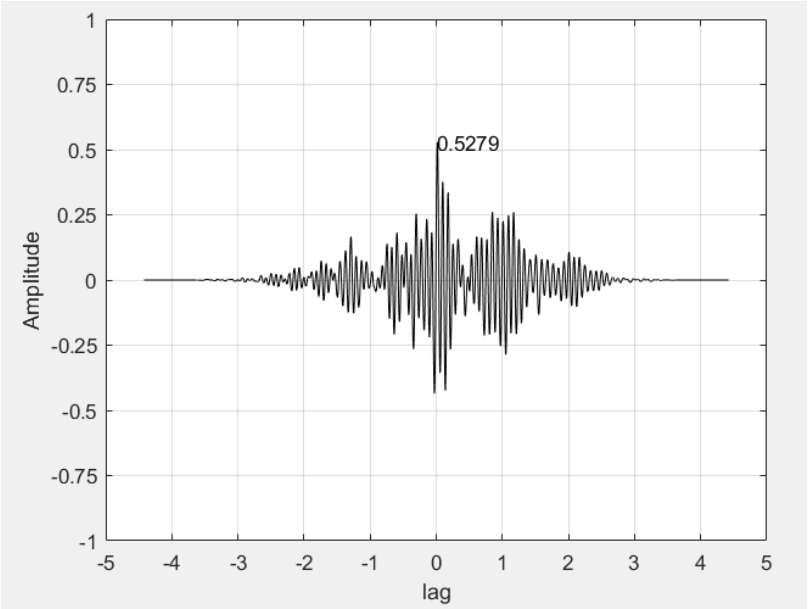

Figure A3. 5: Cross-Correlation Radial Waveform Assembled System vs. Seismograph

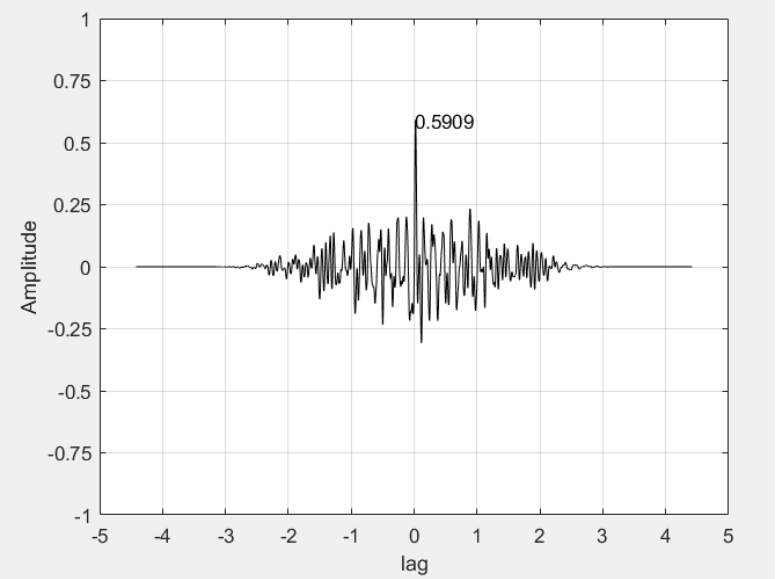

Figure A3. 6: Cross-Correlation Vertical Waveform Assembled System vs. Seismograph

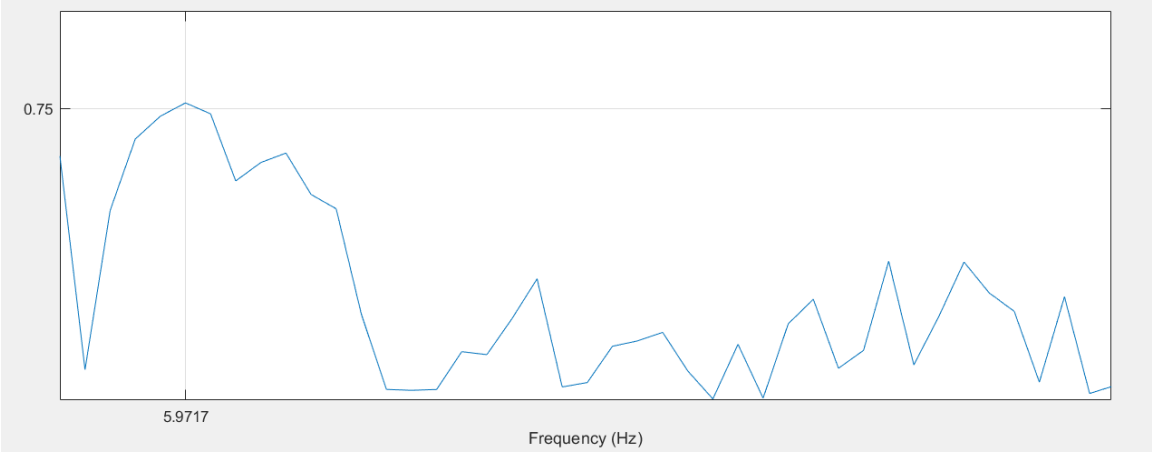

Figure A3. 7: Spectral Coherence Transverse Assembled System vs. Seismograph

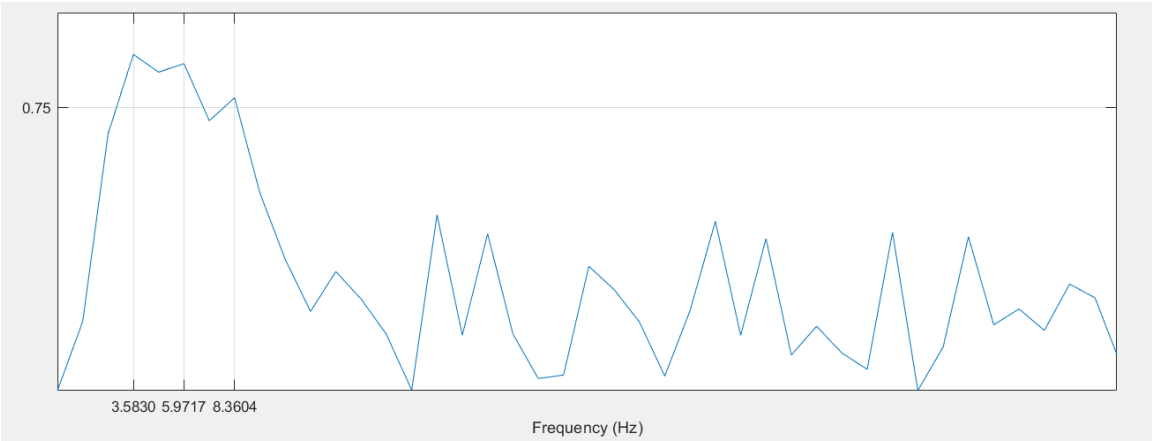

Figure A3. 8:Spectral Coherence Radial Assembled System vs. Seismograph

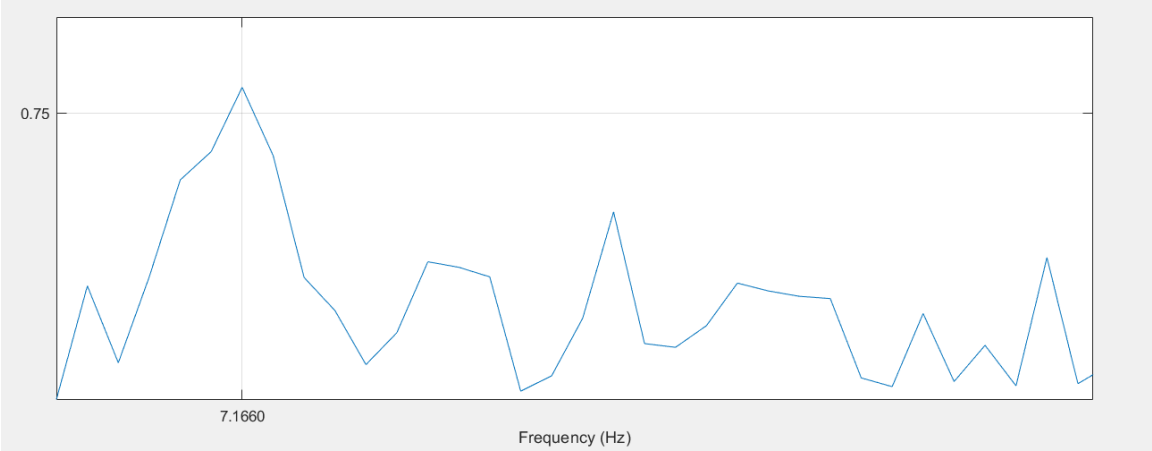

Figure A3. 9: Spectral Coherence Vertical Assembled System vs. Seismograph

Assembled System vs. Titan Accelerometer

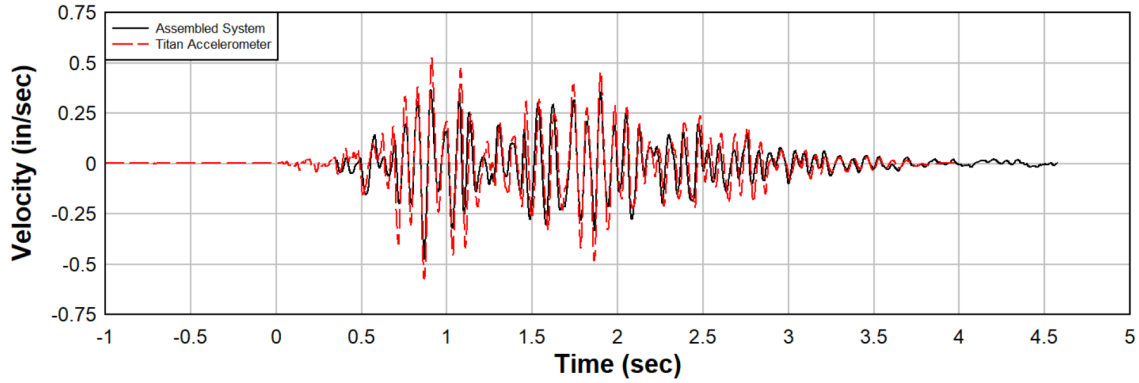

Figure A3. 10: Transverse Waveform Assembled Sensor vs. Titan Accelerometer

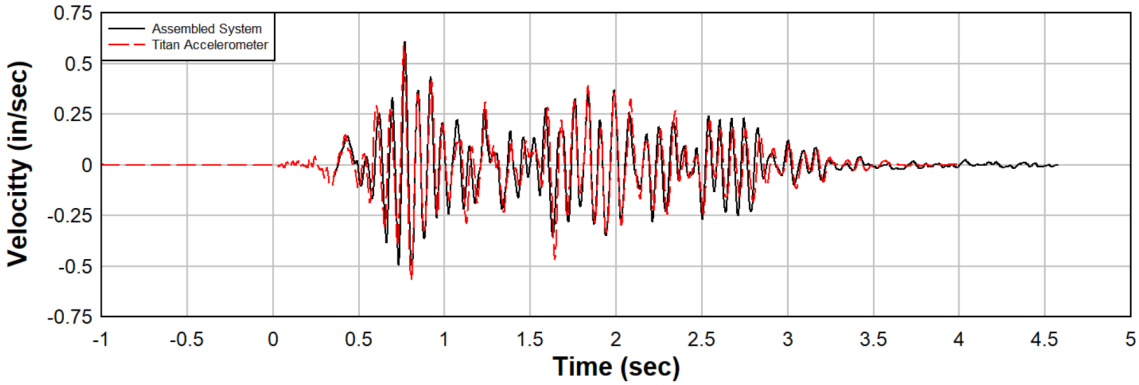

Figure A3. 11: Radial Waveform Assembled Sensor vs. Titan Accelerometer

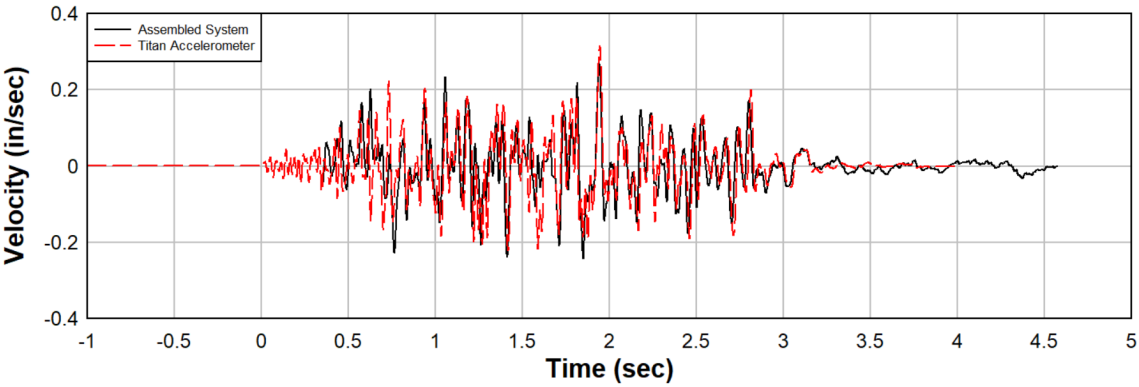

Figure A3. 12: Vertical Waveform Assembled Sensor vs. Titan Accelerometer

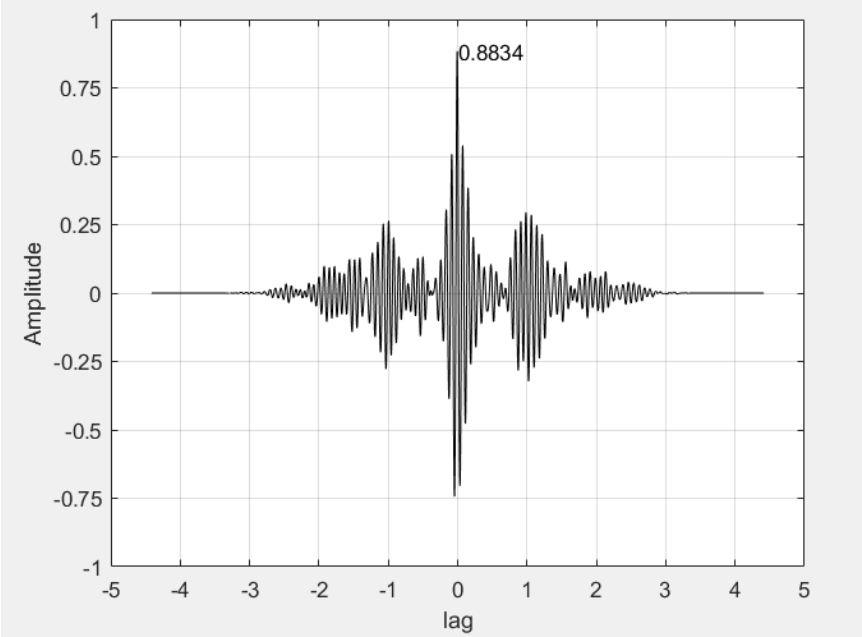

Figure A3. 13: Cross-Correlation Transverse Waveform Assembled System vs. Titan

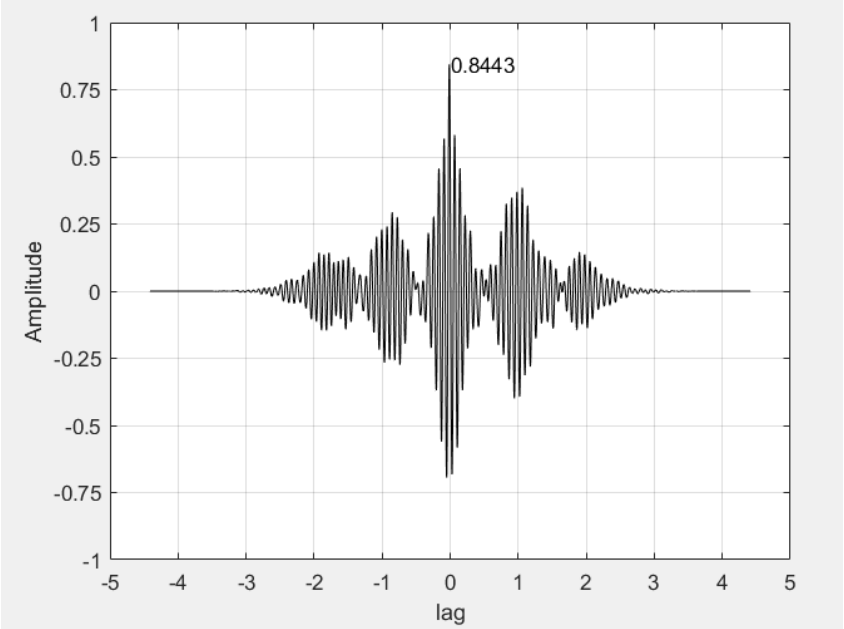

Figure A3. 14: Cross-Correlation Radial Waveform Assembled System vs. Titan

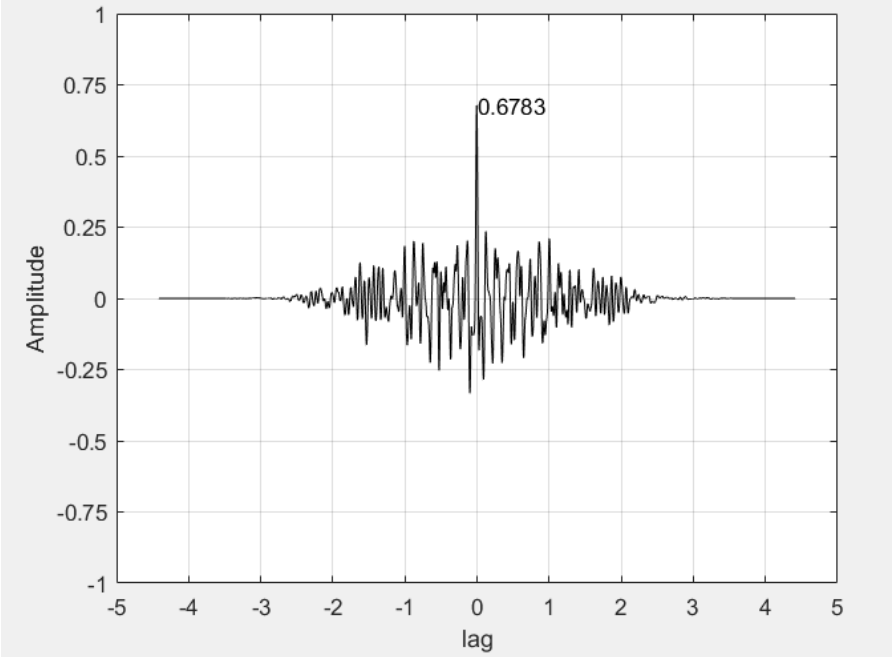

Figure A3. 15: Cross-Correlation Vertical Waveform Assembled System vs. Titan

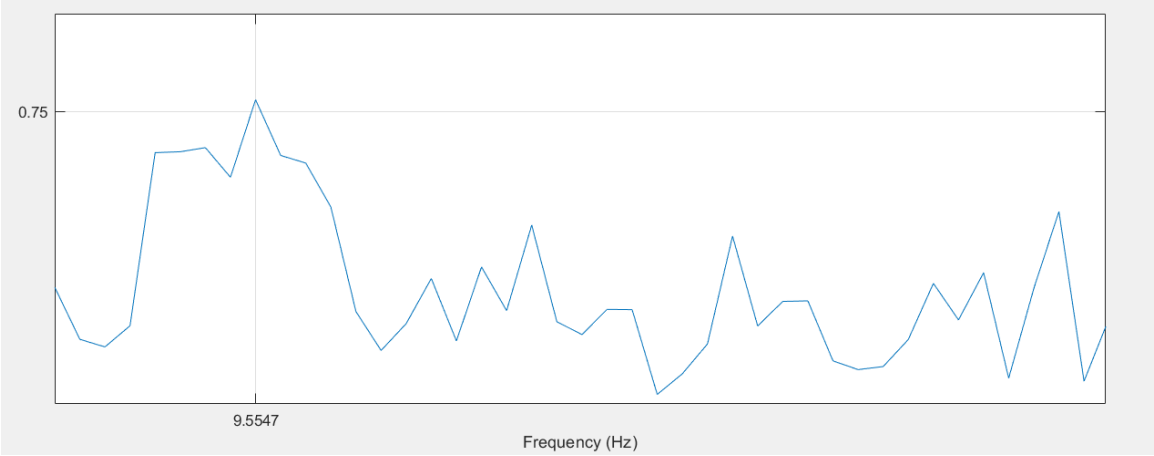

Figure A3. 16: Spectral Coherence Transverse Assembled System vs. Titan

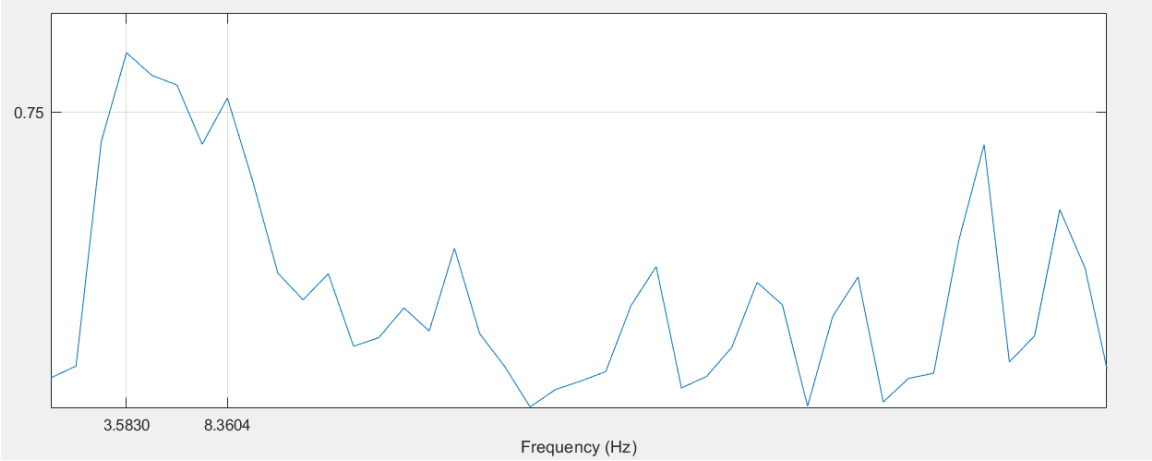

Figure A3. 17: Spectral Coherence Radial Assembled System vs. Titan

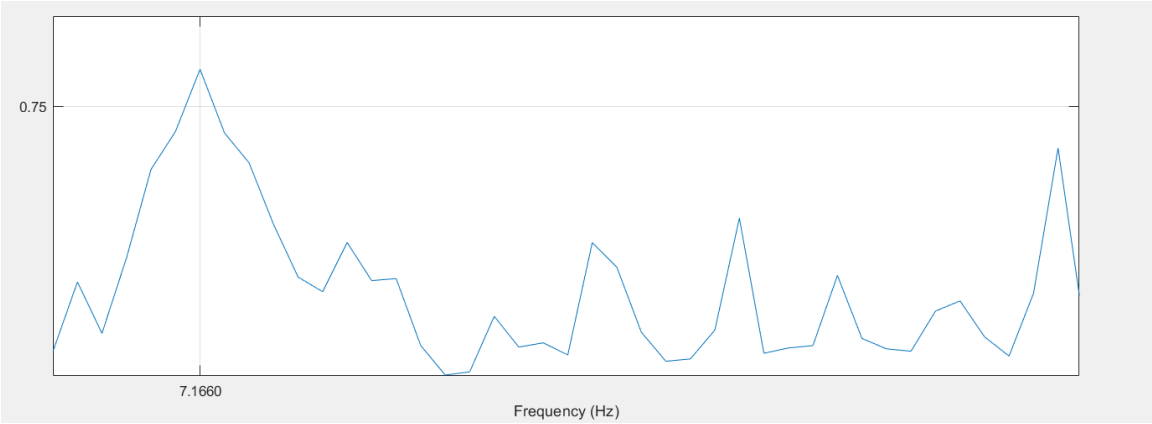

Figure A3. 18: Spectral Coherence Vertical Assembled System vs. Titan

PPV Comparison and Frequency Summary

Table A3. 1: PPVs and Deviations for Event 3

Sensor Type	Transverse PPV (in/sec)	Radial PPV (in/sec)	Vertical PPV (in/sec)
Assembled Sensor	-0.47	0.61	0.27
Seismograph	-0.50	0.45	0.59
Titan Accelerometer	-0.57	0.59	0.32
Assembled System Deviation from Seismograph	0.03	0.16	0.32
Assembled System Deviation from Titan Accelerometer	0.10	0.02	0.05
Assembled System % Deviation from Seismograph	6.00	35.56	54.24
Assembled System % Deviation from Titan Accelerometer	17.54	3.39	15.63

Table A3. 2: Frequencies with Spectral Coherence Values Above 0.75

Spectral Coherence Frequencies	Transverse	Radial	Vertical
Assembled System vs. Seismograph	5.97	3.58	7.17
		5.97	
		8.36	
Assembled System vs. Titan Accelerometer	9.557	3.58	7.17
		8.36	

REFERENCES

Aimone-Martin Associates, LLC. (2016) Supergraph II Comparison Study at the BART Transbay Tube During Underwater Pier Blasting for Caltrans. Comparison Study submitted to Saul's Seismic, Inc.

Ash, R.L., (1963) The mechanics of rock breakage, standards for blasting design. Pit and Quarry.

Bollinger, G. A. (1980). Blast vibration analysis. Carbondale: Southern Illinois University Press, [1971].

Circuit Globe, "Piezo Electric Transducer" Webpage, 2020.

Cook, M.A., (1958) The Science of High Explosives, ASC Monograph No. 139, Reinhold.

Cording, E.J., Hendron, A.J., Hansmire, W.H., MacPherson, H., Jones, R.A., and O'Rourke, T.D. (1975). Methods for Geotechnical Observations and Instrumentation in Tunneling. Vol. 2, The National Science Foundation, Grant GZ 33644X.

Dowding, C.H. (1985). Blast Vibration Monitoring and Control. Library of Congress.

Duvall, W. I. Fogelson, D. E. (1961). Review of Criteria for Estimating Damage to Residences from Blasting Vibrations, Report of Investigation 5968, Bureau of Mines.

Gjodvad, J., Jern, M., (2020) Vibration Monitoring Standards Connected to the use of Explosives in Different Countries. International Society of Explosives Engineers, Denver, CO.

Hunter, C., Fedak, K. and Todoeschuck, J.P. (1993) Development of low-density explosives with wall control applications. Proc.19th Annual Conf. Explosives and Blasting Techniques, Jan 31-Feb. 4, San Diego, California, USA, ISEE.

International Society of Explosives Engineers (ISEE), (2015) ISEE Field Practice Guidelines for Blasting Seismographs. ISEE Standards Committee. Cleveland, OH.

Kisslinger, C., (1963) The Generation of Primary Seismic Signal by a Contained Explosion. VESIAC State-of-the-Art Rept., The Univ. of Mich.

Kisslinger, C., Mateker, E.J., and McEvilly, T.V., (1963) Seismic Waves Generated by Chemical Explosives. AF Cambr. Res. Lab., Bedford, Mass., Rpt. No. AFCRL-63-701, Final Rpt.

Kramer, S.L., (1996) Geotechnical Earthquake Engineering. Prentice Hall.

Leet. L.D., (1960) Vibration from Rock Blasting, Cambridge, Mass., Harvard Univ. Press, 134 p.

Office of Surface Mining Reclamation and Enforcement (OSMRE). Controlling Adverse Effects of Blasting. OSMRE resources, Blasting PDF's.

Prime Faraday Technology Watch. (2002) An Introduction to MEMS (Micro-electromechanical systems). Prime Faraday Partnership, Wolfson School of Mechanical and Manufacturing Engineering, Loughborough Univ., Loughborough, Leics.

Saharan, M.R., Mitri, H.S. (2008) Numerical procedure for dynamic simulation of discrete fractures due to blasting. Rock Mechanics and Rock Engineering, 41

Sheehan, E., Mann, M., Eltschlager, K., Ratcliff, J. (2015) Blasting Seismograph Comparison in Side-by-Side Blast Monitoring Tests. International Society of Explosives Engineers, 2015.

Siskind, D.E., Stagg, M.S., Kopp, J.W., Dowding, C.H., (1980) Structure Response and Damage Produced by Ground Vibration from Surface Mine Blasting. United State Bureau of Mines. Report of investigation; 8506.

Spathis, A.T., (2010) A Brief Review of Measurement, Modeling and Management of Vibrations Produced by Blasting. Vibrations from blasting: Proceedings and Monographs in Engineering, Water and Earth Sciences, Taylor & Francis Group.

VITA

John Meuth

Education:

Master of Science in Mining Engineering at the University of Kentucky, August 2018-present. Thesis title: "Proof-of-Concept for the Development of a ground Vibration Sensor System for Future Research in Blasting."

Bachelor of Science (December 2017) in Mechanical Engineering, University of Kentucky, Lexington, Kentucky.

Academic Employment:

Graduate Research Assistant to Dr. Jhon Silva, Department of Mining Engineering, University of Kentucky, June 2018-present.

Scholastic Honors:

Society of Explosives Engineers Dugan Nelson Scholarship

Society of Explosives Engineers Education Foundation Jerry McDowell Scholarship

Society for Mining, Metallurgy and Exploration WAAIME Scholarship

Presentations and Publications:

Meuth, J. "Active Barrier System Concepts for Underground Coal Mining in the USA," Society of Mining, Metallurgy, and Exploration Central Appalachian Section Meeting 2019, (oral presentation).

Meuth, J. "The Resilience of Underground Communication System Components Subjected to Explosions and Impacts," Society of Mining, Metallurgy, and Exploration Annual Conference 2019, (oral presentation).

Hoffman J., Fryman B., Meuth J. "Debris collection Following a Large-scale AN Detonation," ISEE Conference on Explosives and Blasting Technique 2019.